Vision Based State Estimation For Unmanned Aerial Vehicles - Assist In Vertical Take Off and Landing & Low Altitude Manoeuvre

Ashutosh Natraj

Vision Based State Estimation For Unmanned Aerial Vehicles - Assist In VTOL & Low Altitude Manoeuvre

Ashutosh Natraj

Doctoral Thesis

Submitted for the Partial Fulfilment of the Requirements for the Degree of

Doctor of Philosophy

Modélisation, Information & Systèmes
Doctoral School for Engineering Sciences and Medicine
University of Picardie Jules Verne

Supported by Conseil Régional de Picardie

October 24, 2012

The ISSN serial number is the same for all doctoral theses at UPJV.

ISBN 978-82-471-48xx-x (printed version)
ISBN 978-82-471-48xx-x (electronic version)
ISSN 1503-8181
Thesis at UPJV:xxx

Printed in Amiens by UPJV - MIS laboratory, Amiens

Dedication

This dissertation is lovingly dedicated to my mother, Gyan Datri Shriwastava (25 August 1954 - 13 July 2011). Her support, encouragement, and constant love have sustained me throughout my life.

Abstract

This thesis presents a single camera and laser system depicting an active stereo dedicated to real time state (attitude and altitude) estimation for Unmanned Aerial Vehicles (UAVs) under low illumination to dark, GPS deficient, unexplored environment. The dedicated system consists of a micro fisheye camera and a mini laser projector. The fisheye camera allows to cover a large field of view (FOV) that enables to have the projected pattern available always in the scene even at low altitudes. The state estimation at low altitude is very essential for the UAVs to perform the vertical take-off and landing (VTOL) along with the low altitude manoeuvre for various applications. The approach, close to structured light systems, uses the geometrical information obtained by the projection of the laser circle (under no rotation) or an ellipse (under introduced rotation) onto the ground plane and perceived by the camera.

This thesis presents two solutions for state estimation of UAVs: first one based on algebraic solution and the other one based on geometrical solution. Both the solutions present the mathematical equations with mathematical models developed for both solutions to find the altitude d and the attitude from the relation developed from the normal $\overrightarrow{n}$ of the ground plane with the pattern.

The developed models for algebraic and geometrical solutions have been validated with results. The results consists of two parts: first one for the simulation with ideal and noised data, the second one for the real image sequence from UAV platform compared with commercial sensors on board the UAV. The latter part of the results was expanded for comparison of the results from both the approaches with their robustness check under different illumination conditions, variation in textured surfaces (indoor and outdoor), occluded surface and variation in inclination of the ground planes.

The estimated results from proposed two solutions show good agreement with ground truth values from commercial sensors in terms of its accuracy and correctness. The results also prove its suitability for autonomous VTOL as well as for low altitude manoeuvre under low illumination conditions to dark, GPS deficient, unexplored environment. The use of system also provides room for additional payload to be used for different application due to it being inexpensive and light in weight than the expensive and heavy commer-

cial sensors.

Preface

This thesis is submitted to the Université de Picardie Jules Verne (UPJV) for partial fulfilment of the requirements for the degree of Doctor of Philosophy (PhD).

This doctoral work has been performed at the Department of Robotics and Computer Vision, Laboratory of Modelling and Information Systems (MIS), Amiens, and Laboratory of Electronics, Information and Image (Le2i), Université de Bourgogne under the supervision of Prof. Pascal VASSEUR (Prof. at Laboratory Litis of Université de Rouen, France), Prof. Peter STURM (Director of Research, INRIA Rhône Alpes, France) and Prof. Cédric DEMONCEAUX (Prof. at Laboratory Le2i of Université de Bourgogne, France).

The scholarship was awarded by Regional Council of Picardie department in France to complete PhD at Université de Picardie Jules Verne with a year at Université de Bourgogne as an invited researcher.

Acknowledgements

Contents

List of Tables

List of Figures

Résumé

0.1 Résumé

Cette thèse s'intéresse à l'utilisation d'un capteur actif original pour l'estimation temps réel de l'attitude et l'altitude d'un drone lors des phases d'atterrissage et de décollage. Ce capteur est composé d'une caméra et d'un laser circulaire. Ce dispositif permet de développer une méthode capable de fonctionner même en cas de faible luminosité et d'environnement non texturé. La caméra embarquée est une caméra fish-eye qui permet d'avoir un large champ de vision et peut donc voir le laser à basse altitude ou en prèsence d'angles d'inclinaison importants.

Cette thèse présente deux solutions pour estimer les paramètres de navigation à partir de ce capteur. Une première méthode dite analytique consiste à déduire de la forme du laser dans l'image fish-eye les paramètres recherchés. En effet, nous avons montré que la déformation de l'image du laser est directement liée à l'altitude et l'attitude du drone. La seconde méthode dite géométrique consiste à retrouver le plan 3D du sol à l'aide de l'intersection de deux cônes formés respectivement par le laser circulaire et le cône de vu de la caméra.

Les deux approches ont été validées par des tests synthétiques et réels. Les données de synthèse nous ont permis de vérifier la forte robustesse des deux méthodes proposées. De plus, les tests réels ont montré que nos méthodes pouvaient remplacer les capteurs classiques (centrale inertielle, altimètre) pour estimer l'altitude et l'attitude en conditions difficiles liées à l'éclairage, au type de surface ou à la nature du vol (intérieurs ou extérieurs).

0.2 Introduction

A l'avènement de la robotique, le mot "robot" signifiait un mécanisme imposant muni d'énorme bras-manipulateur. Les progrès de la technique ont conduit à la miniaturisation des capteurs ainsi qu'à celle de nombreuses pièces mécaniques. Ceci a apporté des changements radicaux dans notre vie. Aujourd'hui, il existe de nombreux robots pouvant répondre à différents besoins de notre vie. Grâce aux progrès de l'intelligence artificielle, ces robots sont

désormais pourvus de leur propre intelligence et nécessitent très peu voire aucune intervention humaine. Les différents types de robots peuvent se classer en trois catégorie : les robots mobiles qui opèrent sur le sol appelé "Unmanned Ground Vehicles" (UGV) (fig 1(a)), en milieu sous-marin "Autonomous Underwater Vehicles" (AUV) (fig 1(b)) et enfin la troisième catégorie correspondant aux robots aériens "Unmanned Aerial Vehicles" (UAV).

Dans ce travail, nous nous sommes intéressés à la troisième catégorie. L'intérêt pour ce type de robot (UAV) a considérablement augmenté au cours des dernières décennies. Les drones peuvent être controlés à distance (par un opérateur muni d'une station de contrôle au sol), ils peuvent voler de façon autonome à partir d'un plan de vol pré-programmé ou être totalement autonome. Il existe de nombreuses applications avec ces robots. Les drones peuvent être déployés dans des zones de guerre, utilisés pour surveiller des zones où les caméras fixes sont inefficaces. Ils peuvent naviguer dans des environnements inconnus et ainsi fournir une information rapide sur des zones dans lesquelles une intervention humaine est impossible : catastrophes naturelles, après fuite d'un produit chimique, une catastrophe nucléaire comme par exemple lors de la série de catastrophes qui a frappée le Japon le 11 Mars 2011. Dans chacun de ces cas, les drones permettent d'obtenir une information complète et précise pour aider des opérations de sauvetage. Cependant, les applications ne se limitent pas à ces domaines, nous pouvons aussi trouver des applications dans la surveillance de trafic routier afin d'éviter les bouchons à la périphérie des villes ou encore à l'aide d'urgence pour retrouver des personnes lors d'avalanches. Le principal challenge pour rendre autonome la navigation du robot aérien est d'être capable d'estimer de façon précise l'altitude et l'orientation durant le vol, à partir de capteurs embarqués.

En robotique aérienne, il est très important de distinguer les UAV en fonction de leur voilure. La figure 2 (a) présente un drone à voilure fixe qui ne possède donc pas la capacité de vol stationnaire alors que la figure 2 (b) montre un drone quadri-rotor qui a la capacité de rester à la même position. Le second type est souvent un meilleur choix pour les applications mentionnées dans le paragraphe précédent.

Le fonctionnement autonome de drones est tributaire de l'encombrement des différents capteurs que l'on peut embarquer sur celui-ci. Ces capteurs collectent des données qui sont traitées pour fournir des informations spé-

(a)

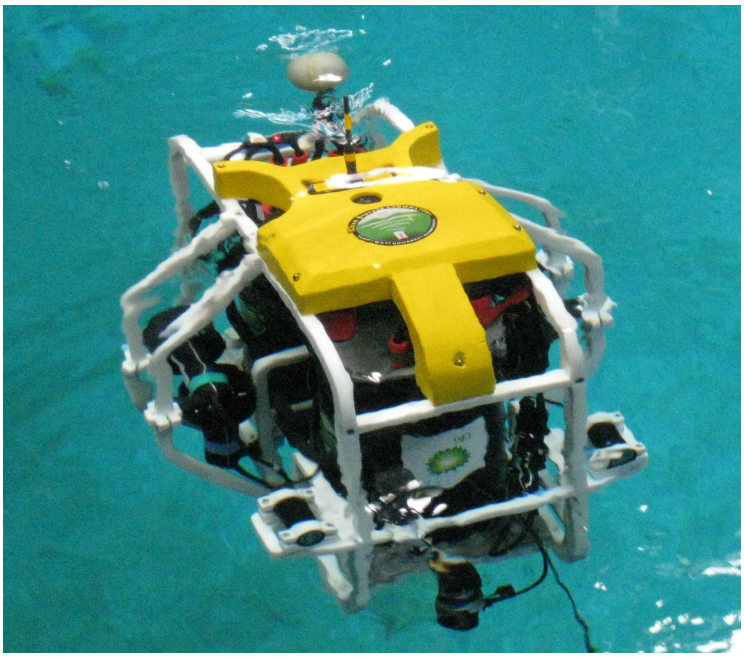

(b)

Figure 1: Different types de robots : (a) robot mobile (UGV), (b) robot sous marin (AUV) Nessie de l'Université d'Heriot Watt

cifiques afin d'aider le drone à naviguer. Nous pouvons citer ici quelques-uns des capteurs illustrés dans la figure 3 essentiels dans le contrôle des drones, l'altimètre et la centrale inertielle (IMU) qui permettent respectivement d'estimer l'altitude du drone et l'orientation, i.e. le lacet (la rotation le long de l'axe Z), le roulis (la rotation le long de l'axe des Y) et le tangage (le

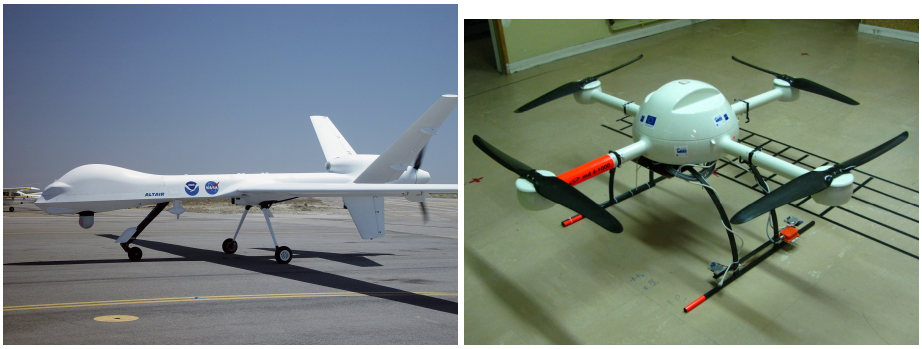

(a) (b)

Figure 2: (a) Drone à voilure fixe (b) quadri-rotor.

long de l'axe X).

(a) (b)

Figure 3: (a) Altimètre (b) centrale inertielle

Les techniques de vision par ordinateur appliquées au domaine de drones sont considérées comme un domaine de recherche difficile tout en connaissant un développement important ces dernières années pour permettre l'autonomie partielle ou totale. Pour ce faire, les méthodes basées vision nécessitent de nombreuses étapes (détection et suivi de caractéristiques, reconstruction 3D, estimation de la pose, ...) souvent très consommatrices de temps de calcul et elles rendent ainsi la contrainte temps-réel très difficile à réaliser. D'autre part, les drones sont souvent sujets à des vibrations qui engendrent des change-

ments brusques dans la séquence d'images et naviguent dans des environnements non structurés. C'est pourquoi les méthodes basées vision sont souvent difficiles à mettre en oeuvre et restent un réel challenge pour la communauté scientifique.

L'estimation de la pose de l'UAV est une tâche importante pour de nombreuses phases de la navigation telles que de décollage et l'atterrissage ([63]), la localisation, l'asservissement visuel, le suivi d'objets, les opérations militaires ([87]), la surveillance du trafic routier et bien évidemment pour le contrôle du drone comme dans [4]. Par rapport à une centrale inertielle traditionnelle, sonar ou des capteurs GPS, la vision apparaît comme un capteur idéal pour la navigation des petits drones ayant des charges limitées en raison de sa taille compacte puisqu'elle peut fournir de nombreuses informations. En conséquence, les méthodes basées sur la vision ont fait l'objet de nombreuses publications [6-8].

Pour rendre autonome un drone, il faut que celui-ci soit capable de manœuvrer vers l'avant ou vers l'arrière, et puisse accomplir les tâches essentielles du décollage et de l'atterrissage [64], ce qui nécessite la connaissance précise de l'attitude et de l'altitude du drone par rapport au plan du sol. Cependant, les systèmes de vision classiques capables de calculer ces paramètres le jour ne peuvent pas estimer ces même paramètres la nuit ou lors de conditions d'éclairage faibles et requièrent donc l'ajout d'autres capteurs pour y parvenir.

Pour rendre le drone autonome, plusieurs solutions ont été proposées par les chercheurs. Certains exploitent un laser pour estimer exclusivement l'altitude. Dans ce travail nous proposons de coupler un laser circulaire avec une caméra afin d'estimer à la fois l'altitude et l'attitude du drone pour effectuer les manœuvres de base : décollage vertical et l'atterrissage.

0.3 Etat de l'art

Ces dernières années, les chercheurs ont mis l'accent sur l'amélioration de l'autonomie des robots aériens. Plusieurs solutions innovantes basées soit sur la vision ou sur une fusion de capteurs miniaturisés ont été proposées.

Pour le décollage vertical et l'atterrissage, des approches basées vision ont déjà été proposées. L'une basée sur les systèmes hybrides avec des résultats de simulations dans [16]. La solution proposée par How et al. dans [45]

(a) (b)

Figure 4: Application de drones lors de sauvetage ou après une catastrophe

permet d'utiliser un matériel commercial en fournissant des informations sur l'altitude. Bien qu'ils résolvent le problème, l'utilisation de ces capteurs est coûteux et nécessite plus de charge utile, ce qui est un frein dans le cas de mini-UAV. Grzonka et al. dans [39] proposent une solution à partir d'un télémètre laser, mais nécessite une carte prédéfinie de l'environnement.

L'utilisation d'une caméra pour estimer les paramètres de navigation du drone est un atout important dans ce type d'applications. En effet, comme les caméras sont de moins en moins couteuses et de plus en plus petites, cela en fait un choix intéressant pour la navigation des robots aériens car elles peuvent aussi fournir d'autres informations. Une question se pose ici, quel type de caméra est le plus intéressant pour la navigation d'un UAV?Il existe principalement trois types de caméras : les caméras perspective, fish-eye et catadioptrique (fig. 2.1).

Mondragon et al. in [66] proposent d'utiliser une seule caméra pour estimer la pose 3D de l'UAV. Cette méthode utilise une caméra perspective calibrée et consiste à suivre un objet de référence. L'estimation de la pose se fait alors par un calcul d'homographie. Cette solution permet de remplacer les méthodes basées GPS souvent inexactes à basse altitude. Toutefois, l'utilisation d'une caméra perspective limite l'application à cause de son faible champ de vue. En effet, le motif est perdu à très basse altitude et cette méthode ne peut donc pas être utilisée lors des phases de décollage et d'atterrissage. La figure 2.2 présente des images d'une vidéo temps réel où le motif est visible car l'altitude est élevée, mais où une partie de l'objet est per-

(a) (b)

(c)

Figure 5: Différent types de caméra: (a) caméra perspective, (b) caméra fish-eye, (c) caméra catadioptrique

due à basse altitude. D'autres méthodes basées vision monoculaire existent dans la littérature. Nous pouvons citer Ettinger et al. dans [33], Todorovic et al. dans [99], Cornall et al. dans [24], Dusha et al. dans [32] qui estiment l'attitude du drone à l'aide d'une détection de l'horizon dans les images. E. Altug et al. [3] ont proposé un système qui comprend deux caméras : une première est à bord de l'UAV et une seconde fixée au sol. Ces deux caméras suivent des marqueurs positionnés sur les deux caméras. Cette méthode exige

donc la fusion de deux différentes données visuelles pour estimer la pose et l'altitude et oblige l'UAV à se trouver toujours à proximité de la caméra au sol.

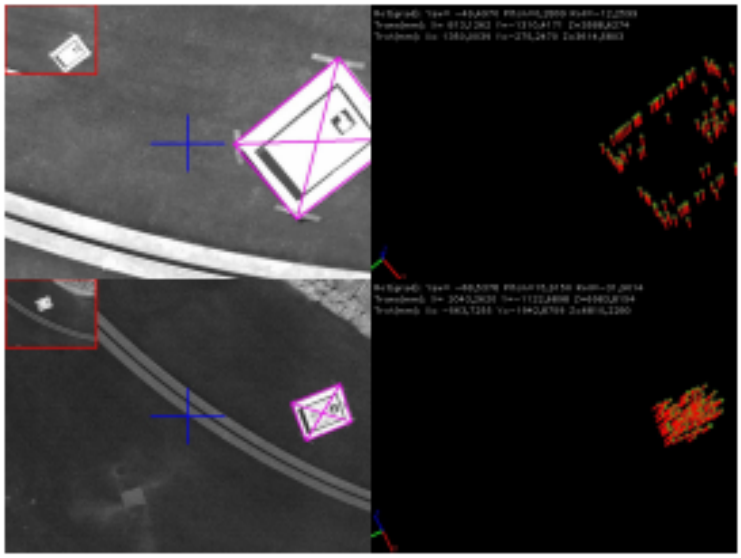

Figure 6: Résultats expérimentaux de la méthode de Mondragon et al. Source: Mondragon et al. [66]

Une autre approche proposée par Demonceaux et al. [28] consiste à utiliser une caméra catadioptrique. Dans cet article, les auteurs proposent d'utiliser des marqueurs naturels comme l'horizon et une caméra catadioptrique. Comme ce type de caméra peut être modélisé par une image sphérique, le principe consiste à détecter un grand cercle (projection de l'horizon) dans l'image sphérique afin de segmenter l'image en deux parties : sol et ciel. Le cercle ainsi déterminé représente l'horizon et permet donc de déduire le roulis et le tangage du drone.

D'autres méthodes int utilisées des marqueurs artificiels. C. De Wagter et. al. [104] ont proposé d'estimer l'attitude du drone à l'aide d'un damier sur le sol. Saripalli et. al. dans [89] et [90] utilisent un câble en mouvement. Rudol et. al. dans [86] ont utilisé plusieurs marqueurs. L'inconvénient de ces approches est qu'elles sont fortement dépendantes des marqueurs et ont donc une zone de déplacement limitée à la visibilité des marqueurs par la caméra embarquée sur l'UAV.

Le choix de la caméra pour effectuer le contrôle du drone est un choix important. Chaque type de caméra a ses avantages et ses inconvénients. Les

caméras perspectives peuvent être considérées comme un bon type de candidat puisqu'elles fournissent une image d'importante résolution. Néanmoins, leur champ de vue est limité, ce qui réduit leur capacité de déplacement pour des méthodes utilisant des marqueurs au sol. C'est pourquoi, augmenter le champ de vue peut s'avérer intéressant. L'utilisation d'une caméra fish-eye peut donc être un bon compris entre résolution de l'image et champ de vue. Mais celle-ci engendre des distorsions importantes dont il faut tenir compte. Pour augmenter encore plus le champ de vue, on peut utiliser une caméra catadioptrique. Mais son utilisation s'avère délicate sur un drone car ces caméras sont encombrantes. De plus, elles ne peuvent pas fournir d'informations sur le sol si elles sont placées sous le drone puisque ces images présentent un trou noir au centre de l'image. Ainsi, les caméras fish-eye semblent être un bon compromis entre champ de vu et résolution de l'image.

L'utilisation d'une seule caméra pour déterminer l'altitude n'est pas une tâche aisée et requièrt l'ajout d'information supplémentaire sur l'environnement ou l'utilisation de deux caméras. La figure 2.3 (a) présente une caméra unique et la figure 2.3 (b) montre des configurations de caméras stéréoscopiques.

Ainsi, des systèmes de vision stéréoscopique ont également été proposés pour estimer l'altitude. Ces systèmes permettent d'obtenir une information 3D métrique de l'environnement et non à l'échelle comme c'est le cas pour la vision monoculaire. Un travail intéressant a été proposé par Eynard et al. en 2010 [34] dans lequel ils présentent une approche temps réel basée sur un système mixte stéréoscopique composé d'une caméra fish-eye et d'une caméra perspective pour l'estimation de l'attitude et du déplacement du drone. Abbeel et al. en 2007 [1] ont utilisé deux paires de caméras stéréoscopiques pour estimer la pose de l'hélicoptère. Cependant, en dépit d'une mise en œuvre intéressante et réussie, la méthode présente plusieurs inconvénients : elle est sensible aux variations de l'environnement puisqu'elle dépend du système stéréoscopique au sol et n'est pas utilisable la nuit.

La solution proposée dans ce travail consiste à associer une micro caméra fish-eye et un projecteur laser. Notre système est léger, précis et moins coûteux que les capteurs commerciaux.

(a)

(b)

Figure 7: Différents types de configurations: (a) mono-caméra, (b) stéréoscopique

0.4 Capteur Fish-eye/Pojecteur laser

Le choix du capteur conditionne bien évidemment l'approche proposée. Dans ce travail, nous souhaitons rendre la phase de décollage et d'atterrissage du drone totalement autonome. Pour ce faire, il est nécessaire de calculer l'altitude du robot et comme nous l'avons vu précédemment, ce paramètre ne peut pas être estimé avec un système mono-caméra sans connaissance a priori sur l'environnement. Il faut donc ajouter un capteur supplémentaire sur le système ou sur le sol. Dans ce travail, nous souhaitons que le drone puisse décoller et se poser dans un environnement inconnu. C'est pourquoi nous ne pouvons retenir une solution basée sur des marqueurs. Ainsi, nous nous sommes intéressés à un système stéréoscopique. Deux systèmes stéréoscopiques

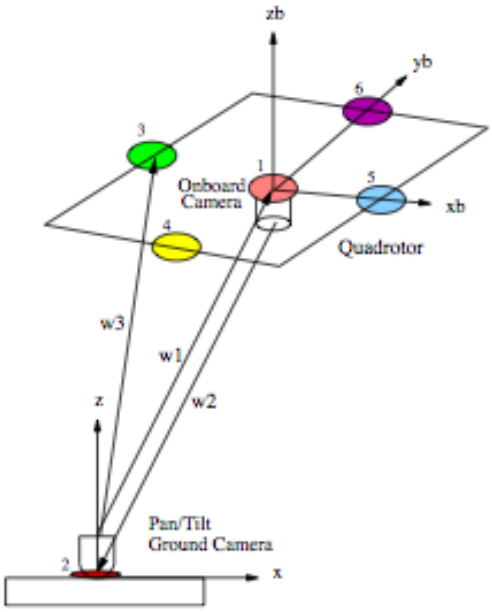

Figure 8: Principe de la méthode de Altug et al. Source: Altug et al. [3].

s'offrent à nous. Le premier dit passif consiste à utiliser deux caméras. Mais cette solution nécessite une phase de mise en correspondance de point parfois très délicate entre les deux images. Ici, nous avons opté pour un système de vision active (fig. 9), consistant dans l'association d'une caméra et d'un projecteur laser.

Il est aussi très important de considérer les différentes possibilités pour construire notre système à savoir, quels types de caméra et de laser devons nous considérer pour notre application? La figure 10 présente notre scénario. A haute altitude, on peut remarquer que le laser sera toujours visible dans l'image même avec une caméra à champ de vue limité. Par contre, dès que le robot volant s'approche du sol, une caméra perspective n'est pas capable de voir le laser et nous devons donc augmenter le champ de vue. C'est pourquoi, nous avons opté pour une caméra fish-eye. Le choix du projecteur laser est aussi important. Deux choix s'offrent à nous. Nous pouvons utiliser une grille de point ou un cercle. Comme dans cette application, nous ne souhaitons pas reconstruire la surface du sol et que nous recherchons juste la pose du drone, il est inutile d'utiliser une grille de point. De plus, on peut montrer que pour estimer la pose (comme pour le calibrage de caméra) il est plus robuste

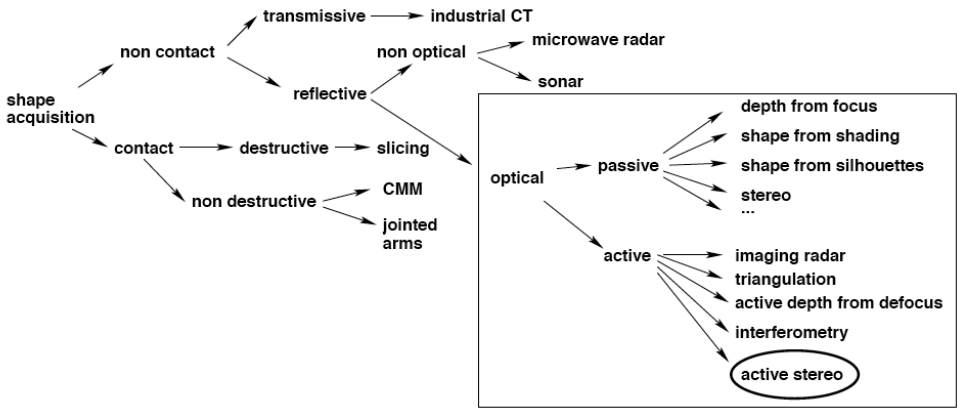

Figure 9: Classification des méthodes d'acquisition. Source: Joaquim Salvi's VIBOT lecture notes on 3D reconstruction by laser triangulation

d'utiliser des cercles que des points. Nous avons donc opté pour un laser circulaire.

0.5 Modélisation mathématique

Dans cette section, nous nous intéressons à la modélisation mathématique du problème. Notre capteur est décrit figure 11. Notons W le repère monde, C le repère caméra, L le repère du laser. Ces deux repères sont distants d'une translation (baseline) b. Pour simplifier les équations, nous supposerons les deux repères alignés ($R = I$) et $b = (b_1, b_2, b_3) = (b_1, 0, 0)$. Il s'agit d'estimer la normale n du plan π et la distance de ce plan relativement au repère C. La caméra fish-eye est elle considérée comme une caméra sphérique pour s'affranchir de ses distorsions et utiliser les propriétés de la géométrie projective [108]. Dans ce travail, nous avons proposé deux solutions pour résoudre ce problème. Une solution analytique qui recherche le lien entre la déformation de l'image du laser et les mesures d'altitude et d'attitude du drone.

0.5.1 Modélisation analytique

Notons X_L, X_C et X_s respectivement les coordonnées d'un point $3D$ dans les repères du Laser, de la Caméra et de la Sphère. Soit π le plan du sol

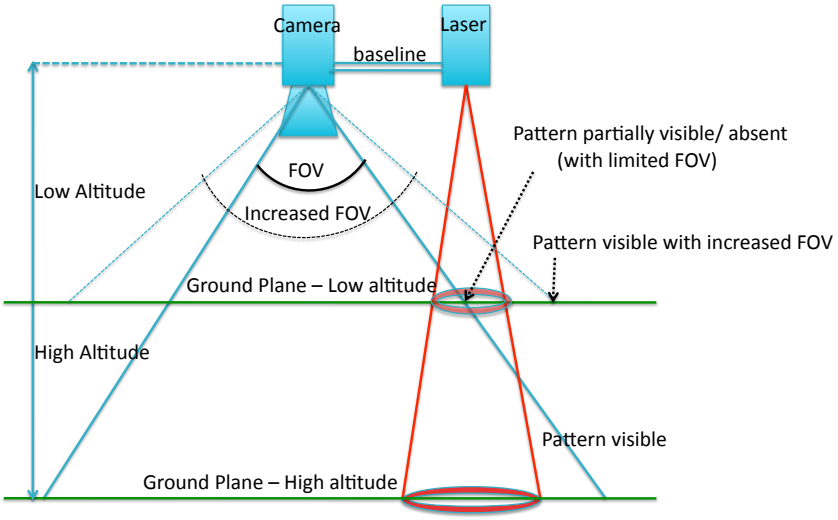

Figure 10: Avantage d'un large champ de vue dans notre application.

d'équation

$$X_L.\overrightarrow{n} + d = 0. \tag{1}$$

dans le repère du Laser. $\overrightarrow{n}$ et d correspondent respectivement à l'attitude du capteur et à sa hauteur relativement au sol. Ce sont ces valeurs que nous recherchons par la suite. En pratique, nous disposons de l'image du laser sur la caméra sphérique. Il s'agit de déterminer comment $\overrightarrow{n} = [n_1, n_2, n_3]^T$ et d modifient cette image.

La projection du laser sur le sol définit un cône de révolution d'équation :

$$x_L^2 + y_L^2 = z_L^2 tan^2\theta, \tag{2}$$

où θ est l'angle d'ouverture du laser supposé connu par calibrage. Les points 3D définis dans le repère du Laser ont pour équation $X_C = RX_L + b$ dans le repère caméra. (R et b sont eux aussi connus par calibrage intrinsèque). Pour simplifier les calculs, nous supposons par la suite que $R = I$ et $b_1 \neq 0, b_2 = b_3 = 0$. Nous avons donc :

$$X_L = X_C - b. \tag{3}$$

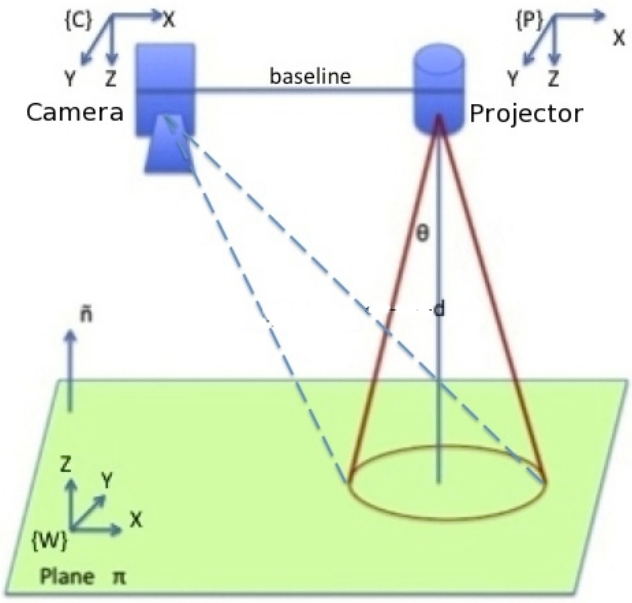

Figure 11: Modélisation du capteur.

Ainsi, le plan π a pour équation dans le repère caméra :

$$(X_C - b).\overrightarrow{n} + d = 0, \tag{4}$$

Soit :

$$x_C n_1 - b_1 n_1 + y_C n_2 + z_C n_3 + d = 0 \tag{5}$$

Or, la relation entre le repère de la sphère et celui de la caméra est donnée par un scalaire λ:

$$X_s = \lambda X_c \tag{6}$$

où

$$\begin{cases} x_s = \lambda x_c \\ y_s = \lambda y_c \\ z_s = \lambda z_c \end{cases}$$

Et par substitution dans l'équation (3.6) on déduit :

$$x_s n_1 - \lambda b_1 n_1 + y_s n_2 + z_s n_3 + \lambda d = 0 \tag{7}$$

Par conséquent,

$$\lambda = \frac{-(x_s n_1 + y_s n_2 + z_s n_3)}{d - b_1 n_1} \tag{8}$$

De plus, d'après les équations (3.3) et (3.2), la conique a pour équation dans le repère caméra :

$$(x_c - b_1)^2 + (y_c - b_2)^2 - (z_c - b_3)^2 tan^2\theta = 0 \tag{9}$$

Soit

$$\begin{array}{c} (x_s - \lambda b_1)^2 + y_s^2 - z_s^2 tan^2\theta = 0 \\ x_s^2 + \lambda^2 b_1^2 - 2\lambda b_1 x_s + y_s^2 - z_s^2 tan^2\theta = 0 \end{array} \tag{10}$$

dans le repère de la sphère. Enfin en substituant la valeur de λ dans (3.11), on obtient :

$$\begin{array}{l} d^2 x_s^2 + [n_2^2 b_1^2 + (d - b_1 n_1)^2] y_s^2 \\ +[n_3^2 b_1^2 - (d - b_1 n_1)^2 tan^2\theta] z_s^2 + [2 b_1 n_2 d] x_s y_s \\ +[2 b_1 n_3 d] x_s z_s + [2 b_1^2 n_2 n_3] y_s z_s = 0 \end{array} \tag{11}$$

Cette équation caractérise l'image du laser sur la sphère en fonction de l'altitude d et de l'attitude $\overrightarrow{n}$. Il suffit de comparer cette équation avec la véritable image fournie par l'image sphérique pour en déduire ces paramètres.

Considérons l'image sphérique du laser, tous ses points $(x_s, y_s, z_s) \in \mathcal{S}^2$ vérifient l'équation d'une quadrique du type (figure 12):

$$A x_s^2 + B y_s^2 + C z_s^2 + 2D x_s y_s + 2E x_s z_s + 2F y_s z_s = 0, \tag{12}$$

où les six coefficients peuvent être déterminés par RANSAC.

Nous avons donc en comparant (3.15) et (3.24)

$$\frac{B}{A} = \frac{[n_2^2 b_1^2 + (d - b_1 n_1)^2]}{d^2} \tag{13}$$

$$\frac{C}{A} = \frac{[n_3^2 b_1^2 - (d - b_1 n_1)^2 tan^2\theta]}{d^2}$$

(14)

$$\frac{D}{A} = \frac{b_1 n_2}{d} \tag{15}$$

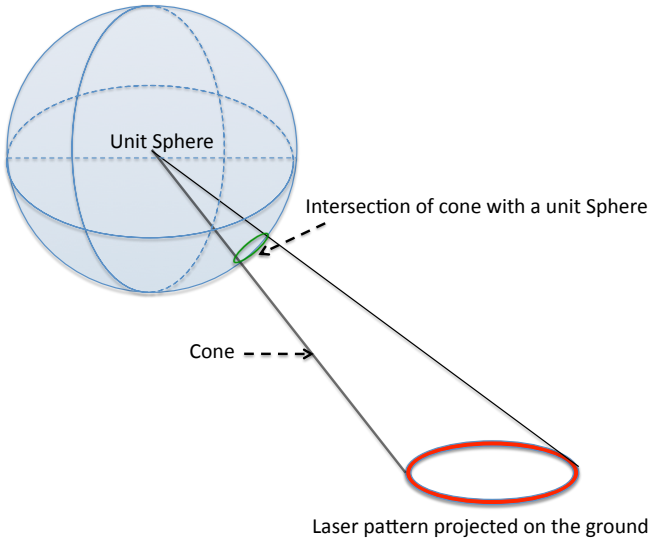

Figure 12: Intersection entre la sphère unitaire et un cône.

$$\frac{E}{A} = \frac{b_1 n_3}{d} \tag{16}$$

$$\frac{F}{A} = \frac{b_1^2 n_2 n_3}{d^2} \tag{17}$$

$$\frac{B}{A} = \frac{n_2^2 b_1^2}{d^2} + (1 - \frac{b_1 n_1}{d})^2 \tag{18}$$

$$\frac{B}{A} = (\frac{D}{A})^2 + (1 - \frac{b_1 n_1}{d})^2 \tag{19}$$

Posons $\frac{b_1 n_1}{d} = G$, G est la solution de :

$$\frac{B}{A} = (\frac{D}{A})^2 + (1 - G)^2, \tag{20}$$

soit :

$$G = (1 \pm \sqrt{\frac{B}{A} - (\frac{D}{A})^2}) \tag{21}$$

A partir de (3.27), (3.28), nous avons :

$$G^2 + (\frac{D}{A})^2 + (\frac{E}{A})^2 = (\frac{b_1}{d})^2. \tag{22}$$

Ainsi, l'altitude a pour formule :

$$d^2 = \frac{(b_1 * A)^2}{(G * A)^2 + D^2 + E^2} \tag{23}$$

et l'attitude $\overrightarrow{n} = (n_1, n_2, n_3)^T$ vérifie :

$$\begin{array}{l} n_1 = \frac{Gd}{b_1}, \\ n_2 = \frac{D}{A}\frac{d}{b_1}, \\ n_3 = \frac{E}{A}\frac{d}{b_1}. \end{array} \tag{24}$$

Notons qu'il existe deux solutions pour G et donc pour d et $\overrightarrow{n}$. Ces deux solutions correspondent aux deux plans d'intersection entre les deux coniques définies à partir de la caméra et du laser. En pratique, nous retenons la solution pour laquelle $\overrightarrow{n}$ définit le plan le plus horizontal par rapport à la *baseline* entre la caméra et le laser.

0.5.2 Modélisation géométrique

Le projecteur laser définit de façon naturelle un cône. De même, l'ellipse formée sur le sol par le projecteur laser définit un cône dont le sommet est situé au centre de la caméra sphérique (fig 13). Déterminer la position de la caméra revient à calculer l'intersection entre ces deux cônes.
Notons $\mathcal{C}$ (respectivement $\mathcal{D}$) le cône de sommet D (reps. de sommet L). A l'aide de $\mathcal{C}$ et $\mathcal{D}$, nous pouvons définir une famille de quadrique $\mathcal{Q}$:

$$\mathcal{Q}_x = x\mathcal{C} + (1-x)\mathcal{D} \tag{25}$$

De façon générale, une quadrique est de rang $\leqslant 4$. Elle est de rang 3 si cette quadrique est un cône ou un cylindre (elliptique, hyperbolique ou parabolique). Elle est de rang 2 lorsqu'elle représente l'intersection de deux plans ou deux plans parallèles. Enfin, elle est de rang 1 si elle représente un plan. Dans le cas de (3.48), $\mathcal{Q}$ est de rang 3 lorsque $x = 1$ ou $x = 0$, $\mathcal{Q}$ est alors le cône $\mathcal{C}$ ou $\mathcal{D}$. Lorsque $\mathcal{Q}_x$ est de rang 2, elle définit les deux plans d'intersection

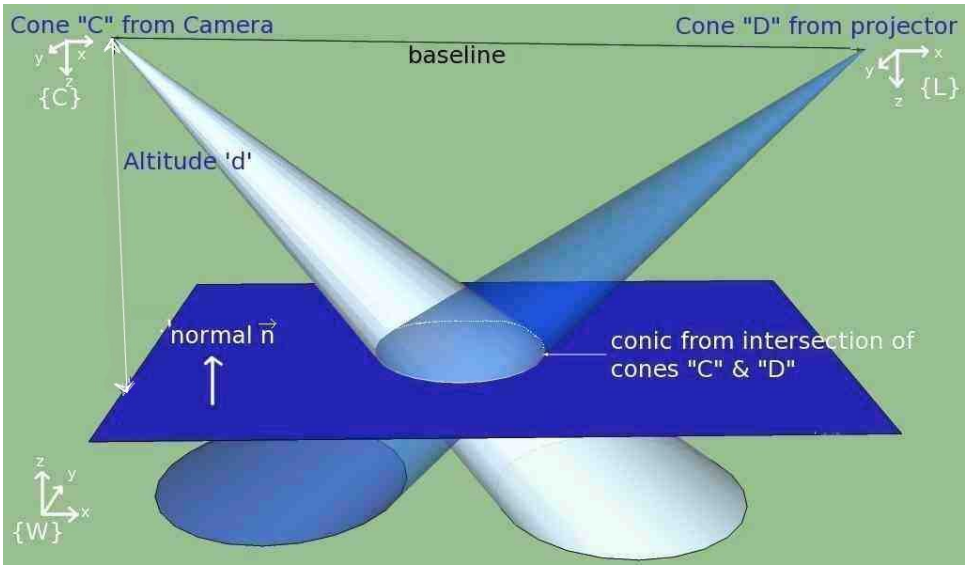

Figure 13: Représentation de l'approche géométrique

entre les deux cônes $\mathcal{C}$ et $\mathcal{D}$.
Par conséquent, pour retrouver l'équation du plan du sol, il suffit de déterminer x pour que $\mathcal{Q}$ soit de rang 2. Pour ce faire, on procède comme suit :

1. Calculer les racines $P(x) = \det \mathcal{Q}_x$. P est un polynôme de degré 4 et admet donc au plus 4 racines réelles. Deux sont évidentes, $x = 0$ et $x = 1$. On peut montrer que les deux autres sont en fait identiques puisque P admet une racine double. Cette dernière solution x_0 représente l'intersection entre les deux cônes.

2. Comme $\mathcal{Q}_{x0}$ est de rang 2, on peut décomposer $\mathcal{Q}_{x0}$ sous la forme :

$$\mathcal{Q}_{x0} \sim VU^t + UV^t = (V\ U) \begin{pmatrix} U^t \\ V^t \end{pmatrix} \tag{26}$$

   où U et V sont en fait les deux plans d'intersection des deux cônes.

3. Le plan du sol π est le plan pour lequel les sommets des deux cônes C et L se retrouvent du même coté.

Montrons désormais comment obtenir 3).
Comme $\mathcal{Q}_{x0}$ est de rang 2, on peut écrire :

$$Q = (A\ B \vdots \vdots)\text{diag}(s_1, s_2, 0, 0) \begin{pmatrix} \pm A^T \\ \pm B^T \\ \cdots \\ \cdots \end{pmatrix} \tag{27}$$

où s_1 et s_2 sont les deux valeurs singulières associées aux vecteurs singuliers A et B. Ainsi, on peut écrire :

$$Q = \pm(s_1 AA^T - s_2 BB^T) \tag{28}$$

U et V doivent donc satisfaire :

$$\begin{aligned} UV^T + VU^T &\sim Q \\ &\sim s_1 AA^T - s_2 BB^T \end{aligned} \tag{29}$$

Les deux plans sont donc des combinaisons des vecteurs singuliers A et B :

$$\begin{aligned} U &= uA + B \\ V &= vA + B \end{aligned} \tag{30}$$

D'après (3.52):

$$UV^T + VU^T = (uA+B)(vA+B)^T + (vA+B)(uA+B)^T \sim s_1 AA^T - s_2 BB^T \tag{31}$$

Soit :

$$\begin{aligned} &2uvAA^T + 2BB^T + (u+v)AA^T + (u+v)BB^T \\ &\neg\dagger \sim s_1 AA^T - s_2 BB^T \end{aligned} \tag{32}$$

d'où

$$u + v = 0 \tag{33}$$

et donc :

$$v = -u \tag{34}$$

En substituant dans l'équation précédente, nous obtenons :

$$-2u^2AA^T + 2BB^T \sim s_1AA^T - s_2BB^T \tag{35}$$

c'est-à-dire :

$$u^2 = \frac{s_1}{s_2} \tag{36}$$

Finalement, les deux plans ont pour équations :

$$U = \sqrt{\frac{s_1}{s_2}}A + B \tag{37}$$

$$V = -\sqrt{\frac{s_1}{s_2}}A + B \tag{38}$$

Par la suite, nous pouvons déduire les paramètres d'altitude et d'attitude par les formules suivantes :

$$Roulis = (\frac{V(3)}{\sqrt{V(1)^2 + V(3)^2}}) * \frac{180}{\pi} \tag{39}$$

$$Tangage = (\frac{V(3)}{\sqrt{V(2)^2 + V(3)^2}}) * \frac{180}{\pi} \tag{40}$$

et

$$Altitude = abs(V(4)/\sqrt{V(1)^2 + V(2)^2 + V(3)^2}) \tag{41}$$

Ainsi, nous avons développé deux méthodes permettant d'estimer le roulis, le tangage et l'altitude d'un drone à l'aide d'un capteur fish-eye et d'un projecteur laser circulaire. Par la suite, nous allons valider ces méthodes.

0.6 Résultats expérimentaux

Nous avons validé nos méthodes sur des données de synthèse et des séquences réelles. Dans le cas des données réelles, nous avons comparé nos résultats avec une centrale inertielle et un capteur de pression pour avoir une vérité terrain. Le capteur expérimental est composé d'une caméra μEye munie d'une optique fish-eye $(Fujininon1 : 1.4/1.8mm)$ et d'un projecteur laser Lasiris

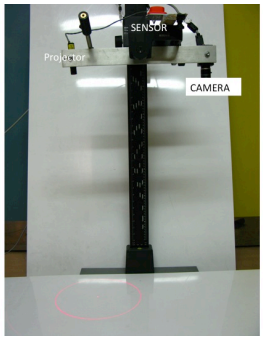

(a)

(b)

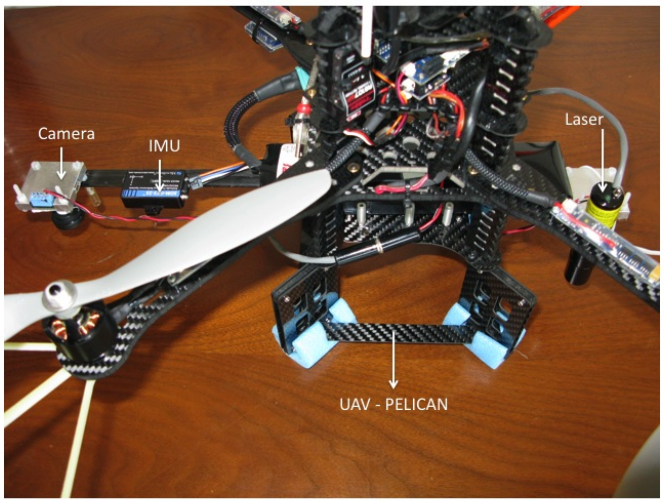

(c)

Figure 14: Notre système (a) sur un bras, (b) un UAV microdrone (c) un Pelican.

$(classII, poweroutput < 1mW, wavelength : 400 - 700nm)$.

La figure 14 montre notre système monté sur un bras, sur un drone Microdrone md-4-1000 et sur un Pelican d' Ascending Technologies.

0.6.1 Approche analytique

L'approche analytique a été validée sur des données de synthèse pour en vérifier la robustesse ainsi que sur des séquences réelles. Dans le cas synthétique, nous avons donc simulé notre capteur sous Matlab (figure 15).

Le tableau 5.1 présente des résultats dans le cas idéal où aucune donnée n'est bruitée. Le tableau 5.2 présente des exemples d'estimation dans le cas où

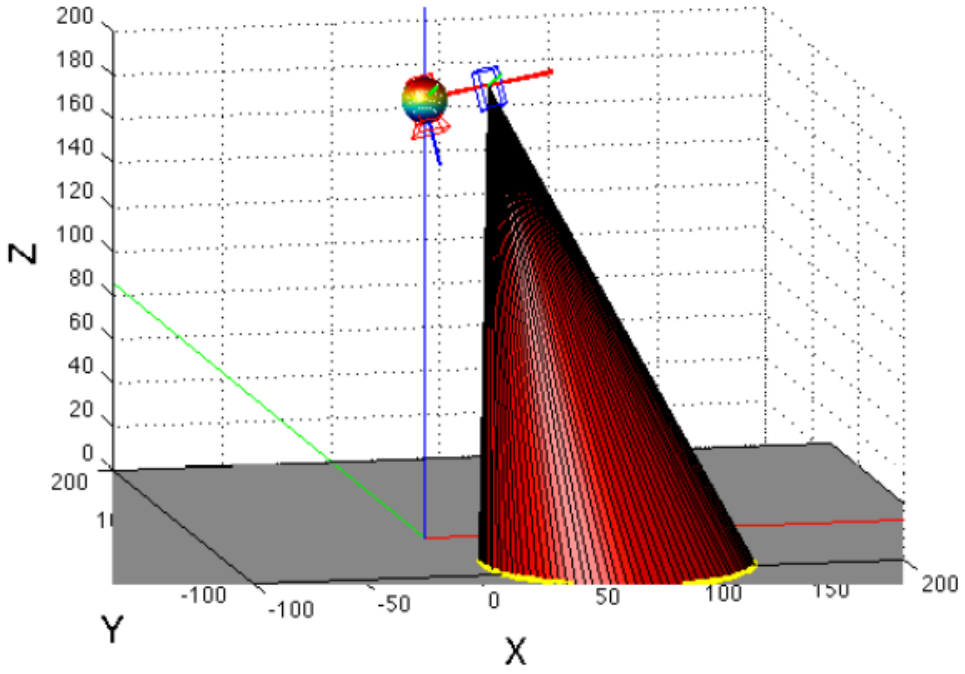

Figure 15: Représentation de la simulation

les points de l'image fish-eye ont été bruités avec un bruit blanc d'écart type 0.5. Ces données montrent une erreur moyenne dans le cas idéal de $4,7$ cm pour l'altitude, de $1,02°$ pour le roulis et de $0.53°$ pour le tangage. Dans le cas bruité, les erreurs augmentent légèrement, $7,8$ cm pour l'altitude, $1,23°$ pour le roulis et $1.26°$ pour le tangage. Cette robustesse de la méthode s'explique par le RANSAC dans la phase d'estimation des coefficients de la quadrique (3.24). La figure 16 montre le comportement de la méthode proposée pour une pose simulée de l'UAV à 150 cm d'altitude, un roulis $6°$ et un tangage $10°$ en fonction du bruit introduit sur les points de la caméra.

Les premiers tests réels ont été réalisés à partir de séquences d'images acquises par notre capteur tenu à la main (Figure 17) dont la caméra fish-eye est séparée d'environ 30 cm du laser. Sur le dispositif, nous avions ajouté une centrale inertielle et un télémètre pour pouvoir comparer nos résultats avec une vérité terrain. Les résultats sont présentés figure 18. Les erreurs moyennes sont respectivement de $7,14$ cm pour une altitude variant entre 50 cm et 2 m, de $2,03°$ en roulis et de $1,65°$ en tangage. Enfin, nous avons embarqué le système sur un quadrirotor (Figure 14 (c)). Les valeurs obtenues sont comparées avec un télémètre et une centrale inertielle et présentées figure 19.

Table 1: Cas synthétique

	Altitude (m)	Roulis (deg)	Tangage (deg)
Vérité terrain	1	0	0
Valeur estimée	1	0	0
Vérité terrain	2	15	1
Valeur estimée	2	13.02	0.03
Vérité terrain	2	0	10
Valeur estimée	1.98	0.02	9.19
Vérité terrain	1	16	24
Valeur estimée	1.07	14.32	22.16
Vérité terrain	1	30	0
Valeur estimée	0.9	30.16	0.07
Vérité terrain	1	5	9
Valeur estimée	1.04	30.16	0.07
Vérité terrain	1	30	12
Valeur estimée	0.901	26.640	11.980

Table 2: Cas synthétique bruité avec un bruit blanc d'écart type 0.5

	Altitude(m)	Roulis (deg)	Tangage (deg)
Vérité terrain	1.2	0	0
Valeur estimée	1.14	0	0
Vérité terrain	7	0	0
Valeur estimée	6.34	0	0
Vérité terrain	2	0	1
Valeur estimée	1.99	0.02	0.05
Vérité terrain	8	12	10
Valeur estimée	7.68	13.56	7.19
Vérité terrain	1	30	10
Valeur estimée	0.93	27.38	10.71
Vérité terrain	2	20	15
Valeur estimée	1.89	17.38	13.71
Vérité terrain	2	12	30
Valeur estimée	1.91	10.15	26.93

0.6.2 Approche géométrique

Comme pour l'approche analytique, nous avons validé dans un premier temps l'approche géométrique sur des données de synthèse. Le tableau 5.4 présente le comportement de la méthode sur différentes mesures avec des données non bruitées ou bruitées par un bruit blanc d'écart type 0.5. La figure 20 montre l'erreur d'estimation des trois paramètres estimées en fonction du bruit blanc

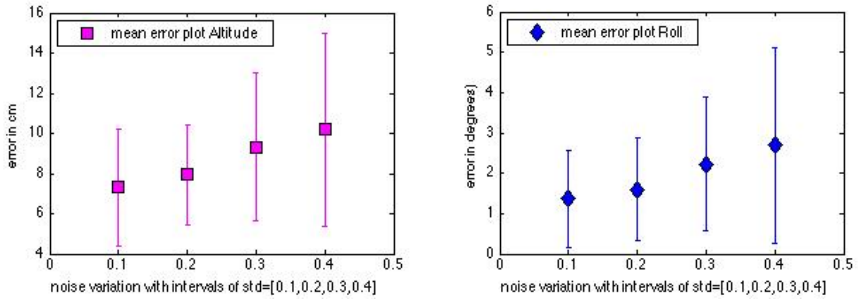

(a)

(b)

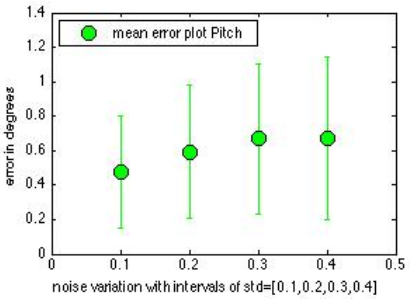

(c)

Figure 16: Erreur moyenne sur le calcul de l'altitude (a), du roulis (b) et du tangage (c) en fonction du bruit dans l'image.

introduit dans le cas d'un capteur situé à 2 mètres du sol avec un roulis de 11 degrés et un tangage de 7 degrés. L'erreur augmente lorsque le bruit augmente mais reste relativement précise.

La figure 21 présente l'estimation de l'altitude et de l'attitude avec la méthode géométrique dans le cas de faible luminosité et d'environnement non texturé. Ces résultats montrent que les erreurs d'estimation sont faibles à basse altitude mais augmente à plus haute altitude. De façon similaire, nous observons que les erreurs sont faibles lorsque le drone est sujet à de petits angles de roulis et tangage mais augmentent lorsque ces angles sont plus importants. Par exemple, pour des angles supérieurs à 35°, l'erreur est supérieure à 3°.

Ainsi, nous avons observé que l'approche géométrique était capable d'estimer le roulis, le tangage et l'altitude d'un drone. Les résultats ont montré que pour des angles inférieurs à 35°, notre méthode estimait ces paramètres avec une bonne précision et rivalisait avec les solutions commerciales (centrale inertielle + altimètre). Cette solution proposée convient donc pour les phases de

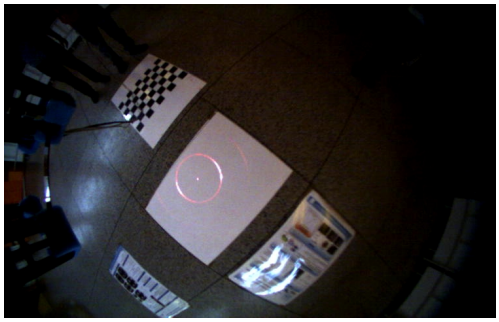

(a)

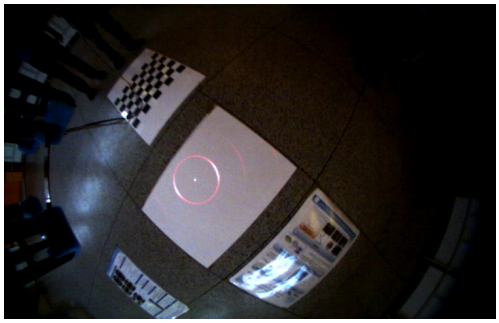

(b)

Figure 17: Images issues d'une séquence réelle.

décollage et d'atterrissage du drone dans le cas d'environnement non texturé et soumis à de faibles conditions de luminosité.

0.6.3 Comparaison entre la méthode géométrique et analytique

La figure 22 présente les résultats de l'estimation de l'attitude et de l'altitude basée sur les approches analytiques et géométriques ainsi que les mesures obtenues par la centrale inertielle et d'un capteur de pression. Le tableau 5.5 montre que la solution géométrique estime de façon plus précise l'attitude et l'altitude que la solution analytique.

0.7 Conclusion

Ce travail a permis de montrer que nous pouvions utiliser un système hybride muni d'une caméra fish-eye et d'un projecteur laser pour estimer le

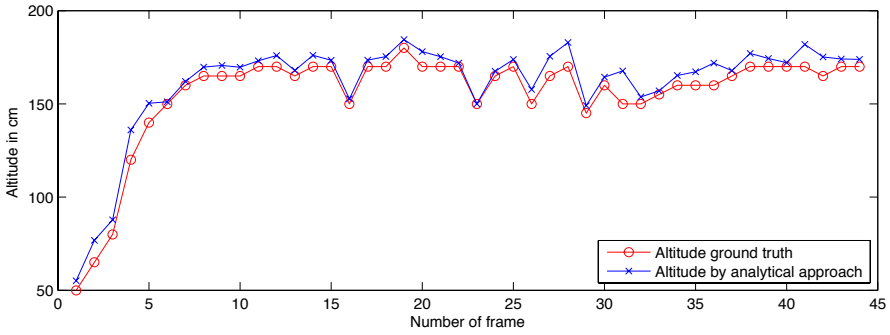

(a)

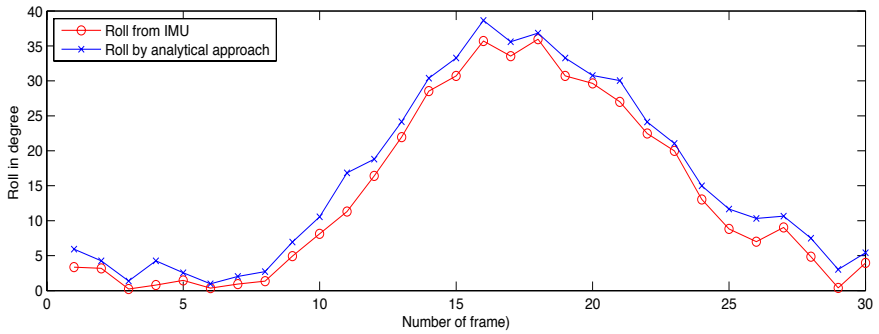

(b)

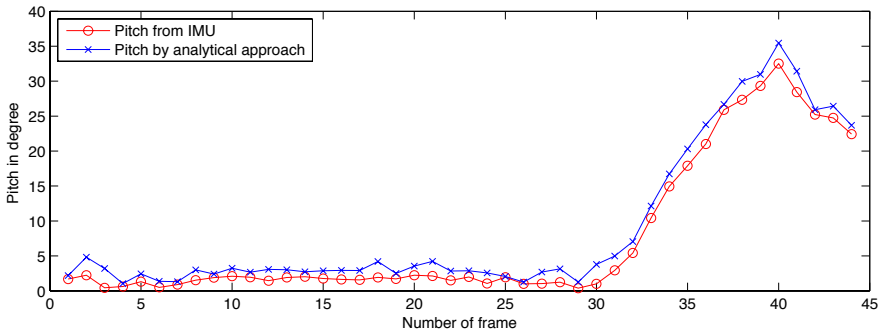

(c)

Figure 18: Estimation de l'altitude, du roulis et du tangage à l'aide de notre capteur tenu à la main.

roulis, le tangage et l'altitude d'un drone durant les phases de décollage et d'atterrissage. Les deux approches proposées aboutissent à des solutions rapides qui peuvent fonctionner en ligne. De plus, ces méthodes peut être utilisées même dans le cas de faible luminosité.

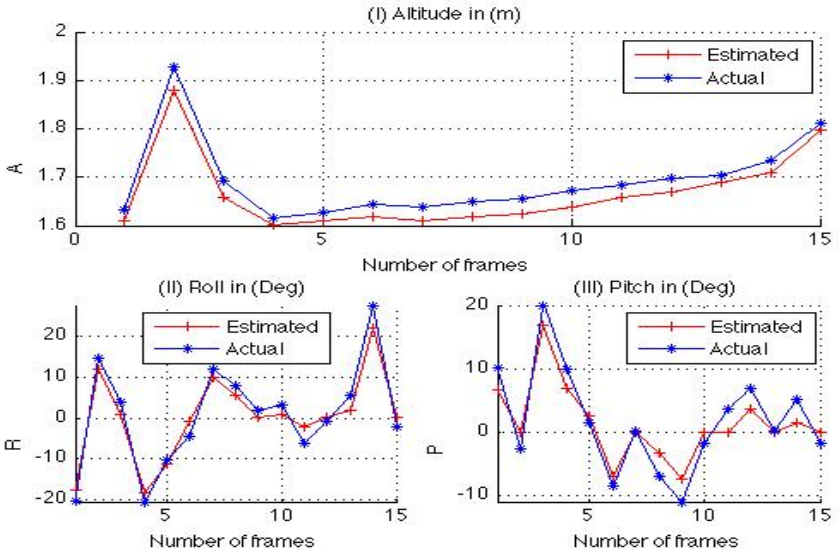

Figure 19: Estimation de l'altitude, du roulis et du tangage à l'aide de notre capteur embarqué sur un quadrirotor.

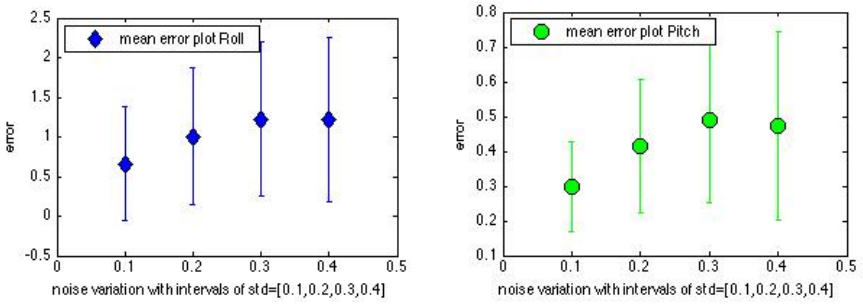

(a) (b)

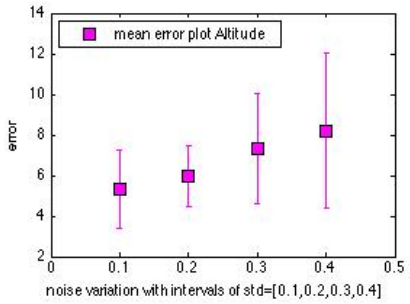

(c)

Figure 20: Erreur moyenne en fonction du bruit (a) roulis, (b) tangage (c) altitude.

Table 3: Résultats synthétiques sans bruit et avec un bruit blanc d'écart type 0.5.

	Roulis (deg)	Tangage (deg)	Altitude (in cm)
Réel	0	0	60
Estimaté	2.68	2.26	60.00
Bruité	2.69	2.16	59.99
Réel	0	1	60
Estimaté	2.82	1.05	59.97
Bruité	2.78	0	59.97
Réel	1	0	60
Estimaté	3.69	2.27	60.05
Bruité	3.67	2.10	60.05
Réel	5	4	60
Estimaté	5.92	4.08	59.70
Bruité	5.88	4.04	59.71
Réel	5	4	110
Estimaté	5.99	4.09	110.31
Bruité	5.96	4.06	110.32
Réel	10	12	200
Estimaté	12.33	12.55	209.07
Bruité	12.36	12.57	209.08
Réel	13	6	1000
Estimaté	13.02	6.27	1032.28
Bruité	14.02	6.77	1068.50
Réel	30	25	100
Estimaté	30.09	27.40	105.12
Bruité	30.19	27.43	105.35
Réel	30	25	1000
Estimaté	31.61	28.38	1160.09
Bruité	31.71	28.40	1198.34

Table 4: RMSE de nos méthodes.

	RMSE Solution algébrique	**RMSE Solution géométrique**
Roulis	2.03°	0.88°
Tangage	1.65°	0.43°
Altitude	7.14 cm	3.91 cm

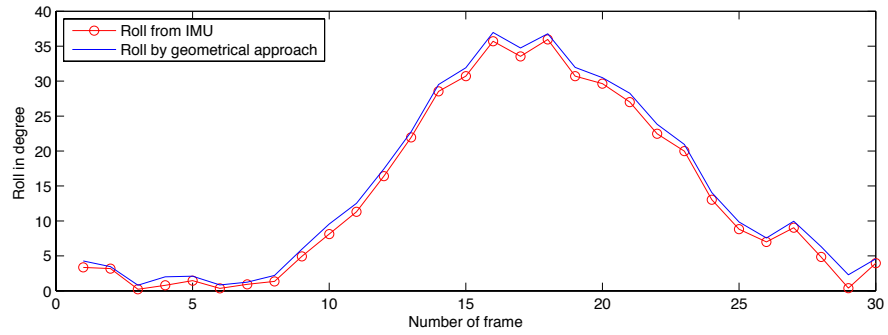

(a)

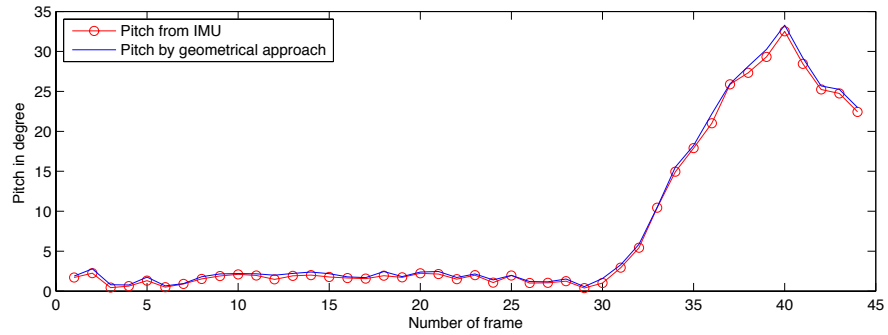

(b)

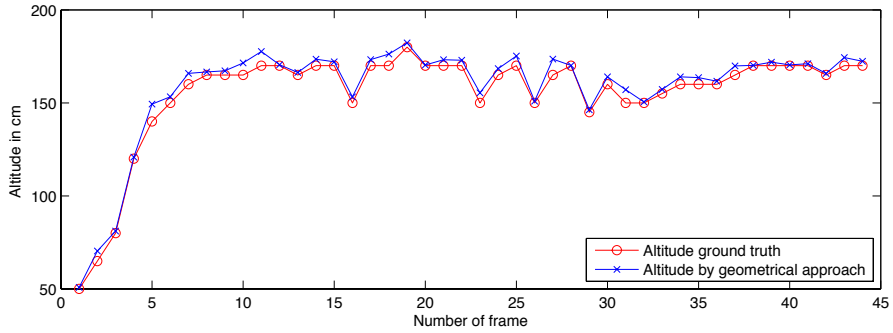

(c)

Figure 21: Comparison de nos résultats avec une centrale inertielle en rouge, l'approche géométrique en bleu (a) Roulis (b) Tangage (c) Altitude.

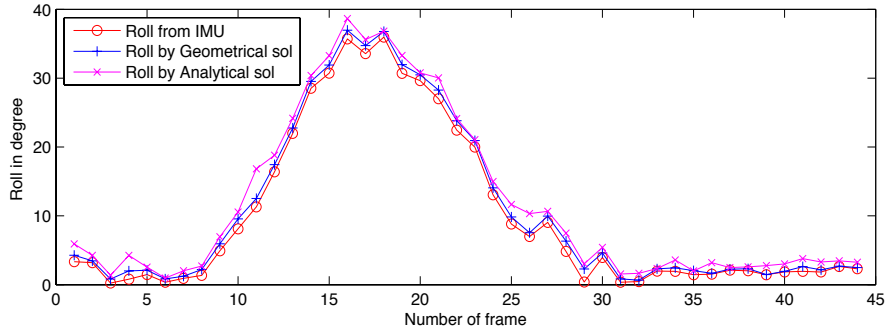

(a)

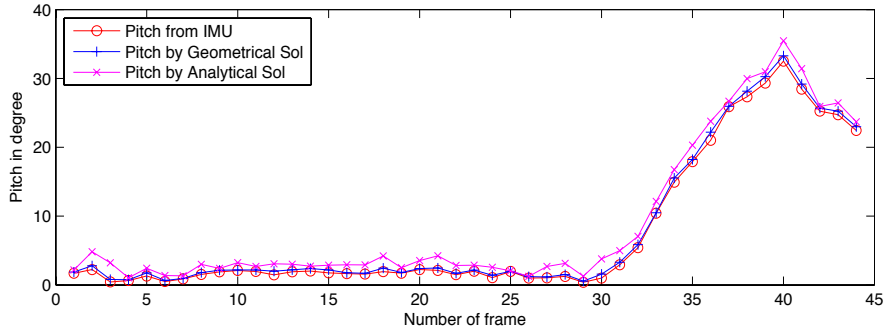

(b)

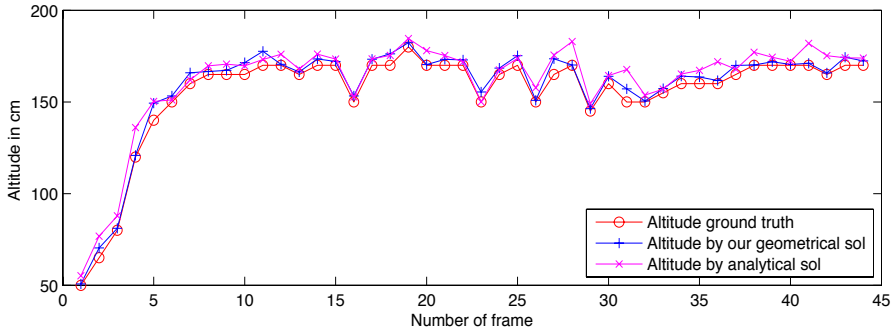

(c)

Figure 22: Comparaison de nos résultats avec une centrale inertielle en rouge, l'approche analytique est en magenta , l'approche géométrique en bleu (a) Roulis (b) Tangage (c) Altitude.

Chapter 1

Introduction

Advancements in engineering led to the miniaturisation of the sensors and many other mechanical parts that have brought in dramatic changes in our lives. In the early era of robotics the word robot always projected a picture of large mechanical parts with a large robot manipulator on its own. Today in there are so many robots to cater different needs of our day today life. Thanks to the advancements in artificial intelligence that these robots have jumped to a higher level of operation, where there is very little or no human intervention and are autonomous in nature. Due to large number of these kinds of robots available today, they have been classified in mainly the following main 3 groups: One that operate on the land ground called " Unmanned Ground Vehicles" (UGVs), second those operate in the water called " autonomous underwater vehicles" (AUVs) and the third one is the one that operated in the air called " Unmanned Aerial Vehicles" (UAVs).

We will trace a part of the first two kinds in brief but will mainly focus on the unmanned aerial vehicles. We can see some of the UGVs and AUVs in the figure 1.1. All these robots are autonomous and serve one or the other purposes they are built for. Today there are several interesting projects that have been realised for practical use, of which we cite a few of them to have a better picture about them. The DARPA's autonomous car [49] later being modified by several academic and industrial [57] research organisations that can navigate in the crowded streets and avoid the obstacles and follow the traffic laws to transport people from a start to the destined end location. Similar are useful application oriented AUVs for the inspection of the hull of large ships [105] to avoid any disaster in future due to wear and tear, similar is the application

(a)

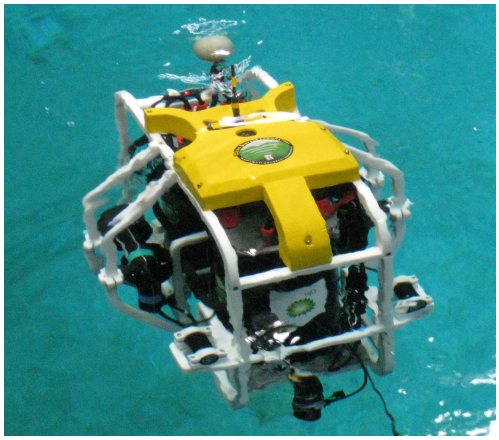

(b)

Figure 1.1: Different types of robots: (a) Unmanned Ground Vehicle (UGV), (b) Autonomous Underwater Vehicle (AUV) Nessie from Heriot Watt University

of the sub sea to deep sea petroleum pipelines inspection to avoid the oil spill disasters [77] that the world and especially the marine lives have experienced. In the following paragraph we discuss on the interest for and types of UAVs.

Since the early age of almost many people are always fascinated by the ability of any object to fly in the air. Psychologist relate this to the fact that humans are always intrigued by the ability to fly, since that is what we humans can not achieve on our own physical built. Henceforth, led the humans to build machines that can make them fly and built aeroplanes and helicopters. Then when we humans entered the field of robotics it was but obvious for the desire of unmanned aerial robots since humans had already mastered their skills for aeroplanes and helicopters. The need for smaller and smaller aerial vehicles led to the complete field of unmanned aerial vehicles, which are small and can

(a) (b)

(c)

Figure 1.2: Different types of aerial robots: (a) Fixed wing UAV, (b) Fixed wing UAV of conventional design aeroplane, (c) Rotor based UAV

easily manoeuvre to address the various application specific needs. Figure 1.2 represents the types of UAVs: one the fixed wing and the latter one rotor based UAVs. With the advent of the need specific UAVs it was desirable to have UAVs that can manoeuvre in a limited space with the capability to hover at the same coordinate for longer time. This capability of hovering at a single coordinate provided with solution to lot of engineering problems and drew lot of interest too. The fixed wing UAVs lacked the ability to hover at the same coordinate due to its nature of build. In turn the rotor based UAVs could and thus our interest for rotor based UAVs was obvious and important.

Figure 1.3 represents the various types of rotor based UAVs. The major interest in rotor based UAVs is due to its ability to operate in a limited space, its ability to perform vertical take off and landing (VTOL), its ability to hover at the same coordinate for a long time. These above stated abilities make it suitable for various need specific applications like monitoring traffic to avoid the bottle neck congestion at the entry and exit of any city, inspection purposes

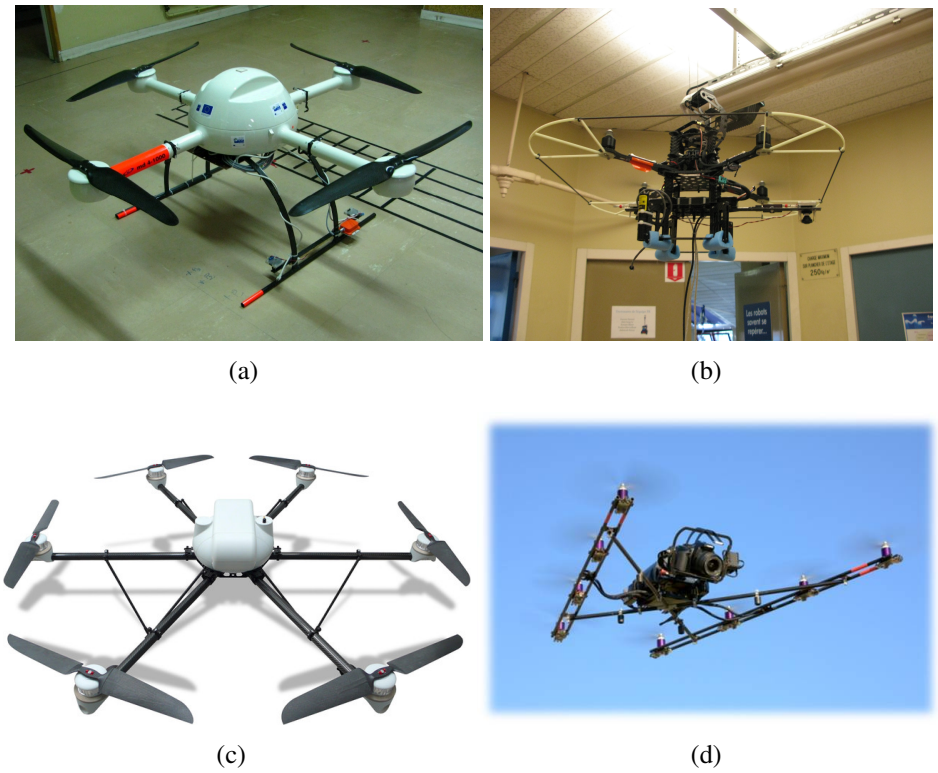

(a) (b)

(c) (d)

Figure 1.3: Different types of rotor based UAVs: (a) Outdoor application large UAV- microdrone, (b) Indoor application quadrotor UAV- Pelican, (c) Six rotor based 'hexarotor' - AR-200, (d) Eight rotor based 'Octarotor' - Falcon.

including the bridges without actually disrupting the traffic and also with a higher precision. UAVs are also help in inter discipline research as used in the monitoring the marine lives in seas by collecting the samples from whales from the water expelled by them using UAVs. UAVs are utilised in so many different sectors ranging from inspection, navigation to defence application and many more to add.

To achieve these tasks it is very essential to have a precise knowledge about the state of the UAV with respect to its environment. This state estimation is mainly carried out utilising the commercially available sensors with specific parameters, the alto-meter is used to estimate the altitude of the UAV and similarly is use inertial measurement unit (IMU) to estimate the values of attitude. Figure 1.4 represents a few of the sensors actually used on board the UAV. Some UAVs also require to have additional sensors to meet the demands of the application one is looking for. For instance the use of lidar or

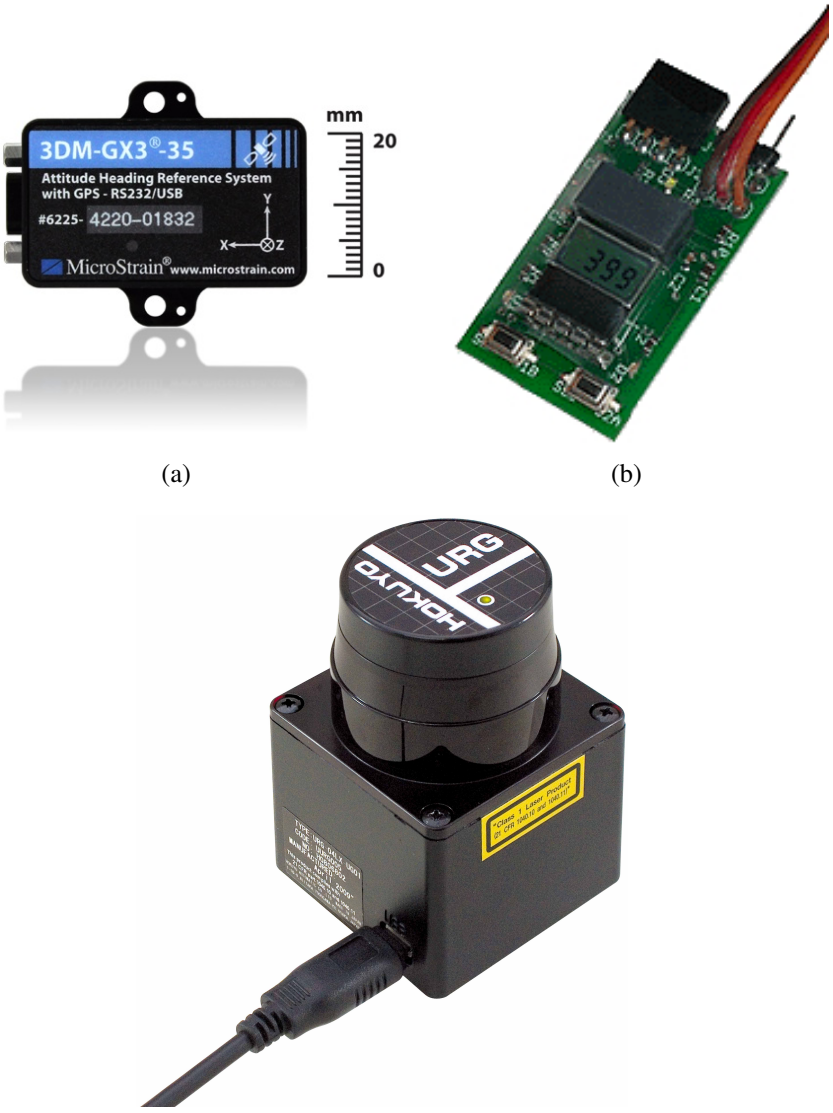

(a) (b)

(c)

Figure 1.4: Different types of sensors on board UAVs: (a) Inertial measurement unit (IMU) for attitude, (b) Altimeter for altitude, (c) Laser range finder.

sonar is been used to develop or update a map of the environment for obstacle avoidance and autonomous functionality in an unknown environment in the lack of prebuilt map and GPS deficient environment.

The advent in the miniaturising the sensors do help for a little increase in payload, but still the miniaturised sensors are heavy and do not serve any other purpose than just providing the control of the UAVs. Since the vision has been

a topic of research in robotics and make use of them for many need specific applications. The miniaturised vision sensors are smaller and lighter than the other sensors we discussed previously. The vision sensor has enormous visual information that can be utilised in many applications due to its strong ability that has been researched recently. Thus we could conclude at this stage that it is wise to replace the mechanical sensors with vision sensors for the following reasons. The vision sensors are:

- Cheaper than the commercial mechanical sensors.
- Light in weight thus provide additional payload.
- Serve multiple applications unlike the previous mentioned commercial mechanical sensors.
- Are smaller and provide additional space for other need specific sensors to be added on board the UAVs.
- Can be used to perform various applications along with the control and navigation at the same time thanks to the various algorithms based on captured images.
- Vision sensors do not require to have the prebuilt map or GPS sufficient environments for their functioning unlike some sensors currently used on board the UAVs.

We note that for most of the applications require the precise control and navigation of the UAVs to achieve their goals. Thus we are curious to make use of computer vision for the control and navigation of the UAVs. Thus in the following section we see the strength and capacity of computer vision in general applied to the robotics that include for UGVs and AUVs. Since this will create the basis of our motivation for using computer vision for UAVs to facilitate in control and navigation with other applications. It is always interesting to look for solutions that not only serve one purpose but instead for multiple purposes. The following section will deal with the various applications of computer vision based tools for robotics in general, since if they are suitable for different applications they can be enhanced to be implemented for UAVs too.

The use of UAVs have a prime limitation of less payload available to implement other need specific application, since the UAVs required multiple expensive sensors for control and navigation alone.

A way to overcome this problem is to replace heavy commercial sensors with hybrid commercial sensors or computer vision. Before jumping to a conclusion, it is important to verify if the vision based tools can assist in control and navigation of robots. Thus in the following section, we will identify and verify the various computer vision based tools replacing commercial bulky sensors, we focus mainly towards the control and navigation for robot application.

1.1 Computer Vision For Robotic Applications

Computer Vision has demonstrated to be a reliable, useful, powerful, fast, efficient, light weight and low cost sensor based tool to cater many applications in robotics and machine vision control systems. Some of the interesting application of computer vision in robotic and machine control as in control of the automatic warehouse for arm robot to perform the automatic storage and retrieval system by Yu et.al in [109]. Saxena et.al in [93] presented an interesting work with computer vision on robotic arm to grasp new objects in an unknown environment to plan the obstacle free path to reach the object to be grasped. Apart from the implementation of computer vision in various robotic application as mentioned, they are widely implemented for medical application, machine vision, control and navigation. These robotic application in conjunction with computer vision has helped solve physically impaired patients as cited by Bailey et al. in [7] for navigational control of robotic wheel chair: wheeley. It already has helped to achieve various difficult applications and still continues to cater more and more everyday. Thanks to the ever growing research interest in computer vision lately that has made it possible and feasible to this extent that we see it today. There are research and developments everyday that reduce, the size of the sensor, the weight, the cost of production and the processing time, but inversely relates to the growth in the capacity of acquiring and processing high resolution images for various need specific applications or control of mobile robots and machines.

Despite the various robotic application we discussed in the previous para-

graph, which mainly addressed various problems but we are interested in the state and pose estimation of the robot for implementation in autonomous control and navigation. Thus we focus on some of the interesting work of computer vision applied in control and navigation of robots that include for unmanned ground vehicles (UGVs) and autonomous underwater vehicles (AUVs) because we can find several work for these robots unlike for unmanned aerial vehicles (UAVs), which intrigued in us on the implementation of computer vision on UAVs will be dealt in the following chapter 2 on state of art.

Generally the control and navigation of the robots can be achieved from visual odometry, Visual Simultaneous Localisation And Mapping (Visual SLAM) and visual servoing for precise state estimation in a confined work envelope unlike the global state estimation in Visual SLAM. We are however interested in the global application of state estimation in an unknown environment, thus we only visit the visual servoing in brief.

The vision feedback control loops are generally introduced in order to have and improve the accuracy of the robotic platforms/ systems. This use of visual feedback to control a robot is commonly termed as *visual* servoing as defined by Hill and Park in [43] and Hutchison et al. in [48]. Visual features, based on the images from visual sensors, such as points, lines, patterns and regions can be used by the robot for their alignment. Hence, vision is an important candidate of the robot control systems that provides feedback about the state of the environment.

The other interesting tool based on computer vision for control of robots is using *visual odometry*. As defined by Nister et al. in [76] their classic paper in 2004. It is the process of estimating the position and orientation of a robot from the images obtained from the video input by a stereo head or a single moving camera, which they demonstrated on various robotic platforms, similar applications were demonstrated in the tutorial by Scaramuzza et al. in [94]. The use of visual odometry has been implemented on the Mars exploration Rovers by NASA as cited in the work of Maimone et al. in [56].

The next interesting tool based on computer vision is Visual SLAM for estimating the pose and location of the robot. This is a technique used by autonomous robots to build up a map within an unknown environment (without a priori knowledge), or to update the map of a known environment. Dissanayake et al. in [29] presented on how to compute the absolute location

and pose of the autonomous robot vehicle from the incremental map it builds of the environment, when it starts in an unknown location in an unknown environment.

The control and navigation by estimating the pose or state of the robot in its environment have been cited using various computer vision based tools in the above paragraphs. However, there are certain findings that indeed motivate and help us develop our research question. These research question is presented in the following conclusion of this part.

Conclusion:

In the process to identify the research context from our literature review, it was noted that there were

- Computer vision based tools could successfully replace the heavy, bulky and expensive commercial sensors,
- Limited but rapidly growing implementation of computer vision based tools for control and navigation from pose or state estimation of robots in their work environment for UAVs, when compared over the UGVs and AUVs.
- Growing interest and demand of applications based on computer vision for UAVs that lead to our research context to be focused on.

1.2 Problem Outline

During the early literature review to identify the research context, one thing that was prominent from our findings as presented above was the rapidly growing interest and amount of work on the application of computer vision based tools for UAVs control and navigation to achieve some additional need specific goals. This motivated us to definitely pursue our research in the control and navigation of the UAVs. However, the research question is yet to be identified defined in section1.3.

The next task was to identify the exact research question. From the use of computer vision based tools for robotic application along with the control and navigation intrigued our interest in computer vision and UAVs. It was also noticed that the importance of precise knowledge about the state of the robot is

equally important for many need specific application as much it is for the control and navigation. From our observation it was noticed that there had been implementation of computer vision for the control, navigation with additional application. We found interesting works in state estimation of robots with fusion of computer vision with GPS information as presented by Soloviev et al. in [96], then was the work on control of robot vehicles based on vision but in GPS-deficient environment as presented by Ahrens et al. in [2]. Then was the interesting work that could work essentially in GPS-denied and unexplored environment but worked in properly illuminated environment as cited in [13] by Blosch et al. In control of UAVs the most crucial stage is the vertical take off and landing (VTOL) and low altitude manoeuvre, since a minor error can cause the UAVs to crash and this emphasises on the need for precise knowledge about the state of the UAVs in their work environment. However there were limited amount of work being performed in low light to dark environment with GPS denied and unexplored environment without prebuilt map of it. Thus we had been interested to find a solution to the problem to estimate the state of the UAVs in such an environment using computer vision based tools due to their stated advantages that addressed for both indoor as well as for outdoor environment.

1.3 Research Questions

The previous section has outlined the problem we want to address in our research work shaping the research question. The research question is identified in parts: first to identify a computer vision based set-up to estimate the state of the UAV in the conditions of environment outlined in 1.2, second to develop the mathematical model based on both approaches of algebraic and geometrical to be suitable for the environmental conditions taken into consideration, third part is to validate the models developed by simulation and implementing them on real UAV platforms.

1.4 Contributions

The main contribution of this work has been to find low cost, light weight, computationally light vision based solution to estimate the state of the UAVs

in improperly illuminated (Low light to dark environment including cloudy day to night), GPS-deficient , unexplored environment that addressed for indoor as well as for outdoor environment. The contribution of this work has been in identifying the research question and development of the solution with a computer vision based set-up, development of the mathematical model for both algebraic and geometrical approach for the solution to address the research question. The solution had been verified and implemented on real time UAV platforms that assist in performing autonomous vertical take off and landing (VTOL) with low altitude manoeuvring capabilities. To the best of our knowledge this is the first work of its kind to have addressed the problem outlined.

The presented research work has helped obtain 3 international conference papers and 1 Journal paper. The 3 conference papers have been in International conference on Intelligent Robots and Systems (IROS-2011) [71], International Conference on Unmanned Aircraft Systems (ICUAS-2012) [72] and International conference on Intelligent Robots and Systems (IROS-2012) [74]. Whereas, the journal paper has been in Journal of Intelligent and Robotic Systems (JINT) published by Springer -Netherlands [73].

1.5 Thesis Structure

This section is to briefly outline the chapters of this thesis work. The first chapter was on introducing the outline of the problem, developing the research question to be addressed with structure of the thesis at the end of the chapter 1. The following chapters are respectively as:

Chapter 2: State of the Art

Chapter 3: Mathematical Modelling

Chapter 4: Calibration Algorithms

Chapter 5: Evaluation and Discussion of Results

Chapter 6: Conclusion Future works

Appendix A: (Spherical Model Of Camera)

Chapter 2 on State of the art addressed on the study of computer vision based tools for UAV applications, identifying the suitable set-up to address the problem outlined to prepare the preface for the modelling the problem mathematically. Chapter 3 is on Mathematical modelling that addressed the right

choice of the set-up as concluded from chapter 2 and develop the mathematical model based on both: algebraic and geometrical approaches. Chapter 4 is on Calibration Algorithms and explained the calibration of the sensors setup used as it being a very essential step in the proposed solution, since a minor error induced in the set-up would lead to a false values in state estimation and concluding with the algorithms devised for algebraic and geometrical approaches to be implemented to obtain the results. Chapter 5 is on Evaluation and discussion of results obtained from the two approaches developed with their robustness testing in different test scenarios of environment conditions. Chapter 6 is on the Conclusion and future works. It being the last chapter of the thesis with discussion on the goals set and achieved, finally concluding with future work that can be performed to improve the proposed solution.

An appendix has been provided at the end that discusses on the spherical model of the camera, this has been done to represent the general camera modelled regardless of the type camera lens being used. This is only to assist the reader to understand proposed solution idea in a general case.

Chapter 2

State of the Art

This chapter provides an overview of the State-of-the-art/practice: Literature review on computer vision and computer vision based tools for UAVs. Concluded by identifying challenges.

2.1 Introduction

Over the recent past few years the research on unmanned aerial vehicles (UAVs) has gained interest in the field of robotics, when compared over to the unmanned ground vehicles (UGVs) and autonomous underwater vehicles (AUVs) because in the latter cases many researches had been carried out, where as research in UAVs is in its early phase. Traditionally, vision-based navigation, state estimation solutions have mostly been devised for Autonomous Ground Vehicles (AGVs) and UGVs and AUVs, but recently, visual navigation, state estimation is gaining more and more popularity among researchers developing UAVs. UAV control is comparatively more complex in nature since they possess more degrees of freedoms (DoF) over the UGVs, when compared with AUVs at-least UAVs are complex to control as AUVs can float without any propelling rotors which is not the case in UAVs. Which is why ? researchers from many institutions of higher education along with research and development (R&D) institutions from public and private sectors in the recent years have been focusing on the improvement of the aerial robotic capabilities. Rotor based UAV have an upper hand over the conventional fixed wing UAV by its advantage to be able to hover in a small area with less difficulty and on top they can easily hover at one place for longer time which is

unlikely possible by a fixed wing UAV. Different types of commercially available rotor based UAV come in the following configurations with single rotor based helicopters (mono), with four (quad) rotor based UAV, with six (Hexa) rotor based UAVs as was explained in chapter 1.

The application of UAVs to multi disciplinary researches and their skills implemented to solve various problems ranging from object position, obstacle & object detection and tracking, attitude and altitude estimation, control, path planing, mapping, navigation, and simultaneous localisation and mapping (SLAM) and many more the list is endless. To answer many of these problems researchers have proposed several innovative and interestingly cheaper solutions based on computer vision. It has been demonstrated that computer vision applications in general are accurate and reliable, on top the vast power of the visual information from camera on board the UAV is harnessed to estimate multiple parameters of interest at once than from previously used multiple sensors. Despite having a "Bird's eye view from the sky" the perfect blend of computer vision with UAV can be implemented in aerial imagery, surveillance, search and rescue, inspection, detection and tracking are among many other applications. Section 2.2 enlightens in brief on the state of the art of computer vision for UAVs.

The introduction on the UAV architectures, various configurations, and control are out of the scope of this thesis, however it has been addressed in brief in the Chapter 1.

To enable such a state of the art research definitely requires large R&D infrastructure, hardware, apart from the superior class of researchers all across the globe. This is the main reason we notice through out the world that UAV research are principally carried out from the academic field that actively research and develop vision systems for UAVs in large public funded educational or R&D institutions. The private industrial sectors focus on the R&D of UAVs for need specific applications and maintained with much secrecy for their profit margins and letting very limited or no access to public unlike the public research.

2.2 Computer vision for UAVs

Computer vision for UAVs intrigues in us to know firstly what does that really mean? The simple answer to this implies to the classification of the use of visual processing on the UAVs, this is the visual processing on the images captured from the camera on board the UAV, where UAV acts like the testbed for the experiments carried out. In [19] Compoy et al. provided brief review on the application of computer vision for UAVs, they emphasised on the importance of computer vision for UAV citing it to be not just an technique to sense and recover environmental information from an UAV, but it should play the main role regarding the UAV's functionality because of the vast visual information gathered, to deploy many possible uses and applications, accounted computer vision as our main natural interface to the world understanding. However, one can say that for environment perception technologies not only include computer vision (camera) but also laser range finders and various other commercial sensors. It is for the following reasons that lead many researchers to make use of camera as primary sensor over the other commercially available sensors: firstly camera acts as the main natural interface to world understanding, vast visual information that can be processed to achieve multiple tasks in one go by the use of miniaturised camera with high resolution. The miniaturised camera means lower in weight over other mechanical sensors, low cost upon large scale production and many more application specific needs and advantages make it the perfect choice among the researchers in computer vision for UAVs. In [55] Liu et al. presented a brief and concise work on general use of computer vision techniques implemented on UAV flight control, visual odometry, visual servoing and aerial surveillance. Above cited works along with many other work make it to be considered as an interesting topic of research in this field of making use of computer vision as the primary sensor system to deploy them in the control and functionality of the UAVs. The solutions based on the computer vision would be definitely cheaper than the conventional commercial sensors available in the market to control the UAVs. Moreover, much recent work prove it to be assert the statement of computer vision based solution can be a replacement to the heavy and expensive commercial sensors, thus our research interest was to find an appropriate and robust but cheaper solution to control the UAVs.

Computer vision for UAVs can be implemented for many applications depending upon the various configuration of the sensor, camera, with the UAV. These can be used for applications varying from the easiest as aerial photography to complex applications as identification and tracking of objects. The conventional method for tracking based on images from ground based camera system had limited field of view. Most of them can not track the object if there be any obstacle in the scene like wall, thus in such situations aerial images come in very practical use due to its capability to view a large area and could look things behind the obstacles where the conventional camera on post fail. Here we classify some these computer vision based UAV applications for capturing of images and processing for aerial photography, monitoring of facilities and industries. This UAV based computer vision system is for better and superior aerial surveillance over one or multiple ground fixed post camera surveillance.

2.3 Computer Vision on UAVs: Why is it interesting ?

In the following section, it discusses on the various interesting cababilities of computer vision for UAVs. Further the subsections discuss on some available or implemented computer vision based tools that can be useful to answer our research question developed in chapter 1.

2.3.1 Aerial Photography And Visual Surveillance

Aerial acquisition of images definitely provide much more information regarding the environment over the images from ground installed cameras. We could see in the near past the developments in the aerial photography, that once started from the ground with human height level photography for field surveying purposes. Then led to installations higher than human height on the buildings for more visual information, later on the high staffs that eventually led to further more and ended on to aerial photography. The aerial photography is one of the most rudimentary applications as cited by Cui et al. 2008 in [25]. Despite being the most rudimentary application, it is being widely explored recently to harness their important uses because of its low cost, re-

liable, fast and hassle free use. K. Ro et al. in 2007 in [84] demonstrated the use of aerial photography for urban highway traffic monitoring, though it was simple but the application helped reduce the big bottle neck traffic congestions to enter the city and monitoring traffic rule offenders and collecting traffic data as is presented by Puri et al. in 2007 in [83].

Sometimes the aerial photography helped in other inter-disciplinary projects on environmental health monitoring, where the information gathered from UAV enabled aerial photography as cited by Myers et al. in 2005 in [70] for monitoring by remote sensing of coastal aquatic environment, so was it used in collecting crucial samples for marine mammal research from whale fishes without disturbing them. The application also finds use in the study of marine life and in more recent times have been deployed in Australia to monitor the health of the coral reefs by analysis the aerial images captured. The natural or accidental wild forest fires cast a lot of impact on our volatile environment and economy, Merino et al. in 2006 in [62] proposed simple solutions to counter this problem. It was also used in 2011 post Earthquake-Tsunami caused nuclear disaster in Japan, when it was declared unsafe for human intervention. UAV based aerial photography with high resolution was used to sense the amount of damage caused.

Aerial photography from the UAVs are very interesting and find their use in military operations against the terrorists groups on the ground before planning a military coup to capture or kill the terrorists. This was heavily used in the Afganistan and Pakistan to act again the Taliban terrorists.

Last but not the least is our entertainment industry where the UAV based aerial photography is used for making movies and also many television news channels also rely on the high resolution video coverage. Thus, we can see how the UAV based aerial photography is taking its important place in our daily life and improving the feel factor.

The visual information from UAV is also in visual surveillance and inspection. The ease of using UAV based visual surveillance and inspection of bridge fault detection is such an useful and important task without actually disturbing traffic on the bridge over the conventional cantilever robot vision based bridge fault inspection as was presented by Metni et al. in 2007 in [65]. Kontitsis et al. in 2004 in [53] have presented the effective use of noise reduction, feature extraction, classification and decision-making in conjunction

with the genetic algorithm on aerial images on automated fire detection alarm system for UAV based aerial surveillance.

Aerial surveillance is finding many more applications based on small micro-copters or quadrotors, since they are becoming feasible and are cost effective than previously assumed only on pilot operated life size helicopters. Aerial surveillance are used these days on monitoring the borders, road traffic surveillance, they are very well used by police in developed countries to track and chase law violators before they abscond by following them on a cheaper solution based on UAVs. However, for all these applications to function normally and effectively, it can only be achieved once we have a robust control system of the UAVs being deployed for the specific purposes. In the following sub section we will see some of the interesting approaches to estimate the state of the UAV using visual tool explained.

2.3.2 Visual SLAM

Simultaneous localisation and mapping (SLAM) based on the visual information from the camera onboard UAV, it is an important tool for robot localisation and to build and update the map of the environment in which the robot is, was well used by Caballero et al. 2009 in [15], where they considered the natural landmarks provided by a feature tracking algorithm, without the help of visual beacons or landmarks with known positions, and used homography-based techniques to compute the UAV's relative translation and rotation by means of the images gathered by an onboard camera as the mosaics. Unlike the previous mentioned work, Artieda et al. 2009 in [6] used a partially structured environment and implemented visual SLAM by relating the features of the object tracked to their distance from the UAV. They also considered the image processing techniques, such as interest point detection, the matching procedure and the scaling factor for a complete 3D visual SLAM.

The proposed solution of MonoSLAM by Davidson in 2003 in [26] was interesting for the fact that he proposed a camera based approach for SLAM. Earlier than his proposed solutions researchers utilised informations gathered from commercial sensors like laser range finder for SLAM. He proposed to use a camera to acquire a series of images from the environment as the robot progressed and detected the features in the images. The mosaics of these images acted as an aid to perform classical SLAM as presented in [31] and

[7]. Davidson focused on the localising than building a precise map of the environment. Thus we observed from the results the UAVs localised well but with a very sparse map. This had to be considered since he mainly tried to consider only 100 features in total. To make it simpler he provided the initial starting pose of the camera in order to have the depth sense at the initial start point. The major drawback lied in this approach were

- The solution was complicated and could not be reliable in outdoor environment since 100 features in total were too little to estimate the position.
- The algorithm was based on the repeatable observation, thus a sudden change in the scene due to a random object or person came into scene the relative position could be lost and result in lot of error in the localisation.
- In dark environment it would fail due to lack of sufficient features in the series of images, still did not counter the above drawback

SLAM based on only visual information have been implemented on UAVs. Angeli et al. in [5] have presented a method for purely vision- based 2D SLAM for micro UAVs that manoeuvre at constant altitude. Their proposed system is good in utilising the visual features and matching them to build a visual map in which it can correctly locate the UAV with its relative starting reference point. Nemra et al. in [75] proposed a visual SLAM approach to estimate the state (attitude and altitude) of the UAV based on a stereo vision system.

2.4 State Estimation

We have already discussed about some of the complex computer vision based tools and applications on UAVs, but what interests many of the UAV research communities across the world is the control of UAV based on computer vision termed 'visual odometry'. Visual odometry focuses on the use of visual information for pose estimation, altitude estimation and navigation. Since odometry is an interesting challenge in the UAV control, thus many researchers use

various expensive, bulky and application specific commercial sensors. However, these commercial sensors not only cost a lot but also consume a lot of battery power to keep them up with the UAV in the air. So it is here when our research interest statement started to be justified. Upon having performed the thorough literature review, it was noticed by us that there did not exist any method for vision based UAV attitude and altitude estimation in the low light to dark environment. It intrigued within us to think of such a system to answer our main research question mentioned earlier on state estimation of UAVs in GPS denied, unexplored and badly illuminated environment.

Several solutions based on commercial sensors for state estimation were proposed as by Cabecinhas et al. in 2010 in [17] proposed a system based on hybrid systems with simulation results. Another interesting work was from Grzonka et al. in 2009 in [40] proposed to make use of commercial miniaturised laser range finder, however, it required a prebuilt map of the environment and yet the laser range finder was bulky and served no other general purpose application. These commercial sensors were of interest to us, but only to keep them as reference ground truth values to compare with vision based estimation methods. Thus it is interesting to explore the enormous and powerful visual information sensor: Camera and its types.

2.4.1 State Estimation From Camera Configuration

The choice to make camera as the primary and most important sensor for several application was easier and practical, since cameras were lighter and less expensive than the commercial sensors. Visual sensor served multiple purpose than the rest available options. Easily available miniaturised camera were not only cheaper but also light in weight. The next important thing to consider was which type of camera configuration and how many to be used? This is discussed in further detail in the following subsections 2.4.2 & 2.4.3.

2.4.2 Mono Camera

As we have seen in the previous paragraph that we had centred to the visual sensor (camera) as our primary sensor. However, there were different types of camera available to be used. We noted down the application of vertical take off and landing (VTOL) and low altitude manoeuvre. This clearly helped us

to look for camera that can be best suited for low altitudes, especially for take off and landing, it was very important to have the attitude and altitude known precisely. The information on the altitude and attitude play a vital role in any UAV's take off and landing. There were mainly three main kind of camera's available to suit our application, which were namely: Perspective camera, Fish-eye camera and Catadioptric cameras, they are presented in the figure.2.1.

Perspective camera: is a standard projective camera P that maps world points X to image points x according to the relation $x = P.X$ [78].
Fish-Eye camera: is camera with an ultra wide-angle lens that produces strong visual distortion intended to create a wide panoramic or hemispherical image.
Catadioptric camera: is a camera that contains mirrors (catoptrics) and lenses (dioptrics) for a complete 360°visual information in one image.

In order to control the UAV the single camera was brought in to use by several scientists. Mondragon et al. in [66] proposed the use of single camera for 3D pose estimation of the UAV, this method explores the rich information obtained by a projective transformation of planar objects on a calibrated camera. The algorithm obtains the metric and projective components of a reference object (landmark or helipad) with respect to the UAV camera coordinate system, using a robust real time object tracking based on homographies. This solution was good a choice at low altitude where the GPS are often inaccurate. However, the limitation of this method lay remain on the tracking of a known pattern due to its limited FOV the trouble of losing the pattern at low to very low altitude, where at low altitude it is very crucial to control the UAV for a safe autonomous VTOL. Figure 2.2 presents the experimental real time video still where the pattern is visible at a higher altitude but a part of the pattern is lost at lower altitude and would be lost completely by reducing the altitude further.

As mentioned earlier that visual information has been used for UAV attitude estimation. The early experiments were based on the images taken by UAV with forward looking monocular camera. These images were used to estimate the roll angle with an horizontal reference based on the skyline segmentation as cited by Ettinger et al. in [33], Todorovic et al. in [99], Cornall

(a)

(b)

(c)

Figure 2.1: Different types of camera: (a) perspective camera, (b) fish-eye camera, (c) catadioptric camera

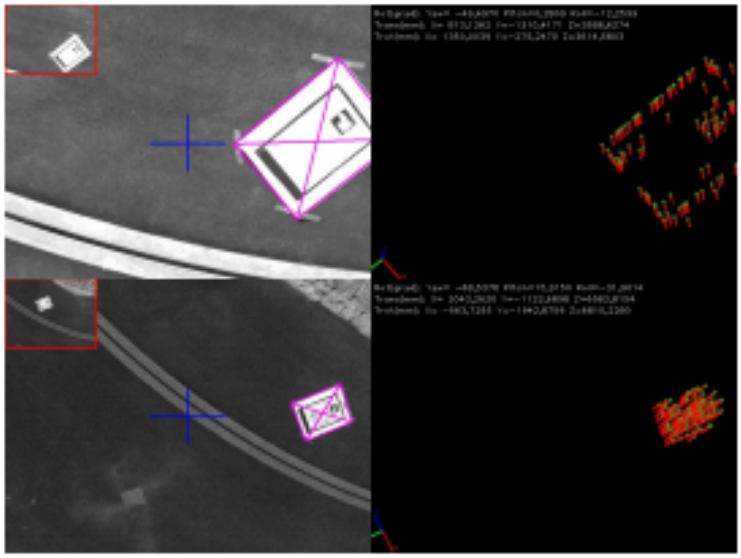

Figure 2.2: Experimental results of state estimation of UAV from single camera by Mondragon et al's method. Source: Mondragon et al. [66]

et al. in [24], Dusha et al. in [32].

The choice of the camera were done on the following reasonings looking at their respective pros and cons. Perspective camera were considered as a candidate camera type by its virtue of its high resolution images, however, the perspective camera even with a small focal length had a very restricted field of view (FOV). This led to only have a limited visual information and a loop hole to still look forward with other available types of cameras. Thus the search for the other type of camera was progressed keeping in mind to have a large FOV for more visual information and helpful to our application. Secondly we considered the fish-eye camera, it was already a better choice over the perspective since it had a wider FOV on comparison with perspective and was very important for our application of VTOL to have the visual information at very low altitude; thus a fish-eye camera with smaller focal length was just appropriate and a better choice. We finally also considered the catadioptric camera, this camera similar fish-eye had a wide FOV, however it draws a major concern of its positioning. The catadioptric camera is a combination of mirror and a camera the structure leaves us with a central blind spot with a complex view of the surrounding environment. What is more important is the positioning of this system on the UAV for our application because we could not use it looking downwards because it would leave us with a very

[]

[]

Figure 2.3: Different types of camera configuration. (a) Single Camera, (b) Stereo Camera

little information about the ground beneath the UAV. These factors led us to consider fish-eye camera as the main sensor for our application. The use of single camera especially to determine the attitude and altitude is an impossibly difficult task and required external information like pattern or marker but this is discussed in details in the following subsections 2.5.1 and 2.6 of this chapter. Fig. 2.3 (a) presents single camera configuration and Fig. 2.3 (b) presents the stereo camera configuration.

2.4.3 Multi Camera

A stereo camera is a type of sensor with two or more lenses with a separate image sensor for each lens. This allows the camera to simulate human binocular vision, and therefore gives it the ability to capture three-dimensional images, a process known as stereo photography. A stereo vision system is generally a standard combination of two cameras, which are separated from each other by a baseline. However, it is not restricted to it but it can be a combination of camera and a laser pattern projector and many more. The stereo camera system comparatively gives more information about the scene of the environment being viewed, thus making it a better choice to determine the attitude and altitude of a UAV utilising a stereo camera system architecture. An inter-

esting work was proposed by Eynard et al. in 2010 [34] in which they present the use of a mixed stereoscopic system consisting of one fish eye camera and other the perspective camera for attitude estimation, which unlike the classical stereoscopic systems based on feature matching, utilised a plane sweeping approach in order to estimate the altitude and consequently to detect the ground plane. They made use of the homography between the two views of the calibrated cameras. They also implemented this on ARM based CPU on board the UAV to estimate the attitude and the altitude on real time.

The use of stereo camera with various approaches have been proposed to estimate the attitude and altitude. We have tried to highlight a few of the interesting researches, we present the work of Abbeel et al. in 2007 in [1] where he deployed two sets of stereo camera and implemented machine learning concepts to estimate the pose of the helicopter. However, despite an interesting and successful implementation the method had drawbacks as follows:

- The solution was sensitive to variation in the environment, since it depended on the stereo ground camera for pose estimation, this could not be implemented for unknown environments for surveillance task for instance.

- During night it would fail, unless there was an improvement on the solution as an illuminated helicopter, still did not counter the above drawback

Altug et al. in 2005 in [3] proposed a system that comprised of two cameras: first one is on board the UAV and second one is a pan tilt zoom (PTZ) camera fixed on ground. Both the camera heads face towards each other to obtain the position and attitude of the UAV with respect to the ground camera rather than utilising the camera on board the UAV to estimate the same. This complex solution to find the camera pose both cameras tracked certain colour markers of known radius, 2.5 cm in their experiments, were attached under each rotor, and also at the centre of the camera and on top of the ground camera as represented in the Figure 2.4. They later tracked the markers and computed their areas to estimate the relative pose of the camera.

This method was good and calculated the desired attitude of the UAV, but it had the following drawbacks:

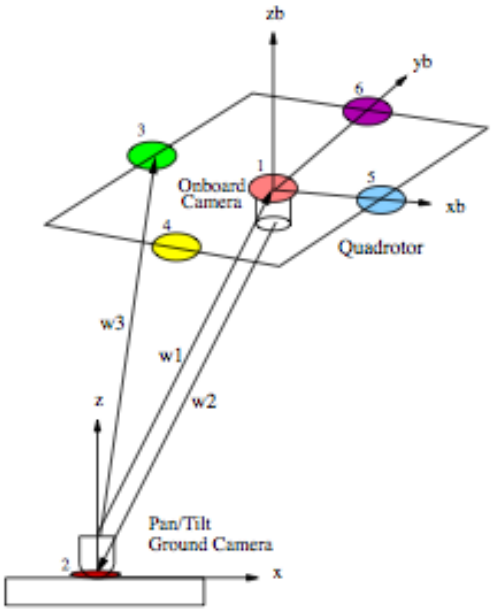

Figure 2.4: Experimental model to estimate the attitude of UAV by Altug et al. method. Source: Altug et al. [3].

- The solution was complicated as it required merging of two different visual datas to estimate the position and attitude.
- In order to realise it in real scenarios, it required an enormous marker to be able to be recognised from a far distance. This makes it unsuitable for survailance or VTOL on an enormous marker that camera could not track.
- The solution was very sensitive to any possible occlusion in outdoor environments, since an occlusion can cause the markers disappear from the FOV of the camera and lose the estimation.
- During night it would fail, unless there was an improvement on the solution as an illuminated markers, still did not counter the above drawback

The following subsections of this chapter will discuss on the intelligent use of the configuration of the camera systems and how some of the researchers made use of different visual features to obtain the attitude and altitude namely by the use of different markers: Firstly natural markers and

secondly artificial markers. Later the artificial markers will give rise to the use of different patterns, where these patterns are again classified: Firstly on fixed patterns and secondly on mobile patterns always available in the scene within the FOV of the camera onboard the UAV.

2.5 State Estimation From Marker

The first and foremost application of UAV to perform various other complex application is to successfully determine its position and attitude (pose, not considering the heading/ yaw angles) in 3D space accurately, efficiently and fast. It is our main interest to estimate the attitude and altitude of the UAV and having already seen the cons and pros of using single and stereo camera system. Since we know the visual information from the use of the configuration of the camera is important but it is important to know about the nature of the feature we are looking in the gathered visual information. As discussed earlier in the previous sections the interesting features of fish-eye and catadioptric cameras.

Landmarks are distinct features that a robot can recognise from its sensory input. Landmarks can be geometric shapes (e.g., rectangles, lines, circles), and they may include additional information (e.g., in the form of bar-codes). In general, landmarks have a fixed and known position, relative to which a robot can localize itself. Landmarks are carefully chosen to be easily identified; for example, there must be sufficient contrast to the background. Before a robot can make use of the landmarks for navigation, the characteristics of the landmarks must be known.

The following paragraphs discuss in detail the use of natural marker and artificial markers in attitude and altitude estimations.

2.5.1 Natural Marker

The use of natural markers are very interesting on its own, since these natural markers helps research to make use of one single camera, since the natural markers carry a lot of information on their own.

What are natural markers ? : The environment contains different kind of informations. Most computer vision-based natural landmarks are long vertical edges, such as doors and wall junctions, and ceiling lights. Some very typical

natural markers consists of horizon and sky separation, plantation in a specific pattern etc that can make more sense for robot odometry.

Researchers have proposed work as by Demonceaux et al. in [28], [27] for attitude estimation based on omnidirectional images by separating the sky from the earth using Markov's random field on the captured images. Another work based on vanishing points to estimate the attitude of the UAV by Bazin et al. in [11] [10]made use of the vanishing points and on combining the horizon and the homography-based approaches for catadioptric images respectively. Some even proposed the visual odometery and simultaneous localisation and mapping (SLAM) for attitude estimation for UAVs as by Caballero et al. in [15]. Similarly as proposed by Merino et al. in [61] make use of natural landmarks. However, these approaches based on natural landmarks had the limitations at times to miss the natural landmarks in the scene, thus it draws our attention towards having an artificial landmark to be always available in the scene.

A very interesting work based on the natural marker was proposed by Demonceaux et al. [28], where they make proper use of the natural landmarker in rural space by working on the spherical model of the camera, where the spherical image helped them to also simplify the problem to separate the horizon from the ground that in turn helped them to calculate the attitude. When the UAV navigates in a free rural space, the horizon in the spherical image is projected into a circle dividing the sky from the earth. Todorovic et al. in 2003 in [99] and Cornall et al. in [24] presented UAV attitude estimation by skyline segmentation, which later on an extended work was presented by Demonceaux et al. in [28] unlike for the perspective camera using the classical segmentation of the horizon and ground based on colour histogram proposed for omnidirectional camera in general with an adapted Markov random fields (MRFs) modelling in [73] and calculated the normal of the plane that best fit the projection these horizon points on the unit sphere, in order to obtain the plane that contains all these horizon points. They implemented RANSAC for robustness of the solution by only keeping the inlier points and avoided the outlier points. Finally based on this obtained plane they calculated the attitude of the UAV.

Ettinger et al. in [33] and Demonceaux et al. in 2006 [27] proposed another work which was in line with the previous work explained on attitude

(a) (b)

Figure 2.5: Attitude estimation of UAV (a) based on MRF (b) based on Optimization

estimation of the UAV based on horizon detection, however, they proposed an extension over the horizon detection method, the use of horizon line as a unit sphere as a circle was later projected on to a plane in 3D space. Thus by doing so it helped them to easily distinguish between the sky points and the ground points. This method was optimised and faster to estimate the plane and so the attitude of the UAV from this plane.

2.5.2 Artificial Marker

As seen in the previous subsection on natural land marker did not prove to be a good option since these natural marker were not really available at different location the most importantly these worked only very well in the rural areas where it was easy to find the natural markers. These methods failed in the urban areas due to the lack of certain natural land markers. In the urban environment pose lot of obstacles and hinder the view. However, researchers made use of those features available in the urban environment as the artificial land markers. They made use of the line matching and bundle adjustment and edge detection and many more methods based on computer vision for UAVs to aid assist to determine the accurate attitude and altitude. We have discussed a few of the interesting methods based on artificial markers. First one was the use of single camera and the artificial marker was in urban area by Natraj et al. in [72], where the authors made use of the man made structures for bundles of lines from them, they used these lines from the scene to determine the

attitude and motion. They proposed a method to determine the parallel lines in the omnidirectional image to determine the attitude by using the fact that equivalent circles of bundles of parallel line projected on the sphere intersect at the antipodal points, which has been verified by Demonceaux, et al. in 2006 in [28]. The proposed method was based on to detect the lines in omnidirectional images by utilising the fast central catadioptric line extraction as proposed by Bazin et al. in 2007 in [10], which detected the edges in the image, chained the edgels (pixels of the edges). Later they selected the two most significant points on each chain of the edges and back-projected them on to a sphere. Then from these bundles of lines projected on to the sphere helped them to determine the attitude.

we cite some approaches based on artificial landmarks to achieve the task, based on hybrid systems was proposed with simulations results in [16]. The interesting work of Rudol et al. in [86] had presented the use of multiple marker. Merz et al. in 2004 [63], Merz et al. in 2006 in [64] used a method that fused visual and inertial information in order to control an autonomous VTOL of aircraft landing on known landmarks.

Several researchers have proposed several solutions based on artificial markers and mainly depended upon different patterns to estimate the attitude and altitude. Thus, they have been dealt in a separate section 2.6 in the following subsection.

2.6 State Estimation From Pattern

As explained earlier that the estimation of attitude and altitude based on UAV computer vision utilising the pattern, can be classified under the family of artificial markers. Since patterns in the scene are nothing bit an artificial marker that help assist to estimate the attitude and altitude of the UAV. The following subsections have been written to highlight the important works based on pattern.

2.6.1 Fixed Patterns

Here we discuss on the work of Tournier et al. in [100] that basically made use of a camera and a pattern. The pattern used was a Moire pattern. He

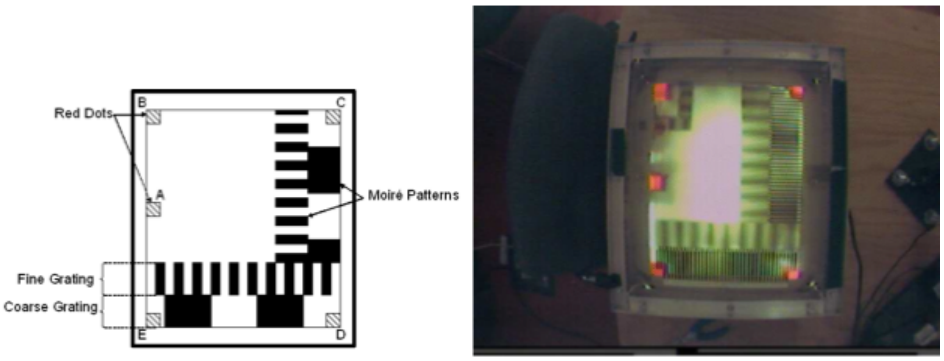

(a) (b)

Figure 2.6: (a) Moiré target model, (b) Moiré actual target

used the property of the Moire pattern to estimate the pose of from a camera mounted on an UAV. A target that consists of the markers to determine relative orientation and locate two sets of orthogonal target moire patterns at two different distance separated from each other. The relative position of the camera on board the UAV to the target with moire pattern was obtained using the concept of similar triangles on the colour light emitting diodes (LEDs) is obtained from the 4 single point discrete Fourier Transform (DFT) on Moire patterns. The Moire pattern used for the research has been presented in the figure. 2.6.

However, this approach has some disadvantages even after its interesting results demonstrated in [100], especially if used in real life implementation.

- The moire effect were sensitive to change in illumination, since the main use the researchers want to harness from UAVs is in research of surveillance, search and rescue, VTOL, proving it not suitable for real life implementation
- The second major problem was how to have a moire pattern always available in the scene or FOV of the camera, as the system failed in the lack of such a target pattern. Making it not a practical solution.
- The pose estimation in the proposed solution was dependent on the moire pattern in the FOV of the camera, thus meant if the pattern was absent in the scene for a small time, it will completely lose its orientation and pose information.

[] 

Figure 2.7: Landing of helicopter on helipad pattern

- Another major drawback of it was with the increase in altitude brought the shortening of the distance between the gratings and making the moire pattern as a single block and led to lose the pose estimation, since it was impossible for the camera to distinguish the target pattern.

It is from here that we thought to have a solution in which we can make use of a pattern that is always available in the scene or FOV of the onlooking camera. Also that we have a system that can carry the pattern always in the scene. The variation in altitude didnot actually effect our approach but instead helped us to estimate the change in altitude.

2.6.2 Helipad

Another application based on the artificial land marker pattern was the known helipad pattern in the scene. The proposed solution in [90] and [89] Saripalli et. al. have proposed an experimental method for autonomous landing of an UAV on a moving helipad target. They used the visual information for identification and tracking a known helipad. They implemented on a real-time, vision-based landing algorithm for an autonomous helicopter. The algorithm to perform the landing was integrated in a feedback loop with the visual information acquired in tracking the known shape target (Helipad in this case). The system was capable to navigate from an unknown initial position and orientation. Figure.2.7 presents Saripalli et al's work on landing on a fixed pattern (helipad).

However, unlike other methods mentioned it had some drawbacks too, which have been presented as below.

- The solution was sensitive to variation in the FOV of the camera, if the known shape target was missing the UAV could be lost.
- Another major drawback of it was with the increase in altitude pattern would vary in size and shape and led to lose the pose estimation, since it was impossible for the camera to distinguish the target pattern.
- During night it would fail, unless there was an improvement on the pattern as an illuminated pattern, still did not counter propose the above two drawbacks

2.6.3 Checker Board

In the work presented in De Wagter et al. in 2005 in [104] , the authors have evaluated the use of visual information at different stages of a UAV control system, including a visual controller and a pose estimation for autonomous landing using a chessboard pattern.

Here, it also made us think there were so many proposed solutions but during night most of them failed. It made our research take a new shape to consider these drawbacks and come up with a proposal that could actually answer the most of the question developed over the time to counter the drawbacks and bring forward a solution that was robust and fast.

2.7 Conclusion

These approaches were good in bright sunny day, where it was easy to identify the horizon and so on to use homography or to find the vanishing points or land markers for attitude estimation, but failed in low light or dark environments. Since most of the approaches were implemented on bright light condition, thus we started to think for a solution to be suitable for low light and dark environments.

Since our approach needs to have a solution suitable in low light to dark environment, we decide to make use of a laser pattern projector mounted on the UAV such that the pattern(artificial pattern) is visible in low light to dark environment. It also enabled to always have the pattern in scene. We also wanted our solution to be suitable to perform VTOL and manoeuvre at low

altitude, thus we decided to use the fisheye camera over the perspective camera. Since the fisheye camera has a large FOV that allows to always have the laser pattern available in the scene which is otherwise unavailable in perspective camera at low altitude.

The main outcomes of our research should be able to answer the following:

- GPS deficient environment,
- Pattern always available,
- Day and night to work,
- Complete darkness where no visual features are generally available otherwise,
- Absence of predefined map,
- Light weight,
- Lower in cost over the commercially available sensors,
- Lower in computational expenditure,
- Lower in power consumption, does not require the UAV to be in the scene from an external camera nor does it require a pattern fixed on the ground or a proper illumination condition to estimate the attitude and altitude.

Chapter 3

Mathematical Modelling

Stereovision is an attractive and widely used, but, it is rather limited to build 3D surface maps, due to the correspondence problem. The correspondence problem can be reduced using a method based on the structured light concept, projecting a given pattern on the measuring surfaces. However, some relations between the projected pattern and the reflected one must be solved. This relationship between them are presented in the latter section on mathematical modelling. This chapter will analyse stereo vision from structured light with enough justification to support our camera-laser system and relate them for the basis of our mathematical modelling .

3.1 Survey on Structured Light

We have seen in the previous chapter 2 in the state of the art how important and interesting is the computer vision based full pose or state estimation for the UAVs. Proceeding further in to the main goal of our research to find a technique that addressed all or most of the cited limitations of other proposed solutions required a new technique as is explained in 2.7 the conclusion part of the chapter 2. The state estimation by vision combines techniques from computer vision, image processing, geometric modelling and computer graphics into one unified framework, thus it can be considered a sub-area if image-based modelling. Since the rapid development of miniature sensors and electronics makes it possible to build low-cost acquisition systems that are increasingly effective.

In order to decide upon our acquisition system we performed a survey on

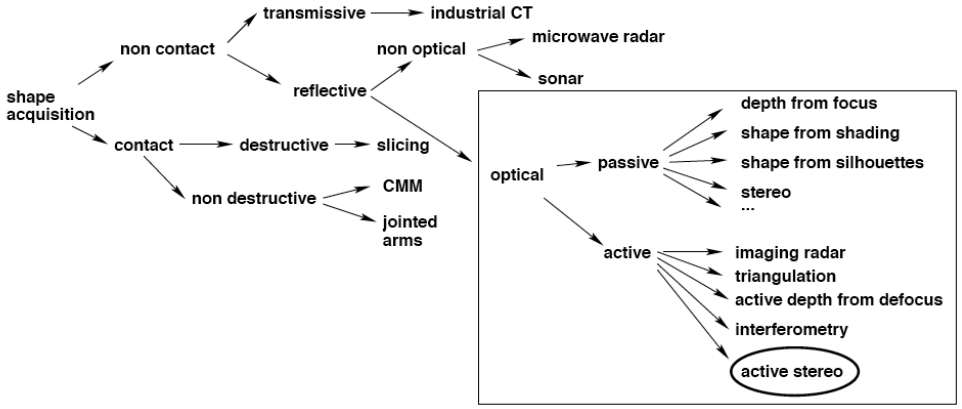

Figure 3.1: The classification of acquisition methods. Source: Joaquim Salvi's VIBOT lecture notes on 3D reconstruction by laser triangulation

the available different acquisition systems and since the geometry acquisition being a mature field of research we focused on it. The reason to concentrate on the shape acquisition methods was to make use of the common goal of attitude and depth of the objects can be assumed as the attitude and altitude of the UAV from the plane on which the scan is being performed. Fig 3.1 represents the classification of shape acquisition methods of which we concentrate on the optical based approach. Which allows us to make use of the off the shelf hardware reducing significantly the cost of the acquisition system.

When 3D information of a given surface is needed, we have to choose between a passive method and an active one. The most widely known passive method is stereo-vision which can be achieved in two different ways. In the first way, an optical sensor is moved to known relative positions in the scene. In the latter way, two or more optical sensors are previously fixed in known positions. The surface to be measured is projected on the image plane of each sensor through each focal point. But using stereo-vision definitely has the well known correspondence problem, however, it is also known that correspondence problem can be alleviated by leaving stereo-vision and opting an active method. One of the widely accepted active methods is based on structured light projection. Here, the second stereo camera is replaced by a light source (pattern projector), which projects a known pattern of light on the measuring scene. The first stereo camera images the illuminated scene and analysing the deformations of the imaged pattern with respect to the pro-

jected one, the desired 3D information can be obtained. Still depending upon the chosen pattern, some correspondences between the projected pattern and the imaged one should be solved. Most of the proposed structured light techniques are based on the projection of regular patterns on the measuring scene.

The branch highlighted in figure 3.1 presents a classification of optical acquisition techniques. One has to consider their advantages and limitations before the choice is made, these choices can be made as per the resolution and accuracy required in the specific application. This makes it important to know the application when choosing the hardware and software to be used to achieve the task. The only limitation that concerns in optical acquisition technique are that it can only acquire visible portion of the plane, it is sensitive to surface's properties like transparency, shininess, textures, lambertian and reflective surfaces.

We can conclude from here so far that it is a wise choice to opt for active stereo to obtain the 3D information from the scene that is suitable to address our stated problem in the concluding part of chapter 1.

Before we implement the active stereo with structured light it is important to understand the basic principles of structured light. We introduce in the following paragraphs the principles of structures light and further investigate on the various coded structured lights. This survey will thus enable us to identify what is suitable for our solution coded structured light or uncoded structured light.

Basic Principles of Structured Light:

The basic principles that allow obtaining 3D shapes and depth informations from images are the same as those of stereo vision. They are based on the fact if two known cameras observe the same scene point X then its position can be recovered by intersecting the rays corresponding to the projection in each image. This process is called triangulation.

The main problem of directly using stereo vision to recover 3D shape and depth lies in the difficulty of automatically matching points in the two images captured. In order to avoid this problem, these passive stereo methods can be replaced by active stereo techniques. In these, one of the cameras is replaced by a calibrated and well defined light source, that marks the scene with some known pattern. For instance, laser-based systems direct a laser beam (contained in a known plane) to the scene and detect the beam position

in the image. By intersecting the ray corresponding to each point with the known beam plane, one can compute the point's position as shown in the figure3.2, the correspondence problem is overcome by searching the pattern in the camera image (pattern decoding).

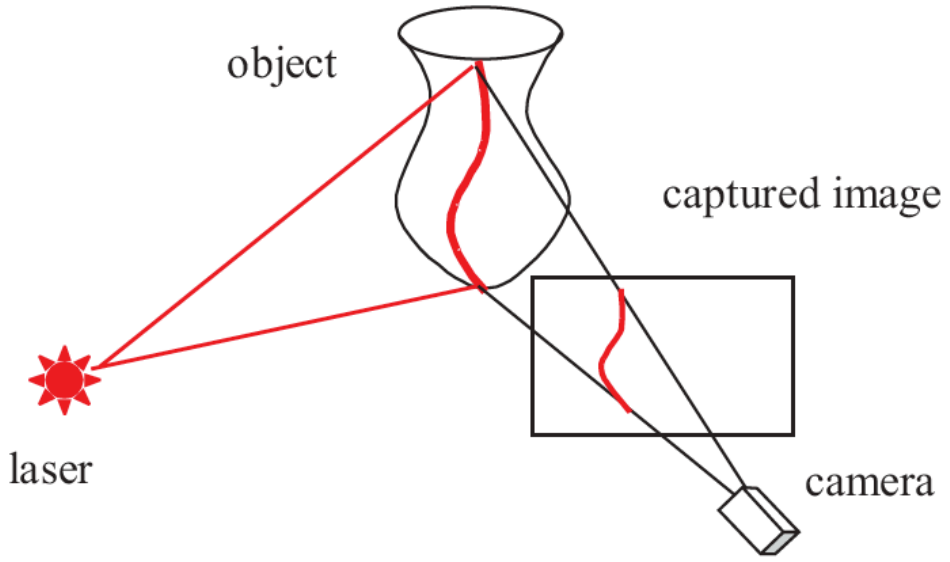

Figure 3.2: The laser beam projected on an objected and its captured image

One can conclude, the basic steps required in recovering the shape or pattern information implementing structured light are the following:

- Camera and projector calibration;
- To establish correspondences between points in the image and the projected pattern;
- To reconstruct the 3D co-ordinates of the points.

However, still it is important to note that the correspondence problem needs to be solved to accurately estimate the 3D depth and attitude information of the object relative to the active stereo system. The correspondence problem is reduced by different approaches of coded structured light by implementing one of the following techniques:

- Single dot projection technique;

- Single Slit;
- Stripe patterns;
- Grid, multiple dots.

Researchers have proposed several interesting approaches in obtaining the 3D information from captured images and we go through some of the works in this field. Early approaches include the temporal coding in which the idea is to project sequentially a binary coded signal corresponding to the binary digit of a coded pattern as is explained by Posadamer et.al in 1982 in [82] and Inokuchi et al. in 1984 in [50] proposed to replace it by a more robust gray binary code as presented in figure 3.3. However, the main problem of a binary temporal code is the large number of slides that have to be projected to achieve the desired resolution and its restriction to static scenes.

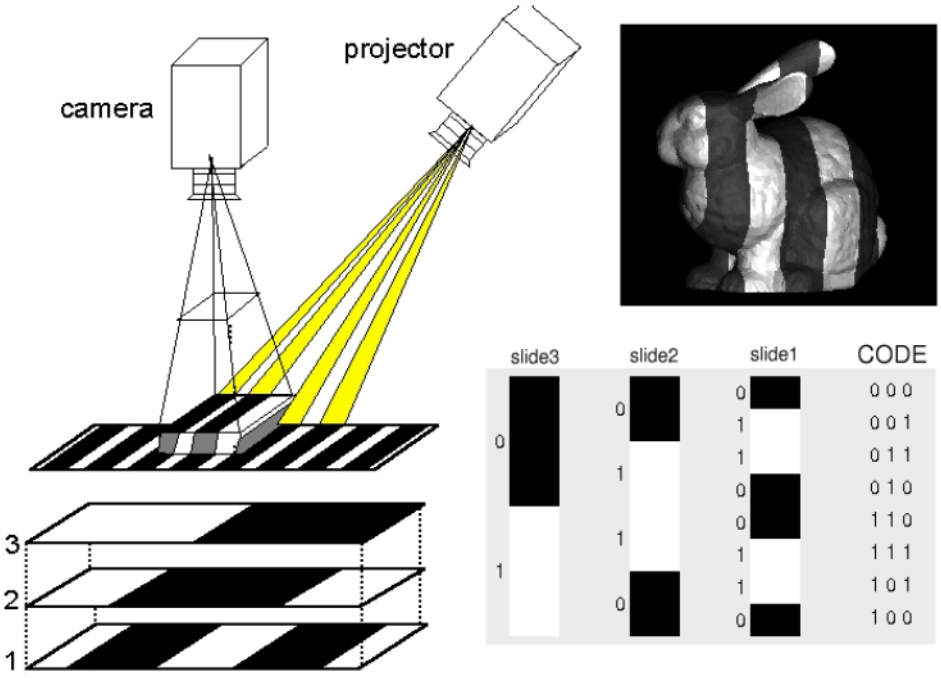

Figure 3.3: The temporal coding (Gray code)

The desire to overcome the restriction to obtain 3D depth information from the restrictions of static scene and to acquire dynamic scenes and also to reduce the number of projected slides leads to codes conveyed by a single slide or pattern. This required a large number of distinct projected patterns to

Classification of coded structured light approaches	
AXIS CODIFICATION	SCENE APPLICABILITY
Single Axis Both Axis	Static Scenes Moving Scenes
PIXEL DEPTH	CODING STRATEGY
Binary Gray Levels Colour	Periodical Absolute

Table 3.1: Classification of coded structured light approaches.

achieve the desired resolution, which is attained by use of neighbourhood of a pixel, known as spatial coding. Moigne et.al in [54] proposed the use of a grid pattern that is partially coded by dots used as landmarks, however, the limitation of this approach that, if some discontinuity on an object surface produces a discontinuity on imaged guidelines, the decoder can get lost. Morita et.al in [69] proposed to use light dots as an M-array code, as an extension to the coded array Vuylsteke in [103] proposed to make use of a coded window of 2×3 pixels to project a coded pattern to obtain the 3D depth and position.

In recent years coded structured light systems have been revisited by many researchers with the motivation to find a theoretical basis that could provide a better understanding of known methods, as well as make it possible to develop new improved systems [9], [110].

The classification on approaches of coded structured light for the 3D information can be obtained from table A.

The coded structured light methods are widely classified as represented in the table A. Of which some are briefly presented with the pattern structures used for getting 3D information of the surface on which the patterns were projected. However, the table 3.2 presents the classification of methods making use of coded structured light for 3D information of the surface on which they are projected. This includes the list of various research methods that fall under each of the classified category.

The table 3.2 presents various approaches that make use of camera-laser system. It is significant from the study of various coded structured lights to obtain the needed 3D information are promising, but then have a dependency on the high resolution image of the projected pattern and mostly have used perspective camera. Perspective is not suitable in our since it can not visu-

Classification of coded structured light		
TIME MULTIPLEXING	Binary codes	Posdamer et al. [82], Inokuchi et al. [50], Minou et al. Trobina [101], Valkenburg and McIvor [102], Skocaj and Leonardis [95], Rocchini et al. [85], ...
	n-ary codes	Caspi et al. [21], Horn and Kiryati [44], Osawa et al., ...
	Gray code + Phase shifting	Bergmann [12], Sansoni et al. [88], Wiora [106], Guhring [41], ...
	Hybrid methods	K. Sato [91], Hall-Holt and Rusinkiewicz [42], Wang et al., ...
SPATIAL CODIFICATION	Non-formal codification	Maruyama and Abe [58], Durdle et al. [30], Ito and Ishii [51], Boyer and Kak [14], Chen et al. [23], ...
	De Bruijn sequences	Hugli and Maître [46], Monks et al. [67], Vuylsteke and Oosterlinck [103], Salvi et al. [79], Zhang et al., ...
	M-arrays	Morita et al. [69], Petriu et al. [81], Kiyasu et al. [52], Spoelder et al. [97], Griffin and Yee [38], Morano et al. [68], ...
DIRECT CODIFICATION	Grey levels	Carrihill and Hummel [20], Chazan and Kiryati [22], Hung [47], ...
	Colour	Tajima and Iwakawa [98], Geng [36], Wust and Capson [107], T. Sato [92], ...

Table 3.2: Detailed classification of coded structured light

alise the pattern at low altitude and can not be utilised for VTOL and low altitude manoeuvring, thus we require something suitable with fish-eye camera. The second draw back in using a coded structured light comes in finding the pico projectors to project these coded structured light that needs to be strong enough to be sensed by the camera viewing them, which was not possible with small and light pico projectors and to achieve the strong intensity for the pattern to be captured required bulky projector that is not in line with our problem outline to have a light weight system. From the above discussion it was concluded to make use of the uncoded structured light projector available in the market. Thus we agreed to use a uncoded structured light source in the form of a red circle laser projector to be used in our active stereo system. This projector was less complicated to project the pattern and the set up was light in weight and with strong intensity to be traced by the camera unlike the pico projector. Also the captured image of the projected pattern did not require high resolution image to develop the relationship to estimate the 3D information required from the surface on which the pattern was projected.

In the following section we present the mathematical model developed using the laser-camera system on board the UAV to estimate the attitude and altitude of the UAV relative to the ground planar plane. The section on mathematical modelling 3.3 focuses mainly on two subsections: first one on algebraic method and the latter one on geometrical method.

3.2 Sensor System

It is very important to discuss our proposed sensor system before we develop our mathematical model. Since in the previous section it has been concluded to make use of an active stereo. The active stereo consists of one camera and a laser projector, that is our sensor system to be used for estimation of attitude and altitude of the UAVs. However, the discussion on the choice of the pattern is addressed later after we have justified the choice of the type of camera to be used in our system to estimate the attitude and altitude of UAVs. The figure 3.4 represents the scenario of using a camera with restrictive FOV, like perspective camera, where the pattern is visible at higher altitude but partially visible or absent at lower altitude. Thus, in order to have a pattern available at lower altitude it is important to increase the FOV. It is here the choice of

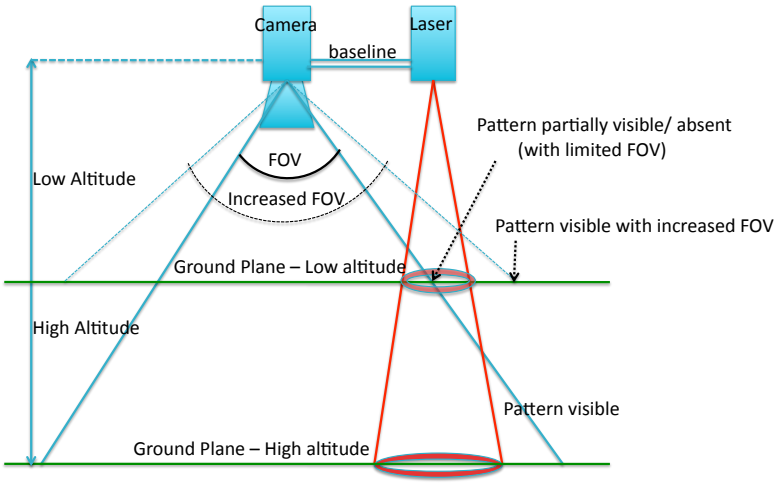

Figure 3.4: A representation for the advantage of large FOV (like Fish-eye) camera to perceive pattern at low altitude.

camera like fish-eye justifies to opt it over perspective camera. Using fisheye camera for this instance we can assure to have the pattern always available in the scene by the virtue of large FOV from the fish-eye.

Choice of pattern:

Of the various available patterns like grid, circle, concentric circles and rectangle projected patterns, we decided to make use of circular laser projected pattern. The reason for the choice is given below:

- Quick and easy to observe the variation in the shape deformation of the circle to ellipse from perfect horizontal to the slightest rotation across any of the axis (except yaw angle, where the circle will remain as it is).

- Accurate in calculations for variation in roll and pitch from circular pattern, thanks to knowledge about the deformation from the respective conic coefficients make it feasible to be accurate in calculation of the roll and pitch.

- Unlike the other patterns used for 3D reconstruction, where it requires multiple points. In our application to estimate the attitude and altitude

requires a fewer points than large number of points required in 3D reconstruction.

- The advantage of using this pattern over other patterns mentioned in the table (A) is because of it's lower computational cost. Our choice of pattern can easily be segmented by the virtue of its red colour intensity.

3.3 Mathematical Modelling

This section of the chapter deals with the mathematical modelling of the system. The mathematical model is an abstract model that uses mathematical language that will include set of equations to describe the behaviour of the system. The mathematical model is essential since it will demonstrate the procedures that have been followed in developing the mathematical model for the state estimation. The mathematical modelling procedures will take in to consideration to

It is important to sum up the points that were concluded in the previous chapter for the need of developing a new solution for which we develop the mathematical model. We are interested in finding a solution that can estimate the altitude d and attitude $\overrightarrow{n}$ of the UAV for application in vertical take off and landing (VTOL) and manoeuvre.

Mathematical modelling for our approach for the proposed solution. The model described in fig 3.5 has been developed with the environment definition. Firstly the world reference coordinate system W is fixed at an initial position namely (0,0,0) of whose X-Y plane be considered as the ground plane π on which the laser pattern be projected on, an assumption is made for the plane to be flat by human experience most places on the earth is flat or with very small variation except for the mountain terrain or man made structures. Secondly the camera coordinate system C for the fish-eye camera mounted on board the UAV. Since we use the fisheye camera it is essential to mention about the spherical camera model as proposed in [108]. Last is the laser coordinate system L. Since we wanted to have the laser pattern always available in the image scene the coordinate frames of camera and the laser, C and L respectively are aligned in the same orientation. However, their orientation with respect to the world coordinate frame W is rotated at 180° along the X-axis to make the camera-laser projector system look downwards to the ground

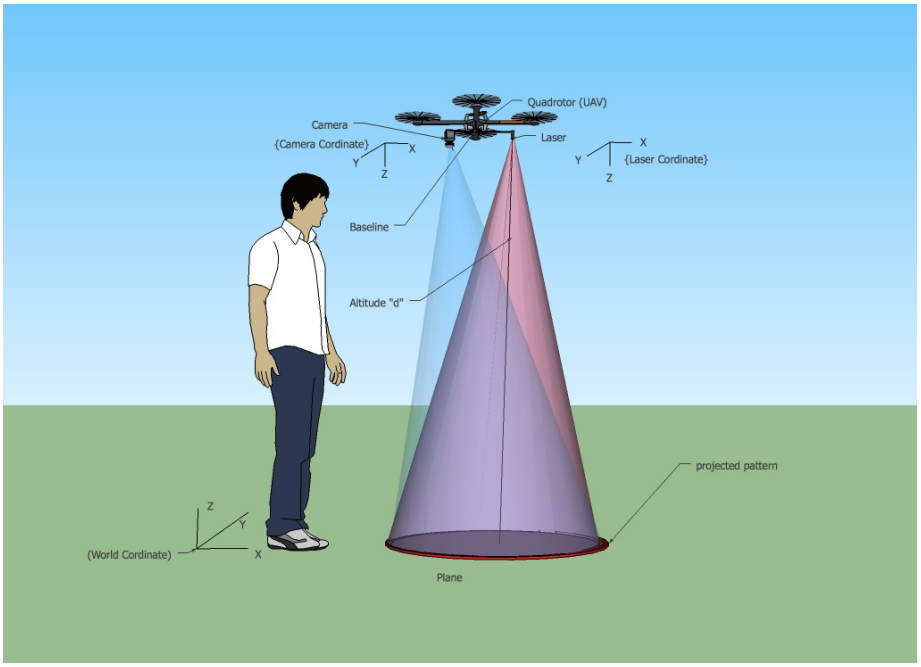

Figure 3.5: A representation of the depiction of the real world problem to be considered for the mathematical modelling.

plane. This alignment makes them keep the same X-axis along all the coordinate frames but reversing their Y and Z-axis in directly opposite to world coordinate frame W. Here the environment coordinates have been defined that in turn helps to directly relate the altitude of the UAV from the distance between the camera-laser system coordinate frames and the world coordinate frame.

For the development of a mathematical model there are always certain assumptions been made. These assumptions play a crucial role in realising the model, thus we also happen to make certain assumptions in the path of mathematical model development that has been explained here. The model has been developed with the consideration of the two normals: first from the surface plane on which the laser pattern is projected and the second from the laser head, do not coincide with each other. This assumption confirms that our active stereo sensor system always looks down towards the ground and not else where.

The experimental setup is described here for better understanding of the proposed solution. The setup consist of a fish-eye camera and a circle pattern laser projector mounted on a fixed baseline b. The camera C and the laser L

coordinate systems are aligned making them to differ only by a small translation distance b_1 along the X axis. The distance b_1 since the baseline b consists of three components b_1, b_2 and b_3 for their XYZ axis respectively as shown in figure 3.6.

Where π represents the ground plane on which the circular laser pattern is projected and $\overrightarrow{n}$ is the normal of this plane, X_L represents the 3D points in Laser coordinate system. X_C represents the 3D points in Camera coordinate system. X_s represents the 2D points in the spherical image plane.

The known parameters are: coordinate frames and their alignment, baseline b, the rotation between the coordinate frames and the open angleθ of the laser pattern projector .

The unknown parameters that we are interested to find: normal $\overrightarrow{n}$ of the plane with the projected pattern for the attitude and altitude d as the distance of the camera-laser system from the plane.

We present our proposed solution for state (altitude and attitude) estimation using the two models: one based on algebraic solution and the other based on geometrical solution.

3.3.1 Algebraic Model

Modeling the conic equation for laser projected circular profile on to the spherical image

The projected laser circle on the ground plane is perceived by the camera as a quadratic on the spherical image model. The key idea from this approach lies in comparing the two equations of quadratic $\mathbf{Q}$ on the spherical image models: one from the circle pattern on the ground plane perceived by the camera as represented in figure 3.6 and the other one from the intersection of the unit sphere with the cone as represented by figure 3.7

X_L, X_C, R and b represent the 3D points in Laser and Camera coordinate system and the rotation and the baseline respectively.

Mathematically the plane on which the laser pattern projector casts the conic is defined as

$$X_L.\overrightarrow{n} + d = 0 \tag{3.1}$$

on the laser frame.

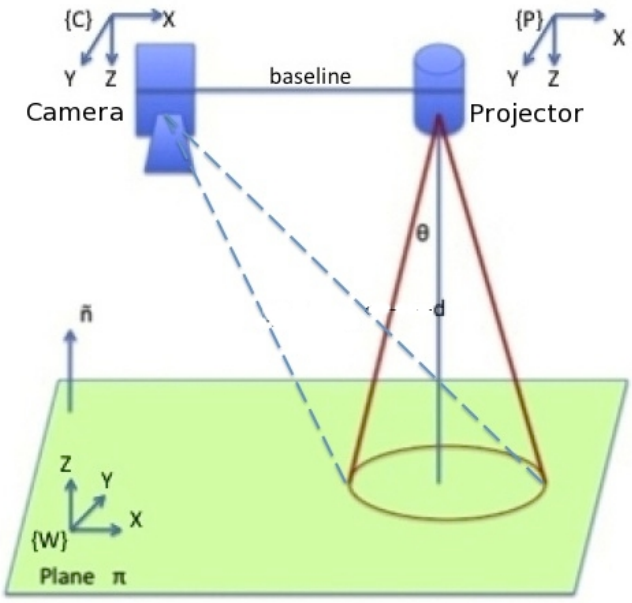

Figure 3.6: The projected red circle on ground plane as perceived by the camera, a quadratic Q on its spherical image model.

Our goal is to determine the values for d and $\overrightarrow{n}$. The d determines the distance of the system from the plane on which the laser pattern is cast, where as the $\overrightarrow{n}$ determines the pose or attitude of the system.

The conic envelope intersecting the plane to form a conic section on the plane π in terms of the Laser coordinate system is given by

$$\{x_L^2 + y_L^2 = z_L^2 tan^2\theta\} \tag{3.2}$$

The θ is the opening angle of the laser projector.

The 3D laser point in terms of camera coordinate is given by the relation

$$X_C = RX_L + b$$

With the assumption been made the rotation to be identity ($R = I$). The 3D laser point in terms of camera coordinate is given by the relation

$$X_L = X_C - b \tag{3.3}$$

We also have the relation between the plane and the camera points by substituting eqn (3.3) in eqn (3.1), thus plane is defined in terms of camera points. as stated below

$$(X_C - b).\overrightarrow{n} + d = 0 \tag{3.4}$$

Now since the normal vector is composed of three components in the respective coordinates axis of X,Y,Z .

$$\overrightarrow{n} = [n_1, n_2, n_3]$$

Upon expanding in term of individual components of the normal, it results in

$$(x_c - b_1)n_1 + (y_c - b_2)n_2 + (z_c - b_3)n_3 + d = 0 \tag{3.5}$$

With the assumption based upon the system the Camera and Laser coordinate systems are alligned, resulting that the components on base line b, as follows

$$b_1 \neq 0, b_2 = b_3 = 0$$

this results in to the eqn (3.5) to be as,

$$x_c n_1 - b_1 n_1 + y_c n_2 + z_c n_3 + d = 0 \tag{3.6}$$

The resulting eqn (3.6) defines the plane in terms of camera points on which the pattern is projected.

$$X_s = \lambda X_c \tag{3.7}$$

where

$$\begin{cases} x_s = \lambda x_c \\ y_s = \lambda y_c \\ z_s = \lambda z_c \end{cases}$$

Thus making eqn (3.6) to be as follows

$$\begin{aligned} &x_s n_1 - \lambda b_1 n_1 + y_s n_2 + z_s n_3 + \lambda d = 0 \\ &\lambda = \tfrac{-(x_s n_1 + y_s n_2 + z_s n_3)}{d - b_1 n_1} \end{aligned} \tag{3.8}$$

Since the conic on the ground plane is perceived by the camera in the

form of a cone with it's vertex being the optical centre of the camera, thus the equation of cone in 3D in terms of camera points can be obtained by substituting the eqn (3.3) in eqn (3.2), it results in

$$(x_c - b_1)^2 + (y_c - b_2)^2 - (z_c - b_3)^2 tan^2\theta = 0 \tag{3.9}$$

The equation of this cone in 3D in terms of spherical points can be obtained by substituting the eqn (3.7) in eqn (3.9) with the consideration that

$$b_1 \neq 0, b_2 = b_3 = 0$$

, it results in

$$(x_s - \lambda b_1)^2 + y_s^2 - z_s^2 tan^2\theta = 0 \tag{3.10}$$

$$x_s^2 + \lambda^2 b_1^2 - 2\lambda b_1 x_s + y_s^2 - z_s^2 tan^2\theta = 0 \tag{3.11}$$

substituting the value of λ from eqn (3.8) in eqn (3.11)

$$\begin{aligned} &x_s^2 + (\tfrac{-(x_s n_1 + y_s n_2 + z_s n_3)}{d - b_1 n_1})^2 b_1^2 - 2\tfrac{-(x_s n_1 + y_s n_2 + z_s n_3)}{d - b_1 n_1} b_1 x_s \\ &+ y_s^2 - z_s^2 tan^2\theta = 0 \end{aligned} \tag{3.12}$$

$$\begin{aligned} &x_s^2 + \tfrac{(n_1^2 b_1^2 x_s^2 + n_2^2 b_1^2 y_s^2 + n_3^2 b_1^2 z_s^2 + 2n_1 n_2 b_1^2 x_s y_s + 2n_1 n_3 b_1^2 x_s z_s + 2n_2 n_3 b_1^2 y_s z_s}{(d - b_1 n_1)^2} \\ &+ \tfrac{(2b_1 n_1 x_s^2 + 2b_1 n_2 x_s y_s + 2b_1 n_3 x_s z_s)}{d - b_1 n_1} + y_s^2 - z_s^2 tan^2\theta = 0 \end{aligned} \tag{3.13}$$

$$\begin{aligned} &(d - b_1 n_1)^2 x_s^2 + (n_1^2 b_1^2 x_s^2 + n_2^2 b_1^2 y_s^2 + n_3^2 b_1^2 z_s^2 \\ &+ 2n_1 n_2 b_1^2 x_s y_s + 2n_1 n_3 b_1^2 x_s z_s + 2n_2 n_3 b_1^2 y_s z_s \\ &+ (d - b_1 n_1)(2b_1 n_1 x_s^2 + 2b_1 n_2 x_s y_s + 2b_1 n_3 x_s z_s) \\ &+ (d - b_1 n_1)^2 y_s^2 - (d - b_1 n_1)^2 tan^2\theta z_s^2 = 0 \end{aligned} \tag{3.14}$$

$$\begin{aligned} &d^2 x_s^2 + [n_2^2 b_1^2 + (d - b_1 n_1)^2] y_s^2 \\ &+ [n_3^2 b_1^2 - (d - b_1 n_1)^2 tan^2\theta] z_s^2 + [2b_1 n_2 d] x_s y_s \\ &+ [2b_1 n_3 d] x_s z_s + [2b_1^2 n_2 n_3] y_s z_s = 0 \end{aligned} \tag{3.15}$$

we talk now about the quadratic on the spherical image obtained through the fisheye camera, which is obtained directly on the spherical image. To show this the general equation of a quadratic can be obtained upon the intersection

of a general cone other than the laser projected cone and unit sphere.

Analytical Equation Of Intersection Of A Unit Sphere :

To determine an analytical equation of the intersection **Q** between the unit sphere and a cone whose apex is the origin as represented in the figure 3.7.

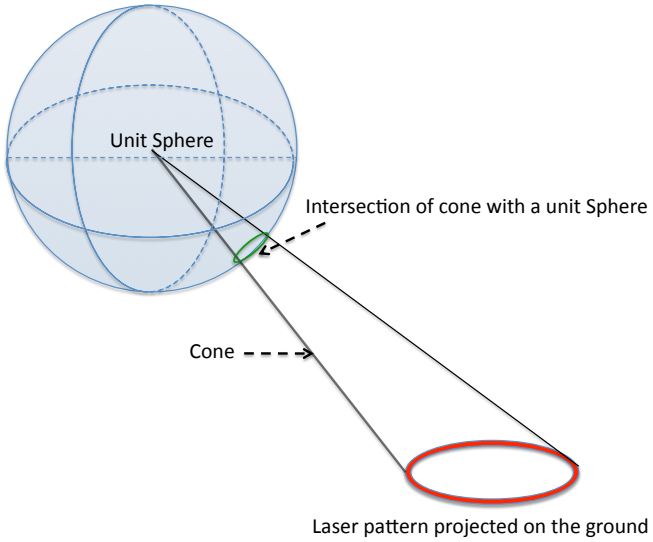

Figure 3.7: The intersection of unit sphere with a cone resulting in the quadratic Q in green colour.

Let us consider an quadric $\mathcal{E}$ centred at $T = (T_x, T_y, T_z)^T$:

$$\frac{(X - T_x)^2}{a^2} + \frac{(Y - T_y)^2}{b^2} + \frac{(Z - T_z)^2}{c^2} = 1 \tag{3.16}$$

and let us consider a 3D plane $\mathcal{P}$ passing through T of normal $n = (n_x, n_y, n_z)^T$:

$$n.P = n.T \tag{3.17}$$

where $P = (X, Y, Z)^T$ is a 3D point.
We define a 3D ellipse $\mathcal{C}$ as the intersection between $\mathcal{E}$ and $\mathcal{P}$:

$$\mathcal{C} = \mathcal{E} \cap \mathcal{P} \tag{3.18}$$

Thus, we can define an oblique cone $\mathbf{C}$ whose apex is the origin as follows :

$$\mathbf{C} = \{\lambda P, \quad P \in \mathcal{C}\} \tag{3.19}$$

Let us note, $P_s = (x_s, y_s, z_s)$ a point on quadratic $\mathbf{Q}$.
$\exists \lambda | P_s = \lambda P, \quad P \in \mathbf{C}$.
Then, eq 3.16 :

$$\frac{(x_s - \lambda T_x)^2}{a^2} + \frac{(y_s - \lambda T_y)^2}{b^2} + \frac{(z_s - \lambda T_z)^2}{c^2} = \lambda^2 \tag{3.20}$$

eq 3.16 :

$$\lambda = \frac{n.P_s}{n.T} \tag{3.21}$$

Thus, if we substitute 3.21 in 3.20, we obtain :

$$Jx_s^2 + Ky_s^2 + Lz_s^2 + 2Mx_sy_s + 2Nx_sz_s + 2Oy_sz_s = 0, \tag{3.22}$$

where

$$\begin{cases} J = \frac{1}{a^2} - \frac{2}{a^2}\frac{n_1 T_x}{n.T} + \frac{n_1^2}{(n.T)^2}(\frac{T_x^2}{a^2} + \frac{T_y^2}{b^2} + \frac{T_z^2}{c^2} - 1) \\ K = \frac{1}{b^2} - \frac{2}{b^2}\frac{n_2 T_y}{n.T} + \frac{n_2^2}{(n.T)^2}(\frac{T_x^2}{a^2} + \frac{T_y^2}{b^2} + \frac{T_z^2}{c^2} - 1) \\ L = \frac{1}{c^2} - \frac{2}{c^2}\frac{n_3 T_z}{n.T} + \frac{n_3^2}{(n.T)^2}(\frac{T_x^2}{a^2} + \frac{T_y^2}{b^2} + \frac{T_z^2}{c^2} - 1) \\ M = \frac{n_1 n_2}{(n.T)^2}(\frac{T_x^2}{a^2} + \frac{T_y^2}{b^2} + \frac{T_z^2}{c^2} - 1) - \frac{T_x n_2}{(an.T)^2} - \frac{T_y n_1}{(bn.T)^2} \\ N = \frac{n_1 n_3}{(n.T)^2}(\frac{T_x^2}{a^2} + \frac{T_y^2}{b^2} + \frac{T_z^2}{c^2} - 1) - \frac{T_x n_3}{(an.T)^2} - \frac{T_z n_1}{(cn.T)^2} \\ O = \frac{n_2 n_3}{(n.T)^2}(\frac{T_x^2}{a^2} + \frac{T_y^2}{b^2} + \frac{T_z^2}{c^2} - 1) - \frac{T_y n_3}{(bn.T)^2} - \frac{T_z n_2}{(cn.T)^2} \end{cases} \tag{3.23}$$

$\mathbf{Q}$ can be modeled by :

$$Jx_s^2 + Ky_s^2 + Lz_s^2 + 2Mx_sy_s + 2Nx_sz_s + 2Oy_sz_s = 0, \tag{3.24}$$

The analytical equation of this intersection is a quadric with 7 coefficients. We can note that there is no constant term thus we are left with 6 coefficients.

J to O are the coefficients of the quadratic obtained by carrying out quadratic fitting on the spherical image.

Upon having obtained the two equations of the conics from the two cases: one from the circle pattern on the ground plane perceived by the camera as represented by equation (3.15) and the other one from the intersection of the unit sphere with the cone as represented by equation (3.24) . The comparison of these two equations representing their respective conic is well visualised in figure 3.8 .

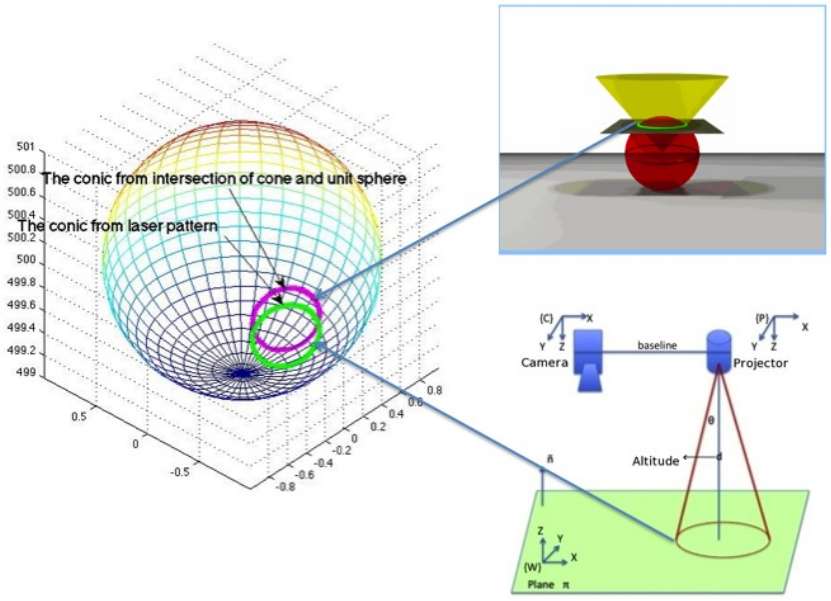

Figure 3.8: Comparison of the two conics: one from conic on the spherical image as perceived by the camera (in green) and the other from the intersection of unit sphere with cone (in magenta)

We now compare the equation (3.15) and equation (3.24) to achieve the goal to estimate the attitude and altitude from the conics normal $\overrightarrow{n}$ of the plane with the projected pattern for the attitude and altitude d .

$$\frac{K}{J} = \frac{[n_2^2 b_1^2 + (d - b_1 n_1)^2]}{d^2} \tag{3.25}$$

$$\frac{L}{J} = \frac{[n_3^2 b_1^2 - (d - b_1 n_1)^2 tan^2\theta]}{d^2} \tag{3.26}$$

$$\frac{M}{J} = \frac{b_1 n_2}{d} \tag{3.27}$$

$$\frac{N}{J} = \frac{b_1 n_3}{d} \tag{3.28}$$

$$\frac{O}{J} = \frac{b_1^2 n_2 n_3}{d^2} \tag{3.29}$$

$$\frac{K}{J} = \frac{n_2^2 b_1^2}{d^2} + (1 - \frac{b_1 n_1}{d})^2 \tag{3.30}$$

$$\frac{K}{J} = (\frac{M}{A})^2 + (1 - \frac{b_1 n_1}{d})^2 \tag{3.31}$$

Let $\frac{b_1 n_1}{d} = G$, where G is variable depending upon the unknowns n_1 and d

$$\frac{b_1 n_1}{d} = G \tag{3.32}$$

$$\frac{K}{J} = (\frac{M}{J})^2 + (1 - G)^2 \tag{3.33}$$

thus now the relation can be rewritten as follows after solving for G. This results in 2 solutions for G.

$G = \frac{(2 \pm \sqrt{4 - 4(1 + \frac{K}{J} - (\frac{M}{J})^2)})}{2}$

$G = \frac{2(1 \pm \sqrt{1 - (1 + \frac{K}{J} - (\frac{M}{J})^2)})}{2}$

$$G1 = (1 + \sqrt{\frac{K}{J} - (\frac{M}{J})^2}) \tag{3.34}$$

$$G2 = (1 - \sqrt{\frac{K}{J} - (\frac{M}{J})^2}) \tag{3.35}$$

We find two solutions of G, which is mainly due to the solutions available from the two planes: one from horizontal and other one from the vertical plane that posses the conic with same coefficients. As was defined in the assumption about the consideration of the normal of the plane and the laser head to look at each other to assure the plane is horizontal ground plane and not the vertical plane where the normals are orthogonal to each other. we are interested in the value of G that comes from the horizontal plane, since the correct value of G leads to the estimate the altitude d which is above the plane, thus positive

value of G2 for this instance is considered for further calculation of unknowns. So we make use of the relationship developed above. We squared and add the equations (3.32), (3.27) and (3.28) thus we generate:

$$G^2 + (\frac{M}{J})^2 + (\frac{N}{J})^2 = (\frac{b_1 n_1}{d})^2 + (\frac{b_1 n_2}{d})^2 + (\frac{b_1 n_3}{d})^2 \tag{3.36}$$

which gives us,

$$G^2 + (\frac{M}{J})^2 + (\frac{N}{J})^2 = (\frac{b_1}{d})^2 (n_1^2 + n_2^2 + n_3^2) \tag{3.37}$$

since we have unit normal vector n, i.e $(n_1^2 + n_2^2 + n_3^2) = 1$, so we now have

$$G^2 + (\frac{M}{J})^2 + (\frac{N}{J})^2 = (\frac{b_1}{d})^2 \tag{3.38}$$

$$d^2 = \frac{(b_1)^2}{(G)^2 + \frac{M^2}{J^2} + \frac{N^2}{J^2}} \tag{3.39}$$

$$d^2 = \frac{(b_1)^2}{\frac{(G*A)^2 + M^2 + N^2}{J^2}} \tag{3.40}$$

$$d^2 = \frac{(b_1 * J)^2}{(G * J)^2 + M^2 + N^2} \tag{3.41}$$

$$d1 = \sqrt{\frac{(b_1 * J)^2}{(G1 * J)^2 + M^2 + N^2}} \tag{3.42}$$

or

$$d2 = \sqrt{\frac{(b_1 * J)^2}{(G2 * J)^2 + M^2 + N^2}} \tag{3.43}$$

depending upon the positive value of G selected.

Since we know that from the relationship of $G = \frac{b_1 n_1}{d}$, we can obtain normal component n_1,

$$n_1 = \frac{Gd}{b_1} \tag{3.44}$$

thus similarly for the values of n_2 and n_3 can be obtained from the previous relations developed.

$$n_2 = \frac{M}{J}\frac{d}{b_1} \tag{3.45}$$

$$n_3 = \frac{N}{J}\frac{d}{b_1} \tag{3.46}$$

We estimate the values of distance d and normal $\overrightarrow{n}$ of the plane that help us to estimate the altitude and attitude respectively.

Since it was observed the two solutions of G as a result from the two planes: one from the horizontal and the other one from the vertical plane that have the conic on each with the same coefficients. However, as was mentioned in the beginning the assumption about having the normals of the plane and the laser head to look at each other, which was mainly to assure the plane is horizontal plane that is considered for the calculation and not the vertical plane. The two solutions of G result in two solutions of distance d and normal $\overrightarrow{n}$ of the plane. Thus, It is important to consider the correct horizontal plane that leads to the correct estimation of the distance d for altitude and normal $\overrightarrow{n}$ for the attitude of the UAVs with the sensor system above this plane π.

3.3.2 Geometrical Model

The approach to estimate the state of the UAV making use of our camera-laser system we were interested to develop the solution based on geometrical approach. The mathematical model development has been discussed in the following section.

The circular pattern from the laser projector is visualised as a conic on the unit sphere of the camera model. Since all the points that belong to the conic converge to the centre of the sphere to form a cone. This appears as an intersection of the camera model unit sphere with a cone, making the centre of sphere as the vertex of the camera cone C subtended by the conic c on the ground plane, whereas the projector that subtends the same conic c on the ground plane forms the cone D as presented in the figure 3.9.

The cone C is visualised from the conic section resulted by the intersection between a unit sphere and the cone is given by the eqn (3.47) as developed in the analytical equation of intersection of a unit sphere in section 3.3.1.

$$Jx_s^2 + Ky_s^2 + Lz_s^2 + 2Mx_sy_s + 2Nx_sz_s + 2Oy_sz_s = 0, \tag{3.47}$$

where J to O are the coefficients of conic obtained by carrying out a conic

fitting on spherical image. Figure 3.9 helps us to visualise it geometrically as a problem of intersection of two cones: one from the camera cone C and the other from the projector cone D. These cones C and D from their respective optical centres, intersect with the ground plane to generate a quadrics Q defined as:

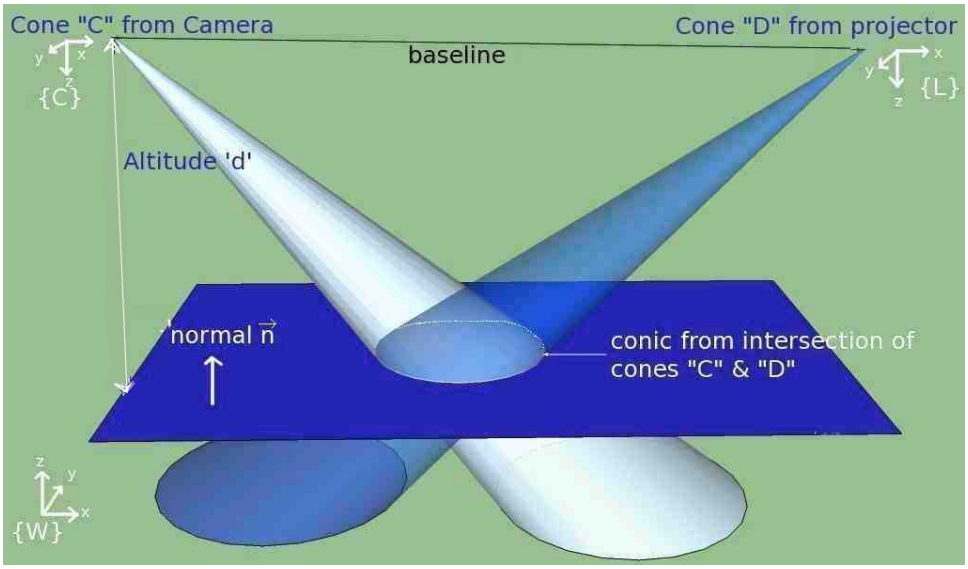

Figure 3.9: A representation of the model for the development of the mathematical model by geometrical approach

$$Q = xC + (1 - x)D \tag{3.48}$$

The quadric "Q" is in general of rank 4. As from the mathematical of family of quadratics it postulates that the quadratic defines a cone, if the matrix "Q" possesses rank 3. Rank 2 defines a pair of planes, whereas rank 1 defines a double plane as explained by Peternell in 1998 in his work [80]. We try to find the ground plane and thus find the determinant of the matrix representing the quadratic that reduces it to quadratic polynomial in x. Since we know the two roots with values of x, for [$x = 0$ and $x = 1$] that reduces the rank of quadratic Q to 3 realising a cone D and cone C for the respective solutions of x [$x = 0$ and $x = 1$]. One of the two solutions correspond to the plane pair. Further when these two cones C and D intersect to give a third degenerate quadric of rank 2 that means there exists a pair of planes on which the cones intersect.

For the estimation process we assume the ground is a plane such that the projector projects a circle that traces out a conic c on the ground, that is seen by the camera. From this information, together with the calibration of the camera projector, the goal is to determine the altitude and attitude of the system relative to the ground plane. We propose an algorithm for finding the ground-plane and may thus be constructed as follows.

1. Determine all x with $det(Q) = 0, (rankQ \leq 3)$. The latter is a quartic polynomial in x. Since we already know two of its roots (0 and 1), we can reduce the problem to solving a quadratic polynomial in x. One of the two solutions corresponds to the plane-pair.

2. The plane-pair is now represented by a 4×4 symmetric matrix Q. Let U and V be the two planes we wish to extract from Q. To do so, let us note that the 4×4 matrix representing the plane-pair U and V , is given by:

$$Q \sim VU^t + UV^t = (V\ U) \begin{pmatrix} U^t \\ V^t \end{pmatrix} \tag{3.49}$$

   The two planes can thus be extracted from Q, by applying an SVD on it and retrieving the two singular vectors corresponding to non-zero singular values.

3. The ground-plane is the one of the two planes relative to which the optical centres lie on the same side. Whereas the second plane passes in general between the optical centres.

Let Q be a rank-2 symmetrix 4×4 matrix and let the following be its SVD:

$$Q = (A\ B \vdots \vdots)\text{diag}(s_1, s_2, 0, 0) \begin{pmatrix} \pm A^T \\ \pm B^T \\ \cdots \\ \cdots \end{pmatrix} \tag{3.50}$$

where s_1 and s_2 are the two non-zero singular values and A and B the associated singular vectors. Hence, we can write:

$$Q = \pm(s_1 AA^T - s_2 BB^T) \tag{3.51}$$

We determine the two planes U and V that form the quadric. Thus U and V satisfy:

$$\begin{aligned} UV^T + VU^T &\sim Q \\ &\sim s_1 AA^T - s_2 BB^T \end{aligned} \tag{3.52}$$

The two planes must be linear combinations of the singular vectors A and B, for example:

$$\begin{aligned} U &= uA + B \\ V &= vA + B \end{aligned} \tag{3.53}$$

We thus need to determine *u* and *v*. We use equation (3.52):

$$UV^T + VU^T = (uA+B)(vA+B)^T + (vA+B)(uA+B)^T \sim s_1 AA^T - s_2 BB^T \tag{3.54}$$

Let us expand this:

$$\begin{aligned} &2uvAA^T + 2BB^T + (u+v)AA^T + (u+v)BB^T \\ &\sim s_1 AA^T - s_2 BB^T \end{aligned} \tag{3.55}$$

thus

$$u + v = 0 \tag{3.56}$$

Hence:

$$v = -u \tag{3.57}$$

Inserting this in the above equation:

$$-2u^2 AA^T + 2BB^T \sim s_1 AA^T - s_2 BB^T \tag{3.58}$$

This is valid for

$$u^2 = \frac{s_1}{s_2} \tag{3.59}$$

Finally, the two planes are

$$U = \sqrt{\frac{s_1}{s_2}} A + B \tag{3.60}$$

$$V = -\sqrt{\frac{s_1}{s_2}}A + B \tag{3.61}$$

From the obtained pair of planes U and V, it is the ground plane that we are interested in, to which the optical centres of the camera and the laser projector lie on the same side. We deduce the altitude and the attitude by solving from the plane which includes both the vertices of the cone modelled as laser cone and the other being the camera cone, V being the said plane in this case.

$$Roll = acos(\frac{V(3)}{\sqrt{V(1)^2 + V(3)^2}}) * \frac{180}{\pi} \tag{3.62}$$

$$Pitch = acos(\frac{V(3)}{\sqrt{V(2)^2 + V(3)^2}}) * \frac{180}{\pi} \tag{3.63}$$

and

$$Altitude = abs(V(4)/\sqrt{V(1)^2 + V(2)^2 + V(3)^2}) \tag{3.64}$$

Thus the conic coefficients helped us to determine the two respective cones: one for the camera and the other for the laser. Upon determining the ground plane we obtained the plane on which this conic lies with its corresponding cone's height determines the altitude. From the ground plane we determined the attitude.

Conclusion

After the survey on structured light to obtain the 3D information needed from a surface, it was noticed that use of active stereo vision system alleviated the correspondence problem based on the structures light concept, projecting a given pattern on the measuring surfaces. It helped justify our camera-laser setup for our devised solution's mathematical model based on: first with the algebraic model and second with the geometrical model. The two mathematical models developed presented the relations on estimating the attitude and altitude of the UAV relative to the plane on which the uncoded structured pattern was projected.

The following chapter will deal on the calibration of the system used with the development of the algorithm that can be used to implement the solution in real application on board the UAVs.

Chapter 4

Calibration & Algorithms

This chapter on calibration and algorithms developed, from the respective mathematical models: one from algebraic and other one from geometrical approach as discussed in chapter 3, will present the necessary steps involved in performing the experiments for real time and also for near to real simulation results by using the calibration values obtained from real setup to be used.

4.1 Calibration

To start with implementation of the solution to any physical problem, it is a very essential step to calibrate the sensors one uses for their accuracy and repeatability of the solution. So one would like to know "what is calibration" ?

Calibration is the setting or correcting of a measuring device or base level, usually by adjusting it to match or conform to a dependably known and unvarying measure.

To begin with the experimental verification of the theory developed it is very important to attain the assumptions made, which initially is the alignment of the laser head and camera with only a fixed baseline with no rotation between the two. This is very essential in our approach because a small rotation introduced on the stereo camera- laser rig will eventually add for a large rotation angle error. This increase in rotational error is introduced with the increase in the distance between the system and the ground plane.

To avoid this additional error to be added to our final estimation, it is very crucial to have the system perfectly aligned. This includes the following

[] []

Figure 4.1: The spirit bubble level of two kinds as shown (a) analog, (b) digital

approaches.

- Mechanical alignment of the camera-laser system.
- Laser calibration.
- Camera calibration.

4.1.1 Camera-Laser Alignment

The process of mechanically aligning the camera-laser system involves a very basic and simple trick. On a rigid fixed baseline with a significant length is used to set-up our experimental set-up, it is very important to make sure the baseline is not too small to be used. At one end we fix the camera, whereas on the other we fix the laser projector. Keeping the entire setup on a levelled work bench. We start to test for the alignment for the perfect horizontal alignment of the camera and the laser individually keeping in mind that no or almost no rotation to be introduced between themselves.

A simple spirit bubble level with marker was used to align the system as shown in the figure 4.1. Since the camera-laser rig placed on the mechanical levelled work bench makes sure the baseline is perfectly horizontally aligned with the work bench. Individually checking with the spirit bubble level the vertical and horizontal alignment. The spirit bubble level ensures that if individually first the camera and later the laser is perfectly vertically aligned to the rigid baseline by showing the correct reading from the spirit bubble. This simple step ensures to avoid the additional rotational angle to be introduced in the alignment. This step ensures the rotation between the camera and the

Figure 4.2: The laser projector used for the experiment.

laser to be identity, keeping their coordinates aligned to each other, and the leaving only a translation which is equal to the length of the baseline.

4.1.2 Laser Projector Calibration

The end application of our method had to be carried on board the UAV, it was essential to decide upon the laser to be used. The laser had to be decided keeping certain requirements into consideration, which included the laser to be:

- light in weight,
- consume less power for operation,
- required less power to trigger,
- not harmful to eyes for operation despite its high intensity (Class II).

Figure 4.2 represents the laser used for this purpose and satisfied the above requirements. Laser calibration step involved the following procedure.

The laser system is aligned on the optical bench. The optical bench is fit with an adjustable rail with pre-etched distance readings. A white plane board

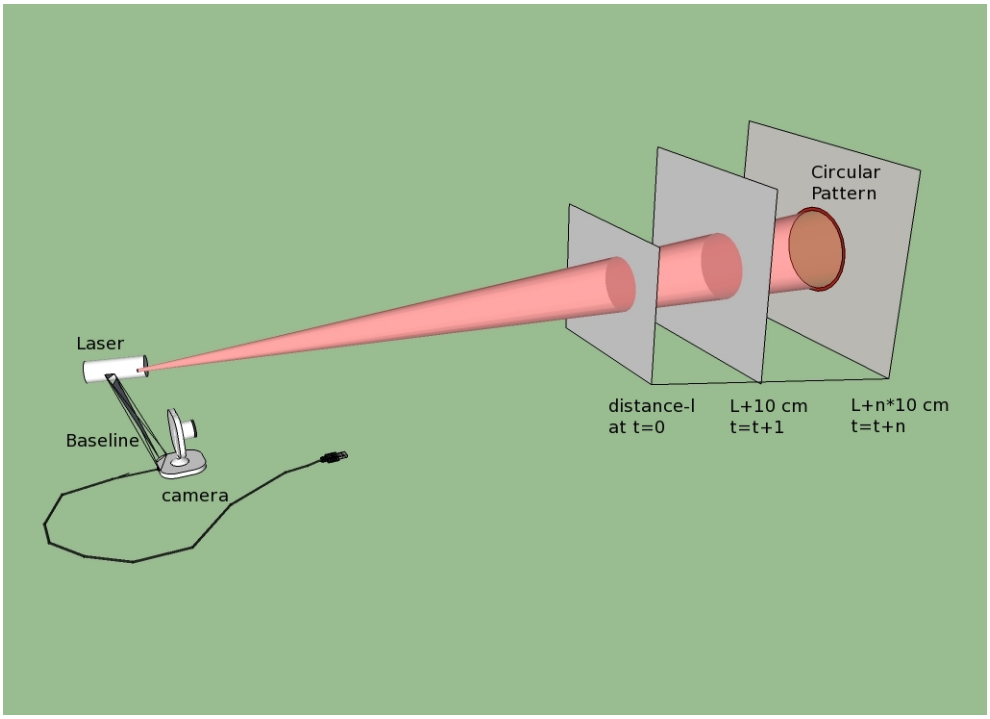

Figure 4.3: The laser projector calibration by moving the plane of projection in regular interval of distance with progressing steps for calibration.

is mounted vertical on the rail placed at a marked distance making sure the circular laser pattern is available on the board, moved until the end of the rail.

The laser circular pattern is projected on white plane board on an adjustable rail. The measurement of the radius (the distance between the centre spot till the circumference of the projected circle) of the circular pattern is noted from a fixed distance from the laser projector. The measurement is repeated upon moving the white board $10cm$ further away on the rail from the laser projector. This step is carried out for 10 readings at equal intervals of $10cm$ away from the laser projector as represented in the figure 4.3. This is carried out to verify the open angle of the laser with the manufacturer's provided value, which plays an important role in the estimation process. This step eliminates possible introduction of error from the laser projector.

4.1.3 Camera Calibration

The camera calibration depends the modelling and only then later finding the numeric value of every camera parameter. The modelling of the camera

involves mainly the following:

- Determine the equation that approximates the camera behaviour.
- Define the set of unknowns in the equation (camera parameters).
- The camera model is an approximation of the physics & optics of the camera.

Camera calibration is primarily, finding the quantities internal to the camera that affect the imaging process

- Position of image centre in the image,
- Focal length,
- Different scaling factors for row pixels and column pixels,
- Skew factor,
- Lens distortion (pin-cushion effect).

It is important when we need to reconstruct a world model or even to interact with the world. It is also because the camera pixels are not necessarily square. Inexpensive single lens systems distort image at its periphery but compound lenses may be used to reduce chromatic effects and pin-cushion effects. There exist variety of techniques to achieve the camera calibration. Some camera calibration techniques are specific to the choice of lens used.

In our experiments we performed the camera calibration for the two type of lens decided to be used for the application: the first one for the perspective camera and the other one for the fish-eye lens. The detailed description on calibration process is out of scope of this research work. However, for detailed understanding by the readers can be obtained from the work of Zhang on calibration in [111] and on the Christopher Mei's work on the calibration tool box used for central catadioptric cameras [60]. Similar is proposed by Bouguet's calibration tool box for the perspective cameras.

The camera calibration tool box implemented to identify the internal and the external parameters is the Christopher Mei's camera tool box. This tool box was practical, since it gave us the opportunity to implement it for the fish-eye camera. The results from the calibration were not only used for the

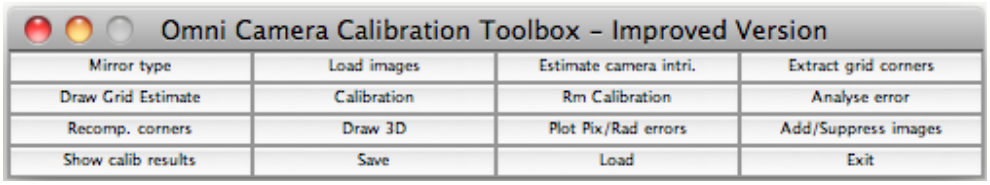

Figure 4.4: The toolbox used for calibration of the camera (Christopher Mei's calibration tool box).

implementation on the real time system but also for the results based on simulation to have the simulated result more closer to real time application.

Following were the steps involved to calibrate. Upon having installed the Mei's tool box, we start the tool box for the selection of the mirror type used in our case fisheye as shown in figure 4.4. The later stage is of loading the images captured from the camera into the toolbox to be used for calibration step. Estimating the camera intrinsic parameter and the grid corners, finally the estimated values of the parameters are obtained.

We have seen the calibration of the camera and then the calibration of the laser projector. We also performed the step to align the camera and the laser. However, it is important to verify if the optical axis of the camera and the projector are aligned to have no rotation. This step of verification if carried out on a fixed table with marking aligned to be orthogonal to the laser projector, on which the checker board would be moved, keeping the projected grid from the laser projector aligned with the checker board grids as represented on the figure 4.5. The idea of aligning the laser grid pattern projected on to the calibration checked board makes sure the optical axis of laser to be orthogonal to the board, whereas the checker board pattern is used for calibration of the camera. Upon calibration the 3D reconstruction of checkerboard with respect to the camera will give the rotation between the board and camera to be orthogonal. Since the checker board being orthogonal from the camera verifies the optical axis of the camera and laser being orthogonal attesting the rotation being identity between the camera and laser. This satisfies the assumption made earlier in the mathematical modelling.

Figure 4.5: The steps to verify for the optical axis of the camera and laser are aligned to each other, it confirms the rotation between the two to be identity.

4.1.4 Baseline Measurement

The baseline measurement might sound simple and an easy step by estimating the distance between the camera and the laser projector. However, it is very essential that the measurement be as accurate as possible. Since calculations for the baseline based on manual estimation can not be accurate and thus to avoid the error induced by the wrong baseline value, baseline being very crucial in the estimation of the desired normal of the plane for attitude ultimately. Computer vision based estimation of baseline was used to be accurate. The method to estimate the baseline is carried out as the calibration stage, where we align the UAV with our vision system fixed under the UAV in a perfect horizontal position mounted on a vertical mount. To assure the perfect horizontal alignment we place a bullś eye spirit level. We then project the circular laser pattern with its centre on the calibration pattern, since we know the exact measurement of the calibration pattern board and its corresponding pixels values in the corresponding image. A simple distance calculation formula between the image centre and the laser pattern projector centre gives the baseline measurement.

For a better understanding an example has been presented: the principal points from the calibration is (363.92, 238.83) the point of central projection from the laser is (274.0, 244.1) thus the distance between the two points in pixels is given by simple distance formula between points.

$$\sqrt{(363.92 - 274.0)^2 + (238.83 - 244.1)^2} = 90.08 \tag{4.1}$$

Thus, we have baseline in pixel points as 90.08 *pixels*. Since in the image the number of pixels of one square side is measured to be 20.12 *pixels* that corresponds to the real world 90mm. From this information we can get the exact baseline by computing.

$$(90.08 \times 90)/20.12 = 402.94mm,$$

thus the exact baseline (distance between the perspective camera and the laser) is 40.29 *cm*.

However, performing the same on the fisheye will not be the correct approach. Thus, in case with fisheye camera the points, the centre of the image and the centre of the laser projector, are transformed on the spherical image and also the side measurement of the square of the checker board. Based on the similar triangles, it is known that the two arcs will correspond to the same common angle subtended by each of them. Since we know the real world measurement of the side of the square grid and its corresponding arc length on the spherical image, and so is the arc length of the base line is known. From the available information the direct relation of the baseline arc length on the spherical image deduces the real world baseline measurement. This is again verified to be 40.29 *cm*.

4.2 Algorithms

The mathematical modelling based on both approaches: first one on algebraic and the latter one on geometrical was developed, but required an algorithm to run to estimated the normal of the plane for the attitude and distance of this plane relative to the camera for the altitude. Thus the following subsections will introduce with the quadratic fitting algorithm and later the algorithms based on two approaches.

4.2.1 Quadratic Fitting Algorithms For Their Coefficients

Fitting data to a quadratic is a very important task for many computer and machine vision problems. Quadratic fitting is a commonly required method but many algorithms perform poorly on data with noise or incomplete dataset. Thus we need to study several available algorithms to perform this task under various noise to the data and identifying the key parameters that affect sensitivity. Then to decide the best suitable algorithm to perform the quadratic fitting to estimate the coefficient to estimate the required parameters of attitude and altitude.

How is this quadratic fitting carried out in general, this requires the dataset of points which are potential to fit one specific quadratic at a given instance of time. The general preprocessing required the segmentation of the image to eliminate the unwanted data points and only keeping the points of interest. In this particular case is the red laser projected circular pattern. This circular pattern transforms into various ellipse depending upon the combined rotation introduced to the UAV, in turn to the camera-laser system. As explained earlier the approach uses the spherical image to maintain the solution as general as possible giving space for all camera types. The segmented image with only the laser pattern is utilised to extract all the points that can satisfy a quadratic at a given instance of time. It is this set of points of interest after the preprocessed image make a complete dataset. The obtained dataset of points from the projected pattern undergoes the conic fitting algorithm to obtain its coefficients after having satisfied the conic.

Fitzgibbon's Conic Fitting

Andrew Fitzgibbon's conic fitting algorithm was taken into consideration to be implemented in our solution to estimate the coefficients of the conic that in turn help us to estimate the state of the UAV. Before one implements the conic coefficients based on this algorithm. Our observations were the previous conic fitting methods rely (when applied to ellipse fitting) either on the presence of good data or on computationally expensive iterative updates of the parameters.

Experimental results illustrated by Andrew Fitzgibbon et al in [35] present the advantages conferred by ellipse specificity in terms of occlusion and noise sensitivity. The stability properties widen the scope of application of the algo-

rithm from ellipse fitting to cases where the data are not strictly elliptical but need to be minimally represented by an elliptical blob. However, this method offered accuracy for ellipse fitting but at the cost of the computation speed. Since in our application that is dedicated for VTOL and control of the UAV for manoeuvring this was inappropriate to trade off with the speed. Thus our need for an alternate relative accurate but quick fitting led us to explore the other solutions.

Quadratic Fitting By Singular Value Decomposition (SVD)

Upon having explored the conic fitting algorithms, to find their coefficients, were trading off with the speed on the computation. Thus, in order to achieve sufficiently accurate coefficients with quicker computation we tried to make use of the singular value decomposition (SVD) on the data obtained from the quadratic on the spherical image that satisfied the quadratic equation developed in equation (3.24). Upon results obtained for simulation were in accordance with the desired coefficients, However, they lacked in the robust solution. This was over come by making use of random sample consensus (RANSAC) initially on the dataset that rejected the outliers from the dataset keeping only the inliers (points that fall within the predefined threshold value to select the points from the point dataset). These inliers were used to estimate the coefficients of the quadratic by the application of SVD on them. Thus finally the quadraticfitting to estimate its coefficients were settled with use of SVD upon RANSAC sorted inlier data points obtained from segmentation of the laser pattern.

4.2.2 Algorithm: Algebraic Model And Geometrical Model

The algorithm developed for the algebraic model discussed in a flow chart in figure 4.6, whereas figure 4.7 represents for geometrical model.

This flow chart explains the algorithm to be implemented on real image sequence. Both the algorithm share some common steps which are highlighted here, both the algorithms threshold the red channel from the image to make use of the laser colour to start the preprocessing stage. This gives the conic on the plane projected as seen by the camera. The dataset that represent that particular conic is projected on to the spherical model of the camera. At this stage

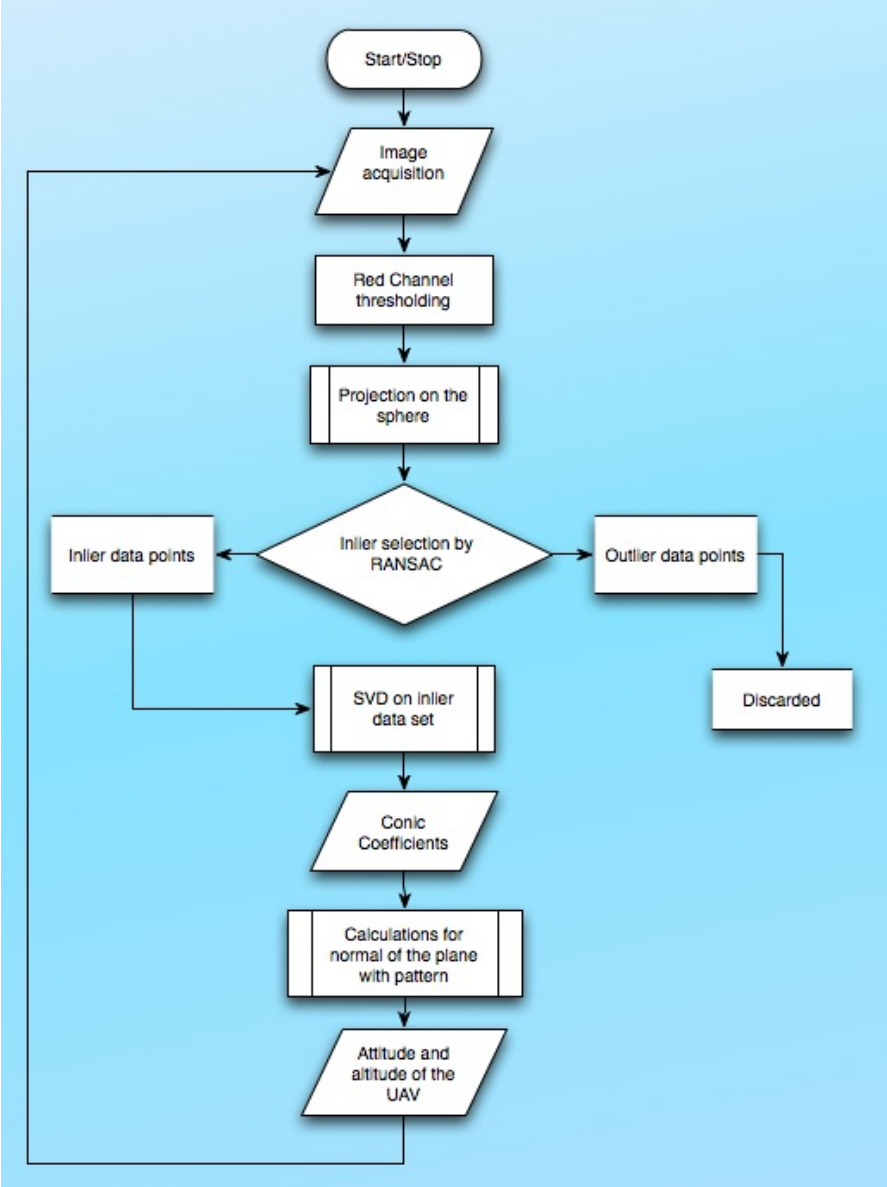

Figure 4.6: The flow chart representing the algorithm for the implementation of algebraic approach based solution.

to ensure the robustness in our solution a tool called RANSAC is applied to only select the point dataset of interest to the estimation process called inliers and discarding the unwanted noisy dataset. The SVD on the inlier points of interest help us estimate the coefficients that is essential part in the estimation of the plane for the attitude and altitude relative to the obtained plane. Until this step both the algorithms share the mentioned steps. Following these steps

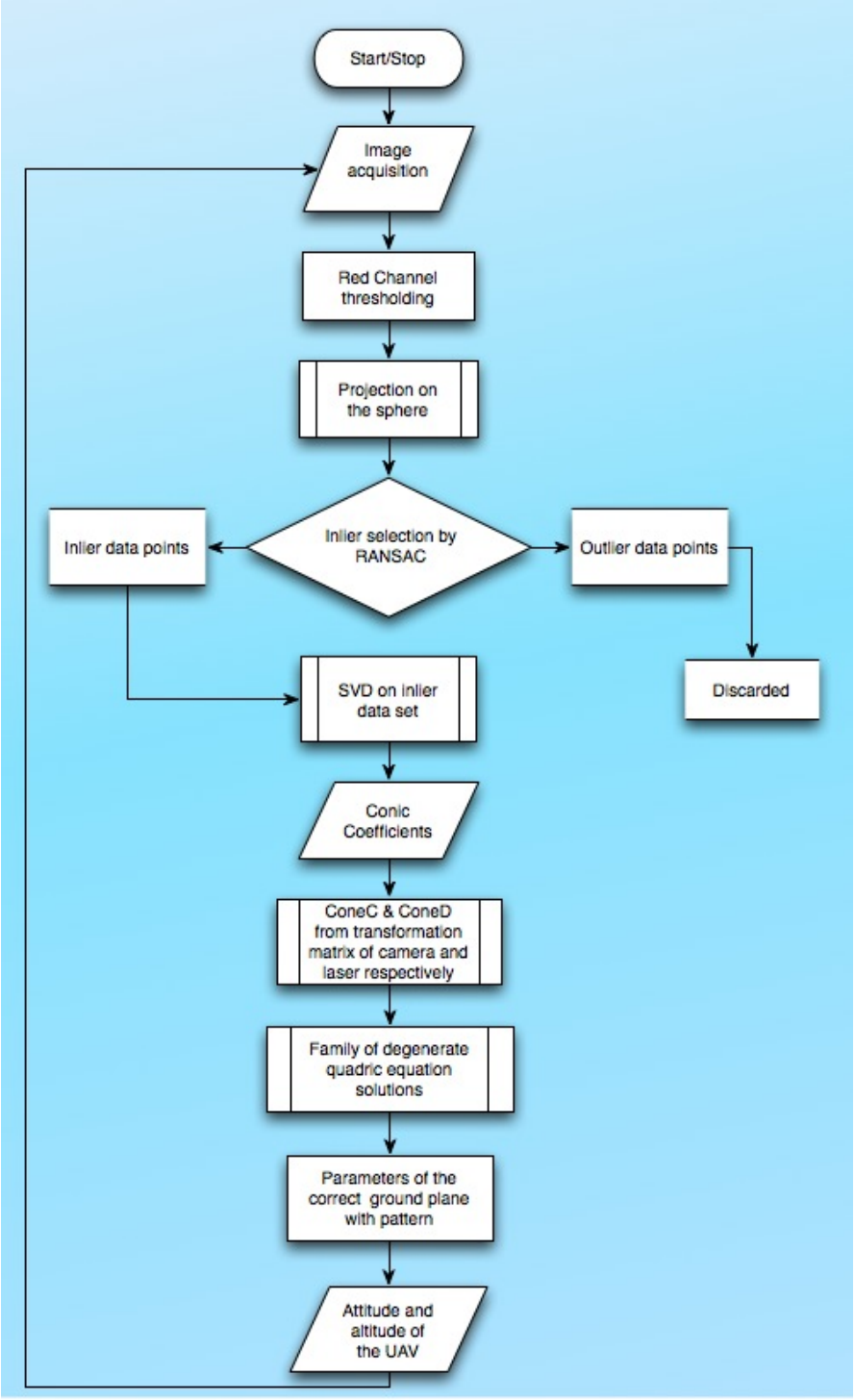

Figure 4.7: The flow chart representing the algorithm for the implementation of geometrical approach based solution.

for respective models developed help estimate the attitude and altitude.

In the following chapter, we would discuss upon the results obtained from simulation as well as from the real image sequence. Later to compare the two approaches by their performance.

Chapter 5

Results

This chapter on results is divided mainly under two major subsections namely: One based on algebraic and other one on geometrical approaches.

However, this chapter will discuss the results on simulations (ideal and noisy cases) and later based on real image sequence on board the UAV results for the individual results cases of algebraic and geometrical results. The chapter will then perform a comparative study between the two approaches and cite their responses to the various scenarios to verify for its robustness. The results have been validated and compared with respect to the available commercial sensors as their ground truth values.

The chapter will include description of the experimental setup being used for the experiments just before the experimental results section to give a better understanding of the implementation in laboratory conditions and field conditions. The chapter will also cite the online video links of the implemented results under various scenarios to get the feel of real time implementation.

5.1 Experimental Setup

Following is the experimental set up being used for our experiments to validate the solutions. We present mainly two stage experimental setup, the basic idea remains the same throughout by making use of a single camera and a laser pattern projector. The two configuration we talk about is mainly for the different stages of experiments. The setup consists of a camera supplied from μEye Cameras, with two different objective lenses: first one perspective lens and the other one fish-eye lens $(Fujininon1:1.4/1.8mm)$ mounted on the camera,

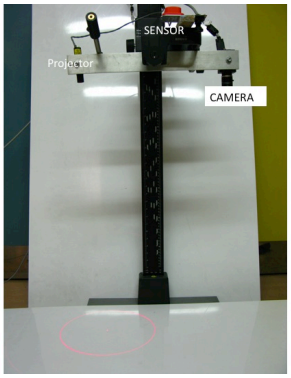

[]

[]

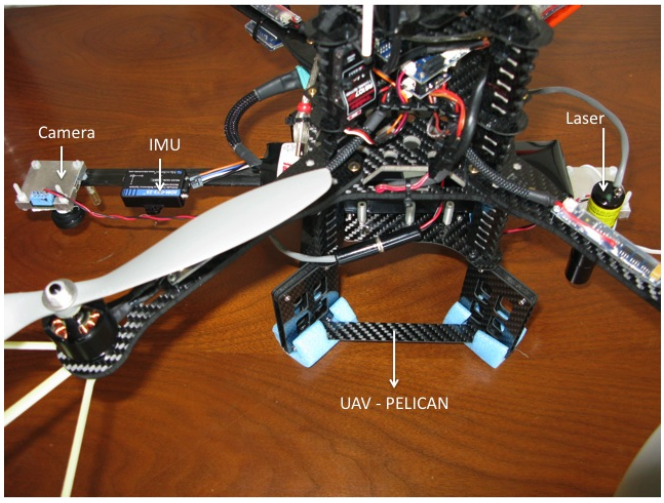

[]

Figure 5.1: The experimental setup of two kinds as shown (a) Laboratory purpose, (b) On-board UAV platform - microdrone (c) On-board UAV platform - Pelican.

and a laser pattern projector ($classII, poweroutput < 1mW, wavelength : 400 - 700nm$) supplied by Lasiris. The $ClassII$ laser projector was chosen by keeping into consideration that it does not harm the human vision by accident, if exposed during the experiment.

Despite the high resolution perspective camera it's limitation lets us with no choice than to discard it. This can be noticed from the limitations of the perspective camera with limited FOV, this hinders in implementing the solution at altitudes lower than $160cm$ for a perspective lens with a small focal length of $6mm$ in our case. The pattern as a whole is only captured at higher altitudes, thus this makes it unsuitable for many indoor applications where the UAV needs to manoeuvre in a tight limited space. Secondly only a small section of visible pattern for estimation can result in false estimation, it is because of the different individual rotations or combined rotations of pitch and roll can subtend different conic. The small and incomplete section through out the image sequence can cause malfunctioning of the algorithm leading to its failure. Therefore the image sequence that captures the entire pattern is considered for a fair state estimation of the UAVs.

Figure 5.1 represents our setup being used for laboratory condition which is mounted on a fixed vertical vernier. Whereas, the other one in micro configuration is the one that is actually mounted on board our test platform UAVs: md-4-1000 supplied from Microdrone GMBH and Pelican UAV from Ascending Technologies GMBH.

5.2 Algebraic Solution Results

This section deals with the results upon implementing our methods developed to estimate the attitude and altitude of the UAV that is useful in implementing vertical take off and landing (VTOL) and also for control of the UAV to perform the low altitude autonomous manoeuvring. However the results under the algebraic solution have been presented in two subsection of simulated results and real time results. Following section only focuses on the results obtained from the algebraic method, the latter section will present the results based on geometrical approach.

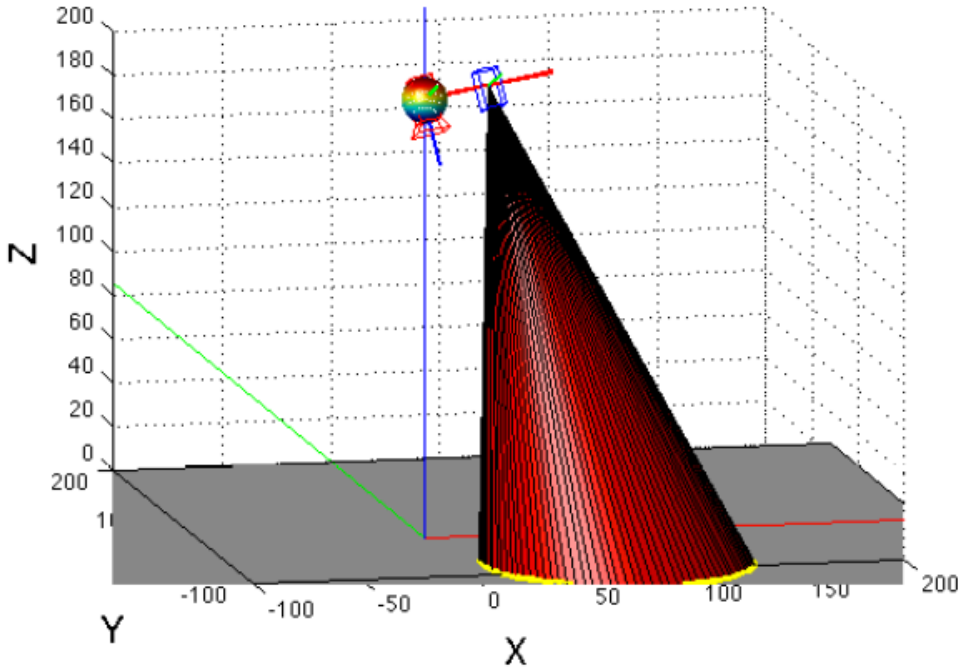

Figure 5.2: Representation of simulation on Matlab to verify our model and its estimation for parameters for attitude and altitude.

5.2.1 Simulation Results

This section on simulated results are very important and help us to realise the accuracy on estimating the required attitude and altitude of the UAV for validation purposes to perform the experiment on the real UAV platform. The expected results from our applied algebraic solution is compared with the supplied input values for simulation. For simulation purpose and real time implementation the coordinate frames of the camera and laser are aligned in accordance with the condition of the mathematical model developed.

In the simulated results part, we present the results initially based on ideal case and then later on noised case. The algorithm based on the algebraic solution to estimate the introduced angle of rotation for testing the attitude with various altitude. In the latter case some additional noise is added to the simulated image points for near to real scenario, when there is some introduced noise in the dataset.

The input for the simulated ideal and for the noisy cases were performed on the circular laser points obtained as a result of intersection of a simulated cone (representing the incident laser cone) with the ground plane as explained in [18]. The results are shown in the tables below. First, the variation with al-

Table 5.1: Simulation Results: Ideal Case

	Altitude	Roll (deg)	Pitch (deg)
Actual	1	0	0
Estimated	1	0	0
Actual	2	15	1
Estimated	2	13.02	0.03
Actual	2	0	10
Estimated	1.98	0.02	9.19
Actual	1	16	24
Estimated	1.07	14.32	22.16
Actual	1	30	0
Estimated	0.90	30.16	0.07
Actual	1	5	9
Estimated	1.04	3.77	7.58
Actual	1	30	12
Estimated	0.90	26.64	11.98

titude with absolute horizontal alignment (presenting absolute horizontal case with no rotation introduced to the UAV) with respect to the ground plane was carried out. The table 5.1 presents the results based on horizontal and rotated ideal cases with simulation as presented in figure 5.2. One can see the estimated values are in a good agreement with the actual input values.

The simulation results carried out with noised case data are presented in the table 5.2, which include both the horizontal and the rotated cases with noise added to the simulated laser image points that represent the projected conic on the ground plane. To introduce the noise we added a noise generated with a standard deviation of 0.5 to the simulated image points of the 3D laser circular pattern. From the table it has been observed the estimation of the values had been very near to the actual input values provided for the verification of accuracy of the algebraic solution in estimating the desired parameters of state estimation (attitude and altitude).

We performed the simulation to verify the algebraic solution proposed in this thesis work to estimate the attitude and the altitude of UAVs in low illuminated conditions to dark environment, this is assumed with noisy data to represent the low light conditions where as the ideal and near to ideal image data points for the complete dark environment. The noise was introduced by adding normally distributed noise with the standard deviation from [0.1 to

Table 5.2: Simulation Results: Noised Case

	Altitude	Roll (deg)	Pitch (deg)
Actual	1.2	0	0
Estimated	1.14	0	0
Actual	7	0	0
Estimated	6.34	0	0
Actual	2	0	1
Estimated	1.99	0.02	0.05
Actual	8	12	10
Estimated	7.68	13.56	7.19
Actual	1	30	10
Estimated	0.93	27.38	10.71
Actual	2	20	15
Estimated	1.89	17.38	13.71
Actual	2	12	30
Estimated	1.91	10.15	26.93

0.4] varying at equal interval of 0.1 to the image image points. Figure 5.3 represents the mean error response for one of the simulation input value (Roll = 06°, Pitch = 10°and Altitude = 150cm) run for 1000 iterations. From the results on varying noise level as presented in figure 5.3, it is inferred that the error increases with the increase of noise introduced to the image points.

From the results obtained by simulation are in good accordance with the input test values provided, It is practical to perform the experiments on the real sequence. Thus the following subsection presents the results on the real time image sequence obtained from on board the UAV platform.

5.2.2 Real Image Sequence Results

The real time experimental results were carried out on the real image sequence to verify the solution proposed in the algebraic approach to be comparable with the values obtained from the commercial sensors to measure the the attitude and the altitude of the UAV. The experiments were carried out on the image of laser circle pattern captured by the fish-eye camera. The image enhancement was carried on the raw image captured. For the treatment process only the red channel of the captured image is used. This was carried to make use of the red colour of the laser circle in order to speed up the estimation process. Later a threshold was imposed on the obtained image to keep only

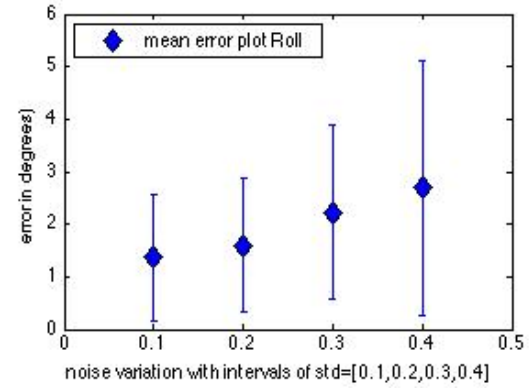

(a)

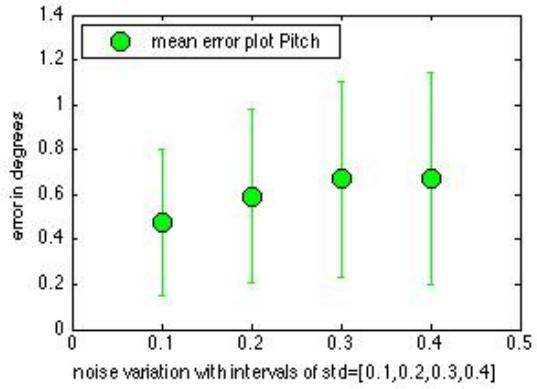

(b)

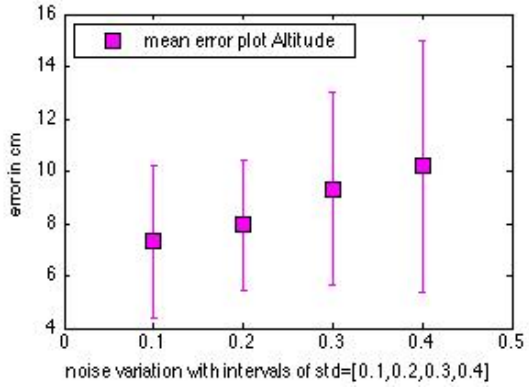

(c)

Figure 5.3: The mean error responses with their respective confidence intervals for different intervals of standard deviation [0.1 to 0.4] for (a) roll, (b) pitch and (c) altitude.

the desired pixels and suppress the rest by forcing them to be black. Then the image is converted into a grayscale, which allows us to achieve the exact profile of the conic subtend by the laser on the ground plane and later perceived by the camera. As explained in the development of the mathematical model, it is this very important step during the estimation process where the estimation of coefficients play an important role in final estimation of the attitude and altitude of the UAV relative to the ground plane over which the UAV is manoeuvring or is to perform VTOL. The correct estimation of the coefficients help obtain the exact values for the normal of the plane provides the attitude in turn, whereas the distance of the plane from the system provides the altitude as derived in the mathematical modelling.

To obtain the coefficients, a quadratic fitting by the singular value decomposition (SVD) was used. However, in order to obtain a best and robust fitting, we introduce all the obtained points that define the quadratic profile on the spherical image, by RANSAC. RANSAC is a very useful tool which helps us to only keep the points that satisfy a predefined distance threshold for the defined quadratic equation developed as a result of intersection of a cone and unit sphere called the inlier points discarding the unwanted noisy data points called the outlier points. Upon only utilising the inlier points from RANSAC help us to estimate the best quadratic coefficients from the fitting utilising the SVD.

The obtained coefficients were put into the developed model to obtain the attitude and the altitude by calculating the normal of the plane the distance of the system from this plane respectively. It is achieved by comparing these obtained coefficients of the quadratic with the coefficients obtained as a result of intersection of a cone with an unit sphere. The steps of the process in obtaining the altitude and attitude are shown in the figure 5.4.

The results of the estimations were compared with the data from the commercial sensors: for altitude a laser telemeter (DLE 50) supplied by Bosch was used where as for the attitude an attitude heading reference system (inertial measurement unit - IMU) was used supplied by MicroStrain ltd.

It is observed from figure 5.5 and table 5.3, the estimation of attitude and altitude by algebraic method were in good accordance with the synchronised commercial sensors ground truth vales.

Conclusion It is observed the solution from the algebraic method to esti-

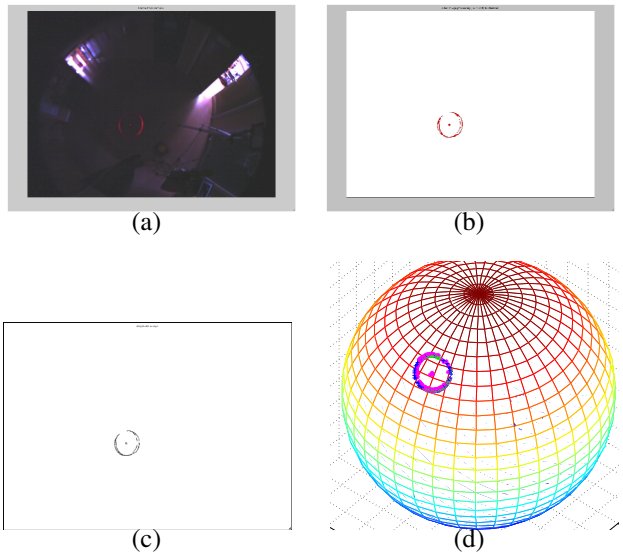

Figure 5.4: Different stages of estimation process are depicted in sub-figures [a] the capture from the camera, [b] segmenting out the red pattern on the ground, [c] converting the image to grayscale and [d] representing the conic fitting carried on spherical image for estimation of coefficients to be able to estimate the attitude and the altitude.

mate the state (attitude and altitude) of the UAVs is suitable and is in good accordance with commercial sensors. The results show the errors are small for small rotation angle but the error is large for larger angles of rotation above 30°, where the error was determined up to 4°in estimation. The approach with the proposed system is light in weight and suitable to perform Vertical take off landing (VTOL) and low altitude autonomous manoeuvre. The solution also validates its suitability to operate in low light to dark environments, in unstructured and GPS deficient environment.

5.3 Geometrical Solution Results

This section presents the results obtained from the geometrical method to estimate the state (attitude and altitude) of the UAVs deduced from the plane on which the laser pattern is projected. The results are presented first for the simulation and later on real image sequence obtained from on-board the UAV platform. The results for simulation are subdivided under the ideal and noised cases.

Table 5.3: Real Case

	Altitude	Roll (deg)	Pitch (deg)
Actual	1.63	20.30	10.40
Estimated	1.60	17.79	6.87
Actual	1.92	14.7	2.6
Estimated	1.88	12.11	0.03
Actual	1.69	3.8	20.2
Estimated	1.66	0.89	17.01
Actual	1.61	20.6	10.1
Estimated	1.60	18.46	7.14

5.3.1 Simulation Results

For simulation purposes to verify the solution developed based on geometrical approach, the camera co-ordinates are assumed as the world co-ordinate frame.

The projector, represented by the larger blue cone above in the figure 5.6 represents the cone and plane intersection giving rise to the conic on the horizontal ground plane. The image planes for the respective camera C and laser D (Laser modelled as camera) are shown in the figure 5.6 in magenta and in green coloured image planes respectively.

From the respective image planes of camera C and laser D, we obtain all the points on their respective image planes to obtain the coefficients using the SVD, we generate the conic equations of conic C and conic$D$ respectively from their conic coefficients.

We now with the help of these conic equations on the image plane determined and the vertices of the cameras C and D extended infinitely thus forming the two required cones: $coneC$ and the $coneD$. Thanks to the mathematical relation to realise a cone from the conic equation along with the help of obtained transformation matrices for the individual cameras C and camera D, where camera D is modelled for laser.

It is of much interest of the geometrical solution to obtain the intersection of the two obtained cones: $coneC$ and $coneD$, which results to produce the quadratic ${}_1Q_1$.

It can be noticed during the simulation that the rank of the matrix of this quadratic is calculated to be 3 or 4 depending upon the execution of the simulation code on matlab, which is due to the mathematical approximation. In

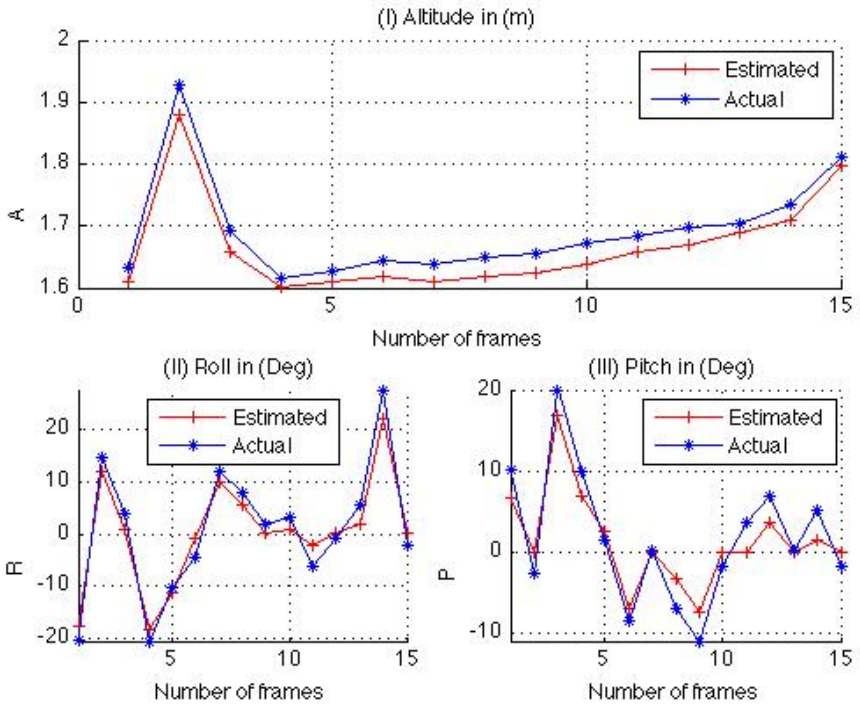

Figure 5.5: The comparison between actual sensor readings and estimated altitude and attitude (Roll,Pitch) from algebraic method.

practice it is supposed to be of rank 2, but when we observe the matrix representing the quadratic Q, it only has 2 elements of its diagonal matrix of non zero values and the others tend to zero. It is from here that we must only calculate the 2 non zero significant elements for the calculation of the rank of the conic Q.

Generally the rank of quadratic matrix is of 4. However, a rank 3 of the quadratic matrix represents cone, while rank 2 represent a pair of planes. As mentioned in the previous paragraph that the rank is of 2, so must have a pair of plane one on the horizontal plane and other the vertical plane. The interest is on the horizontal plane, since it is the plane that keeps the optical axis of the laser and camera in the same side, whereas the vertical plane separates the two optical axis.

It is from this quadratic Q that helps us determine the attitude (Roll, Pitch) and the altitude. This is obtained by obtaining the values of the planes on which the conic are formed. Practically there are 2 conic that arise from the intersection of the 2 cones C and D (for camera and laser respectively) infinitely extended in the world co-ordinate frame with exactly the same conic

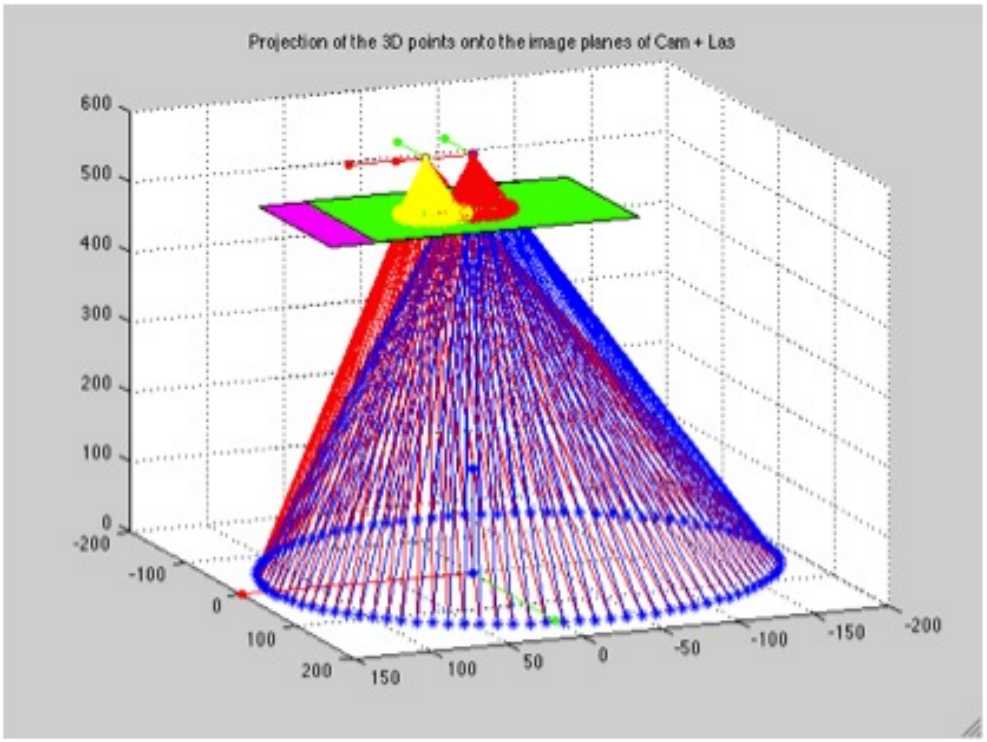

Figure 5.6: The representation of the intersection of two cones: one from the laser projector and the other from the camera. The image planes are also represented in the simulation for camera (in magenta colour) and laser (in green colour), further extended to perceive the common conic on the ground plane.

equation, one is formed on to the horizontal plane that we are actually interested in and the other is on the vertical plane orthogonal to the previous mentioned horizontal plane.

We discard the vertical plane, since it is not the plane we are interested in, to estimate the attitude and the altitude because this conic on the vertical plane bisects the optical centres of the camera and the laser signifying the wrong plane with the conic.

We are interested for the correct horizontal plane with the desired conic to obtain the normal of this plane for estimation of attitude and altitude. The parameters of attitude and altitude are obtained from the vector representing the plane that consists of the 4 elements of which the first three represent the attitude, where as the fourth represents the altitude. However, they are computed up to the scale. To avail the exact true values, we divide the plane vector with the third element (the Z) and calculate the desired attitudes (Roll

Table 5.4: Results from simulation for ideal and noised case with standard deviation of 0.5 : Geometrical Solution

	Roll (deg)	Pitch (deg)	Altitude (in cm)
Actual	0	0	60
Estimated	2.68	2.26	60.00
Noised	2.69	2.16	59.99
Actual	0	1	60
Estimated	2.82	1.05	59.97
Noised	2.78	0	59.97
Actual	1	0	60
Estimated	3.69	2.27	60.05
Noised	3.67	2.10	60.05
Actual	5	4	60
Estimated	5.92	4.08	59.70
Noised	5.88	4.04	59.71
Actual	5	4	110
Estimated	5.99	4.09	110.31
Noised	5.96	4.06	110.32
Actual	10	12	200
Estimated	12.33	12.55	209.07
Noised	12.36	12.57	209.08
Actual	13	6	1000
Estimated	13.02	6.27	1032.28
Noised	14.02	6.77	1068.50
Actual	30	25	100
Estimated	30.09	27.40	105.12
Noised	30.19	27.43	105.35
Actual	30	25	1000
Estimated	31.61	28.38	1160.09
Noised	31.71	28.40	1198.34

and Pitch) along with altitude at which the UAV is hovering.

We performed the simulation to verify our geometrical solution proposed in this thesis to estimate the attitude and the altitude of UAVs from low illuminated conditions to dark environment. The simulation were carried out for the following cases: one in true ideal case with no noise introduced and second one with noisy case. The table 5.4 presents results of estimation in ideal case and noised case with standard deviation of 0.5 compared with the ground truth value provided for simulation. The noise was introduced by adding normally distributed noise with the standard deviation from [0.1 to 0.4] varying

at equal interval of 0.1 to the image image points.

Figure 5.7 represents the mean error response for one of the simulation input value ($Roll = 11°, Pitch = 7°, Altitude = 200cm$) run for 1000 iterations. It shows the error increases with the increase of noise introduced to the image points.

5.3.2 Real Image Sequence Results

The results in this subsection are on the image sequence obtained on the test bed UAV-Pelican and later on the vertical vernier or by hand to test our results to imitate large angles of rotation, which otherwise could not be obtained on the UAV flight due to the chances of the UAV to crash at large rotation angles. The test were carried out on two different setups: the first system consisted the fish eye camera (*Fujinon 1:1.4/1.8mm mounted on a μEye camera*) and a laser pattern projector (*class II ,power output <1mW, wavelength: 400-700nm*) supplied by Lasiris had been used with a fixed baseline, whereas the second one consisted of a perspective camera (*μEye camera with 6.5 mm focal length*) with a laser pattern projector as mentioned earlier and separated by a fixed baseline.

In this section we do not show the results based on perspective camera system but only on fisheye camera and the laser pattern projector set up, since the setup consisting the perspective camera was unsuitable for applications such as the VTOL due to its limited FOV and lacked pattern until an altitude of 160cm. However, the fisheye camera had an upper hand over the perspective by virtue of it's large FOV that facilitated to detect the laser pattern at very low altitude, making it a better choice to estimate the attitude and altitude for VTOL along with various other control applications that required UAVs to manoeuvre at low altitudes.

To perform the quadratic fitting for the estimation of the coefficients of the associated conic c in equation (3.47) that related the system with the n images laser points projected on the sphere.

The estimation was carried out with the help of the coefficients of the associated conic that can then be estimated by Singular Value Decomposition (SVD) with a minimum of five points. In order to estimate robustly the quadratic, we propose to perform a RANSAC algorithm that allows to select only the set of inliers points that satisfy within the threshold of the quadratic

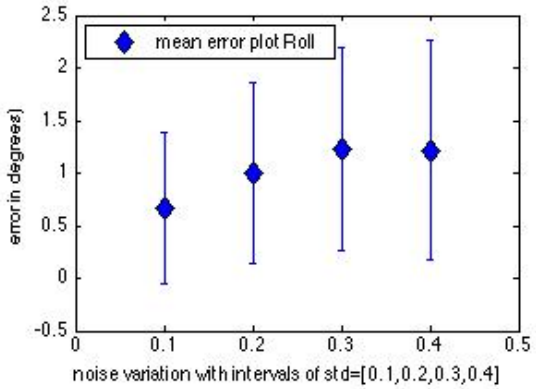

(a)

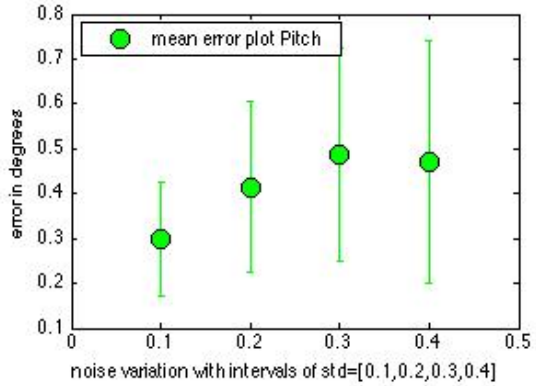

(b)

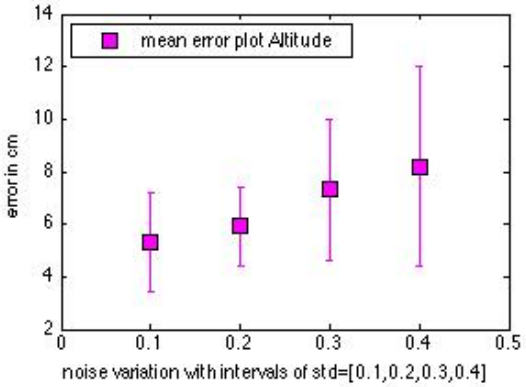

(c)

Figure 5.7: The mean error responses with their respective confidence intervals for different intervals of standard deviation for (a) roll, (b) pitch and (c) altitude based on geometrical solution.

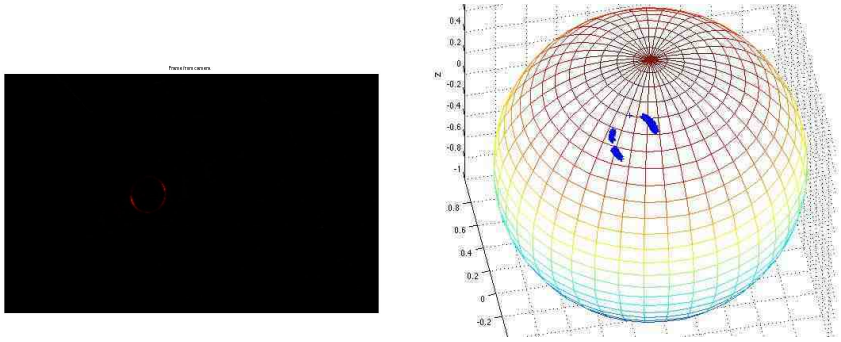

(a) (b)

Figure 5.8: Different stages in estimation process: (a) captured fish-eye image, from which only red channel is allowed to obtain laser pattern and converted to gray scale upon thresholding, (b) inlier points selection by RANSAC for conic coefficients by SVD on spherical image.

fitting and by rejecting the outlier points. A new SVD is then applied to this set for an accurate estimation of the coefficients. These steps of the algorithm are shared by both algebraic and geometrical solutions.

Figure 5.8 describes the various steps for the estimation. Figure 5.10 represents a few stills from the video sequence obtained from UAV flight to implement the geometrical solution in indoor environment. Figure 5.9 represents the estimation of attitude and altitude of the UAVs in badly illuminated, unstructured environment showed the errors were low at lower altitude but increased with the higher altitudes. Similar was the observation in error for large angles of rotation where the errors were small for small individual or combined rotation but large for big angles of rotation. The error was large for angles above 35°resulting to errors in estimations above 3°.

Conclusion It is observed the solution from the geometrical method to estimate the state (attitude and altitude) of the UAVs is suitable and is in good accordance with commercial sensors. The results show the errors are small for small rotation angle but the error is large for larger angles of rotation above 35°, where the error was determined up to 3°in estimation. The approach with the proposed system is light in weight and suitable to perform Vertical take off landing (VTOL) and low altitude autonomous manoeuvre. The solution also validates its suitability to operate in low light to dark environments, in unstructured and GPS deficient environment.

[]

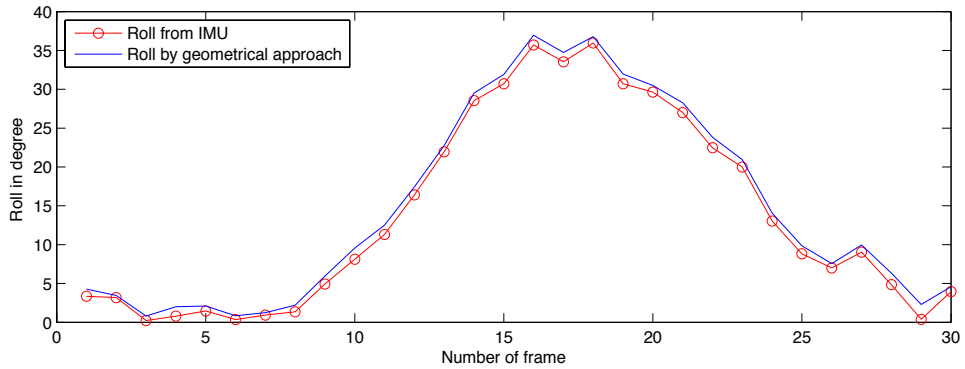

[]

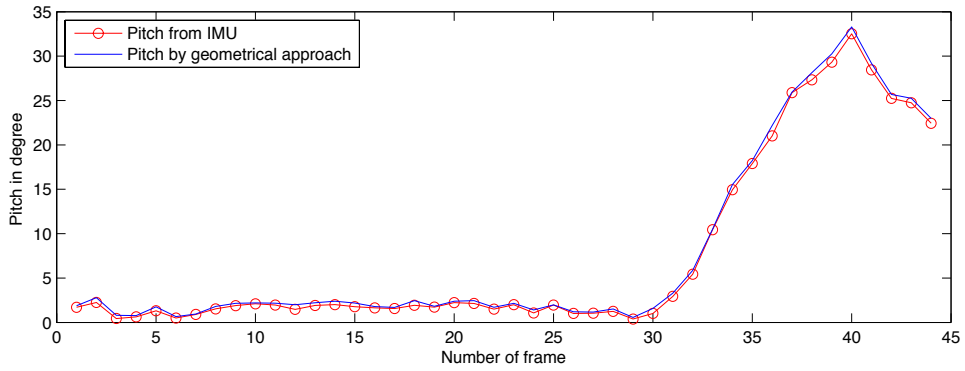

[]

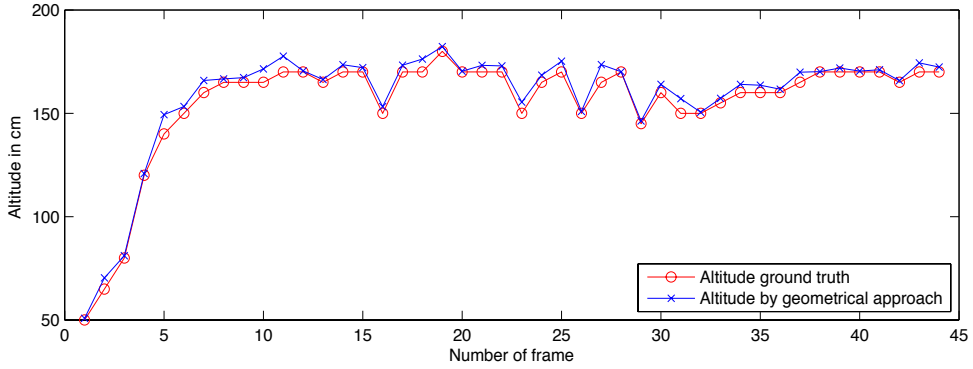

Figure 5.9: The comparison of results obtained from IMU (ground truth) in red with geometrical solution in blue for (a) Roll Comparisons (b) Pitch Comparisons (c) Altitude Comparisons.

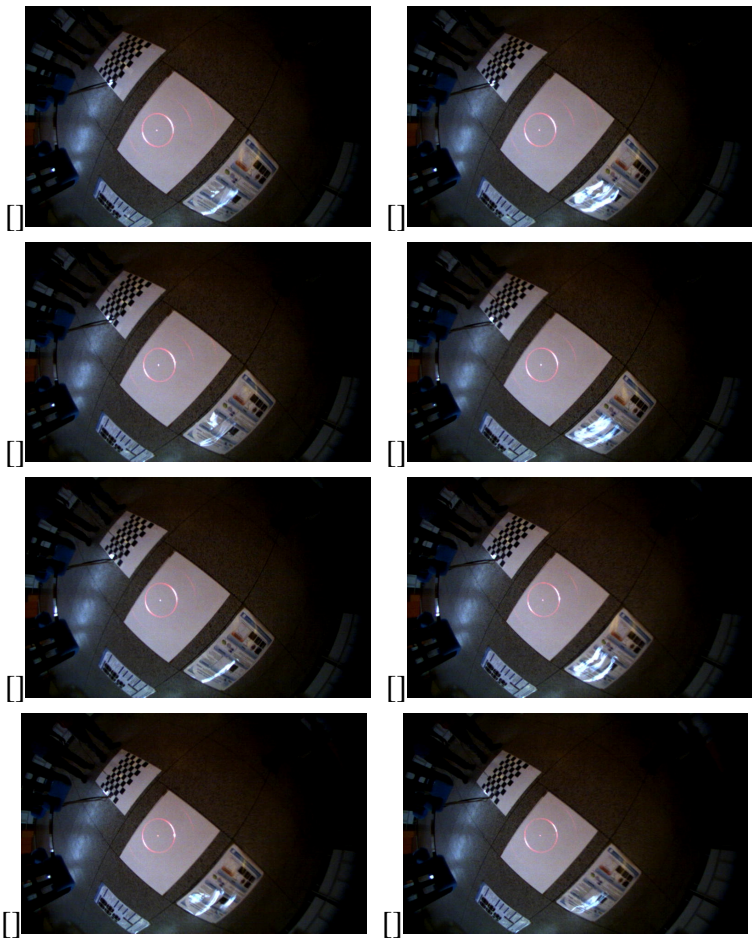

Figure 5.10: Stills from the video sequence of from the test flight over the various surface for indoor environment for comparison between the algebraic and geometrical solutions with their respective synchronised camera-IMU sensor for ground truth values.

5.4 Comparison Between Algebraic And Geometrical Solutions

Figure 5.11 presents the results of estimation of attitude and altitude based on geometrical approach compared with the one obtained from the commercial inertial measurement unit (IMU) for the attitude. We have also compared our results by geometrical solution to the analytical solution proposed from analysis for this particular experiment it presents that the results from the geometrical approach to estimate the attitude and altitude of UAVs performed better than the analytical solution proposed at times but at some instances of experiment algebraic solution also did perform better than geometrical solution for badly illuminated conditions to dark environment. We also carried out the root mean squared error (RMSE) analysis for individual parameters of attitude and the altitude to verify how accurate is our solution. Table 5.5 endorses our finding that the geometrical solution for estimating the attitude and altitude is better than the analytical solution as proposed in an improperly illuminated conditions to dark environment. It was however noted for small rotations the errors were small between 1°- 3° but for large angles of rotation as 35°the percentage error calculated was larger than 3% otherwise low.

Table 5.5: Root mean squared error (RMSE) Analysis for estimations

	RMSE Algebraic Solution	**RMSE Geometrical Solution**
Roll	2.03°	0.88°
Pitch	1.65°	0.43°
Altitude	7.14 cm	3.91 cm

5.5 Robustness Test

It is here to our interest to find out of the two proposed solutions: one based on algebraic and other on geometrical solution, which solution of the two is more robust and better for estimation of state (attitude and altitude) for the UAVs. Thus to verify it the experiment was extended to various surfaces in indoor and outdoor applications. Following are the test scenarios that were considered in indoor environment:

[]

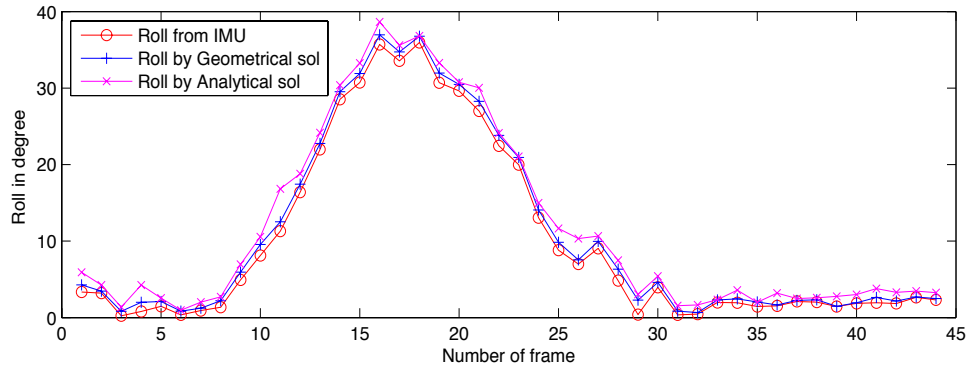

[]

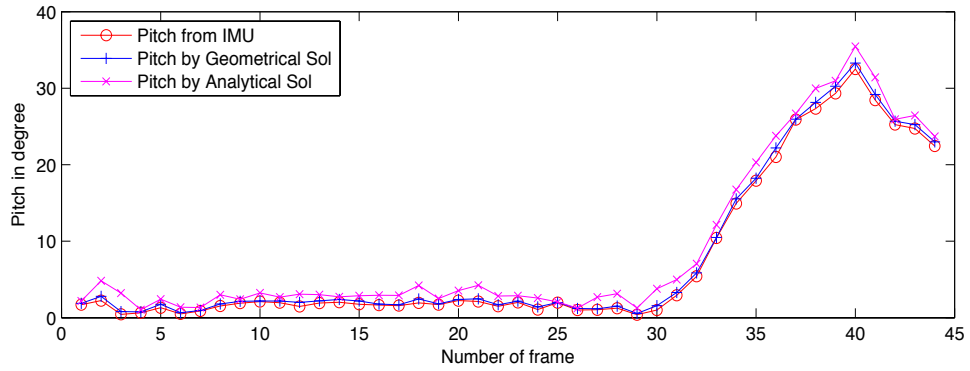

[]

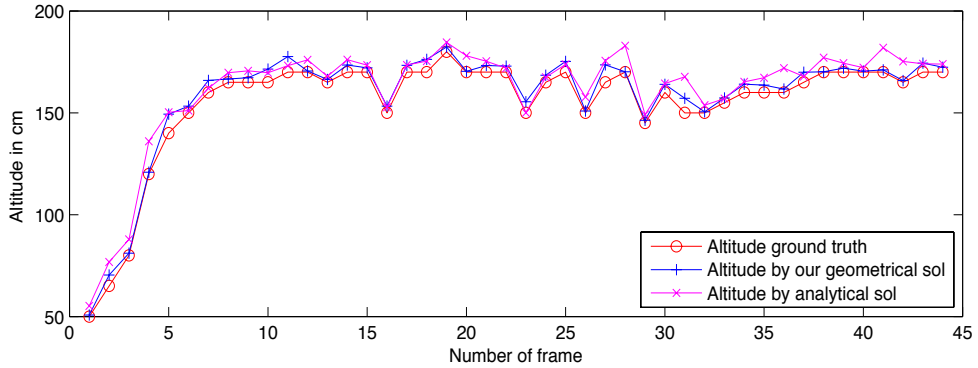

Figure 5.11: The comparison of results obtained from IMU (ground truth) in red, the algebraic approach in magenta and with geometrical solution in blue for (a) Roll Comparisons (b) Pitch Comparisons (c) Altitude Comparisons.

- Variation in illumination conditions.
- Variation in textured surface
  a) Indoor Environment: highly reflective, lambert surface, checkered, coloured surface.
  b) Outdoor Environment: vegetation and road.
- Occlusion on the ground plane.
- Variation in inclinations.

Figure 5.12 represents a few of the stills from some of the test scenarios used to perform the robustness test with comparison between the algebraic and geometrical solutions.

Conclusion

Variation in illumination condition: The state estimation for UAVs in the test scenario for the variation in the illumination condition clearly showed both the estimation processes to be similar in performance, however, the illumination variation from properly illuminated to poorly illuminated or dark environments the estimation results shifted from poor to better estimation. This improved state estimation was mainly due to the ease of tracking the pattern in the image sequence. The performance increased due to less computation time in a better quadratic fitting.

Variation in textured surface: Figure 5.13, 5.14, 5.15 and 5.16 present the state estimation on dark surface, lambert surface, checkered and coloured surfaces respectively for indoor environment conditions that showed the performance of the algebraic and geometrical solutions performed equally, but the estimation performed better with less error on the dark and coloured surface where the quadratic fitting was the best due to large number of inlier points that were part of the quadratic, though the time spent on computing the coefficients from fitting was large when compared to other textured surfaces. The results on checkered surfaces as shown in figure 5.15 showed a bigger error in the estimation especially due to the large number of outlier points due to the dark parts of the checkered surface. The estimation on lambert surface is difficult due to the error caused due to the improper segmentation of the pattern, that leads to the poor quadratic fitting which in turn introduces large errors in estimation.

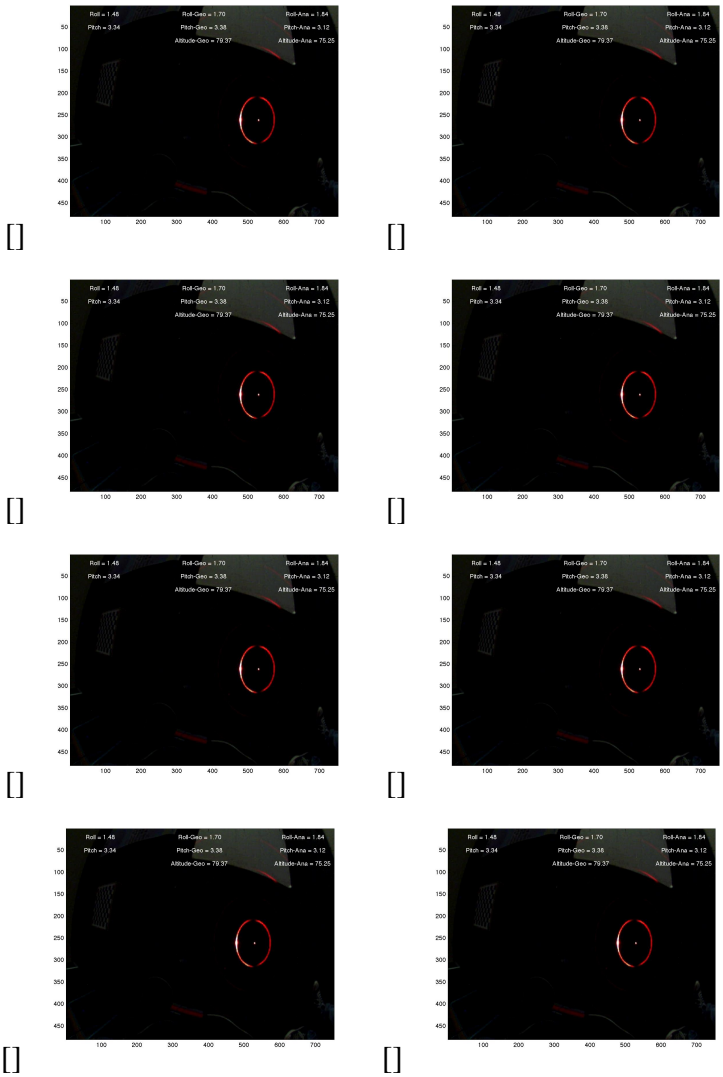

Figure 5.12: Stills from the video sequence of from the test flight over the dark textured surface for comparison between the algebraic and geometrical solutions with their respective synchronised camera-IMU sensor ground truth values.

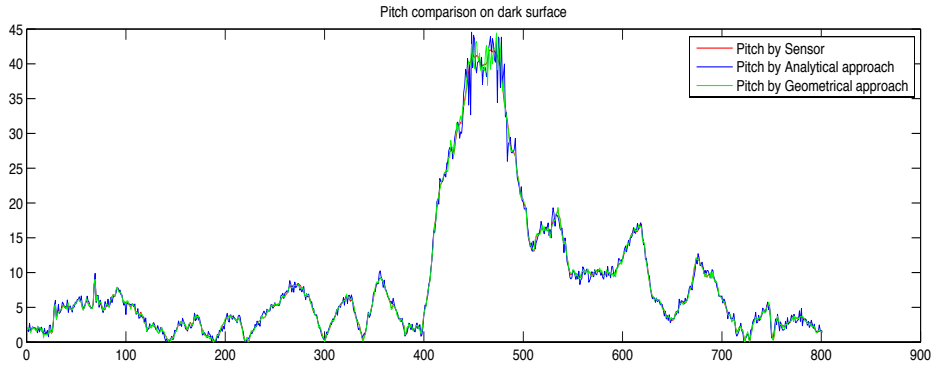

[]

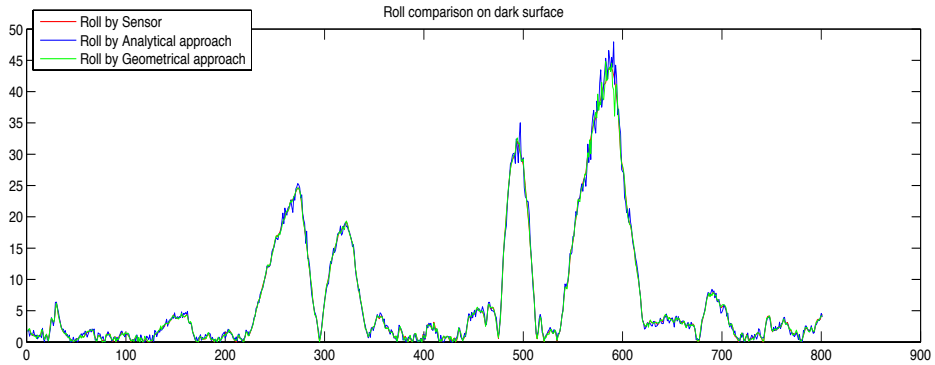

[]

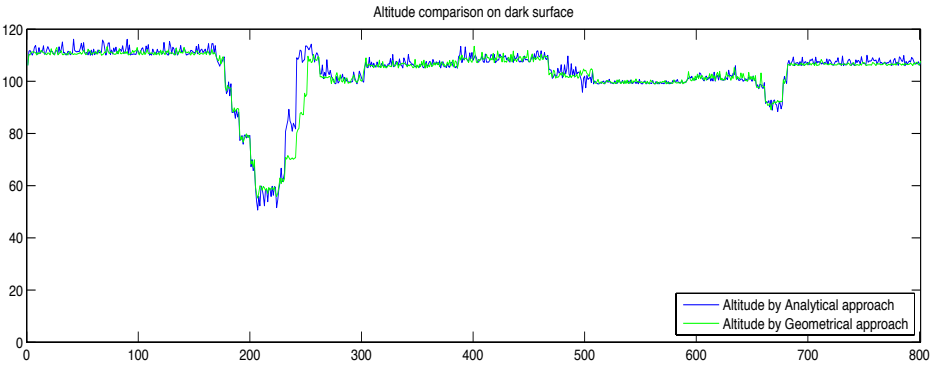

[]

Figure 5.13: Comparison on dark textured surface from Analytical and Geometrical approaches, (a) Pitch, (b) Roll, (c) Altitude.

The state estimation for outdoor environment is challenging when compared with the indoor environment mainly due to poor segmentation of the pattern, the other major reason is due to large noisy data as the vegetation is in general an uneven distribution leading to non planar surface for the projected pattern. This non planar ground makes it difficult for quadratic fitting that leads to large errors in estimation than in indoor planar environments. The

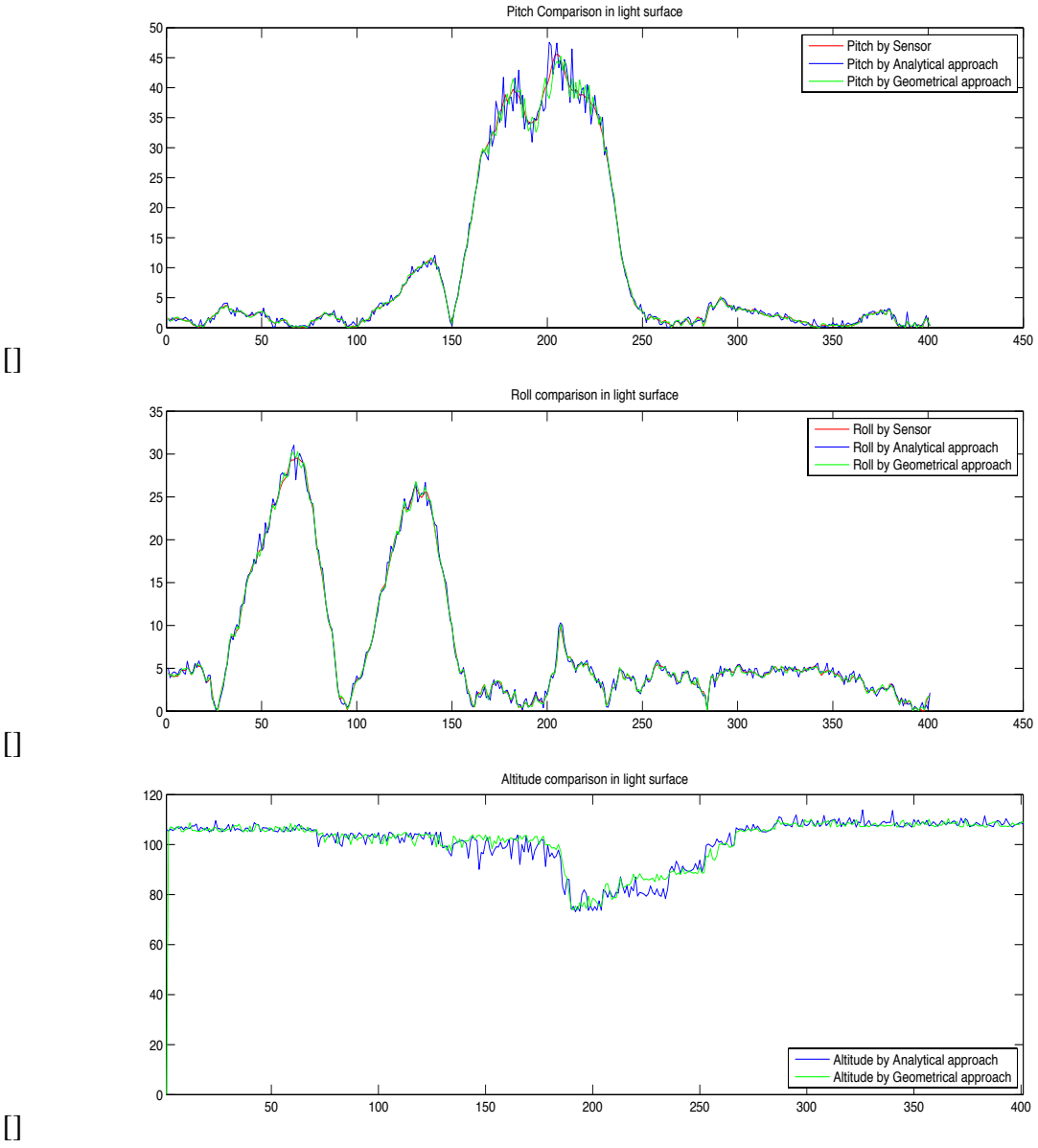

Figure 5.14: Comparison on lambert surface from Analytical and Geometrical approaches, (a) Pitch, (b) Roll, (c) Altitude.

estimation on road in outdoor environment gives better results than the grass for instance due to the virtue of its planar surface. The estimation in outdoor environment is challenging due to its illumination condition, mostly outdoor environment has more light than in indoor environment. Thus, it makes the visibility of pattern difficult unless it be a cloudy day or time from evening till late night. Figure 5.17 (a) and (b) represents the outdoor environment

[]

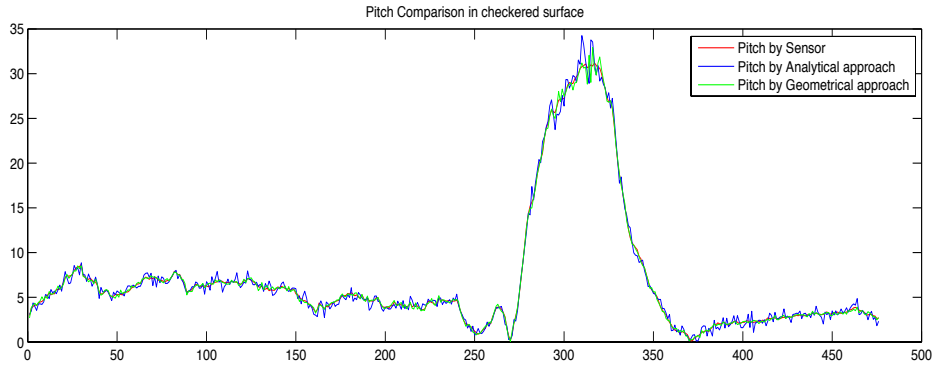

[]

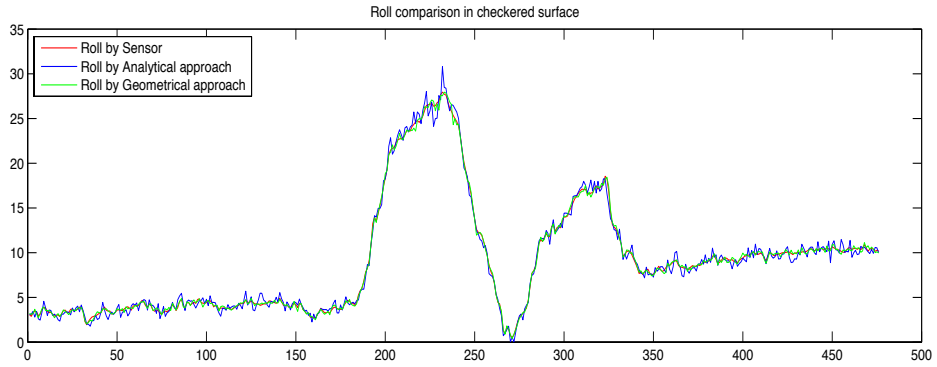

[]

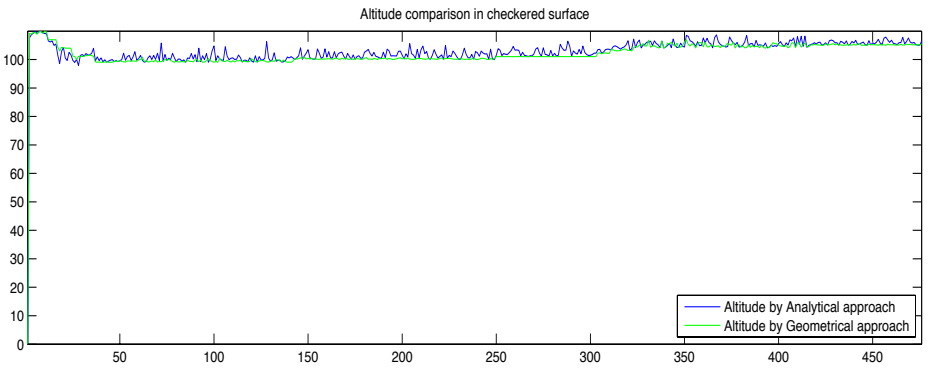

Figure 5.15: Comparison on checkered surface from Analytical and Geometrical approaches, (a) Pitch, (b) Roll, (c) Altitude.

experiments on grass and the latter one on the road on a cloudy day.

Occlusions on ground plane:

The figure 5.18 represents the results based on occlusion. It is interesting to see that both the approaches based on algebraic and geometrical solutions give large errors on occluded ground planes, since the occlusion introduces large errors in estimation of the coefficients of the quadratic after its fitting

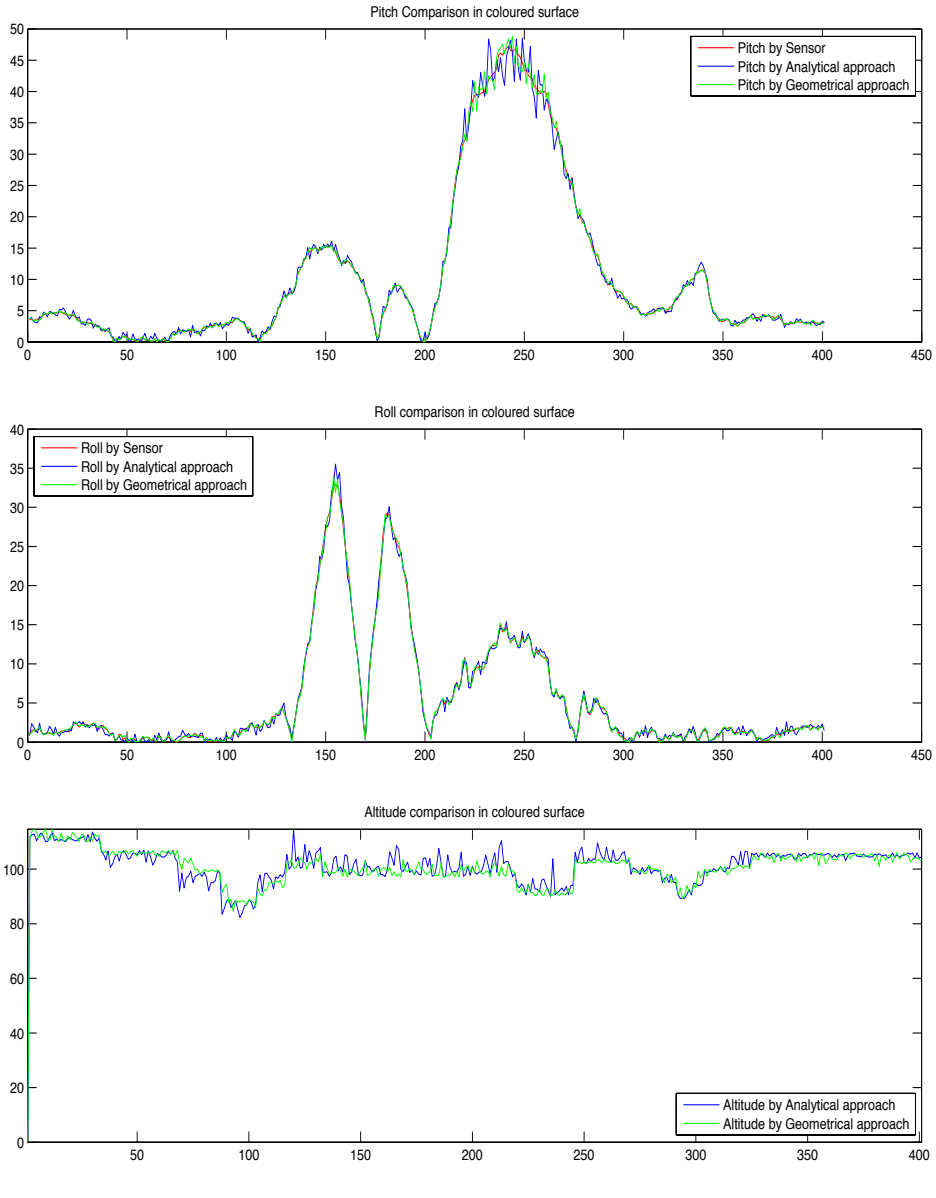

[]

[]

[]

Figure 5.16: Comparison on coloured surface from Analytical and Geometrical approaches, (a) Pitch, (b) Roll, (c) Altitude.

that lead to false ground plane. In this particular example we try to present the solutions of in which there is an occluding inclined ground plane. The UAV is horizontally aligned with respect to the ground plane but our methods sense them as variation attitude and altitude. This results that both solution are not robust enough to inclined occluding ground surfaces. Both the solutions performs fairly good with flat planar occlusions.

[]

[]

Figure 5.17: Results based acquisition carried in outdoor environment (a) on grass, (b) on road.

Variation in inclinations:

The results suggest that both the approaches the algebraic and geometrical solutions fails after increase in the inclined ground planes. It is so because of the strong assumption made during the mathematical modelling for the ground plane to be flat as is the general case on the surface of the earth. Now for an instance the ground plane is inclined but the relative attitude of the UAV is still horizontal to the ground plane, but still the two solutions sense for variation in the attitude and altitude. The same is applicable for when the UAV is inclined relatively to the ground plane, it shows no attitude variation since the angle of inclination of the UAV is same as the inclination of the inclined plane.

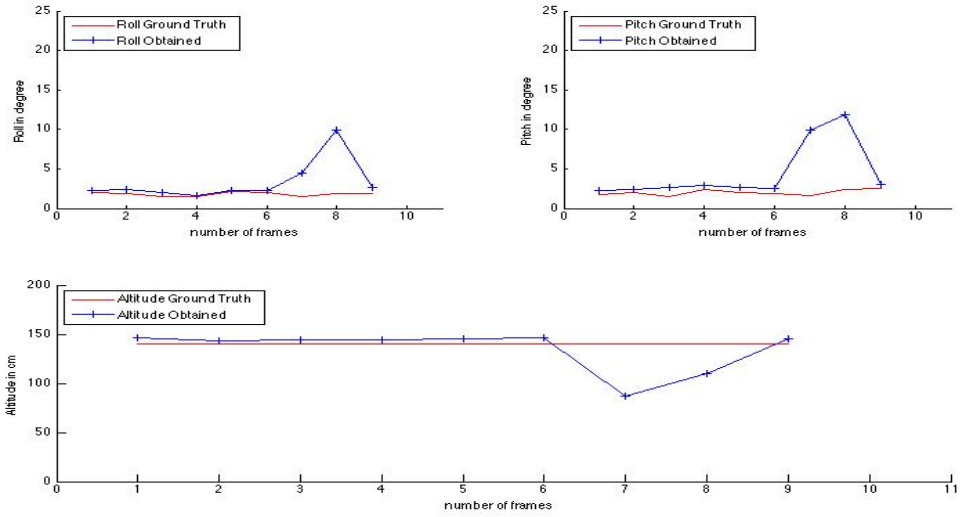

[]

Figure 5.18: Results based false estimation of attitude and altitude as resulted from inclined occluding ground plane.

5.6 Video Links

This section presents the links to the video on the results implemented and their respective responses in indoor and outdoor environment.

Indoor Environment: ” Results from our proposed methods for indoor environment (http://www.youtube.com/watch?v=pO5EfMkZWngfeature=relmfu)

Outdoor Environment: ” Results from our proposed methods for outdoor environment (http://www.youtube.com/watch?v=wXdTn9Hh7owfeature=relmfu)

Chapter 6

Conclusion And Future Works

This chapter discusses the results of state estimation for UAVs from the two mathematical models developed: one based on algebraic solution and the other based on geometrical solution, which is deduced as a function of normal of the plane and the distance of the plane from the UAV. The robustness of the results based on various testing criteria have been checked. Later section presents the future works that need to be carried out in order to overcome the limitations of the proposed solution.

6.1 Conclusion

The state estimation (attitude and altitude estimation) for the UAVs have been developed that can perform in low light to dark, unstructured (without prebuilt maps of the environment) and GPS deficient environment. The mathematical models: first one based on algebraic and the other based on geometrical solutions have been developed as a function of normal of the plane and the distance between the UAVs and the ground planar plane. The main to idea behind the solutions developed is to deduce the attitude and the altitude in functions of the deformation of the circular pattern on the fish-eye image.

It has been observed from the chapter 5 based on the individual results of algebraic and geometrical approaches for both simulation as well as the real sequence, that the estimations from both the approaches are in good agreement to the ground truth sensor datas making both the approaches usable in the estimation of parameters for the attitude and altitude. It is observed that the errors in the state estimation increase with the altitude and decrease with

lower altitudes. The errors also happen to increase up-to 4°for large angles of rotations after 35°. Upon comparing the results between algebraic and geometrical solutions, it is observed that both the solutions have similar response. However, the state estimation by geometrical solution is smoother than algebraic solution. The verification of robustness of the two solutions suggest that the solution is suitable to work in the variation in the illuminations conditions, varying from low light to dark environments. It is also observed from the variations in textured surfaces that in indoor environments the solutions tend to perform better due to availability of flat planar surfaces than uneven surface in outdoor environment.

It is observed that both the solutions fail to perform on inclined surfaces and inclined occluding surfaces. The error is introduced due to the strong assumption made during the mathematical modelling for the ground plane to be planar, which is the case in most of ground planes. The solutions otherwise perform in accordance within the agreeable range of 3%.

It can overall be concluded that the geometrical solution is better than algebraic solution, since the estimations is smoother than the algebraic solution in most of the cases. However, both the proposed solutions are suitable to be implemented for vertical take off landing (VTOL) with low altitude manoeuvre in low light to dark environments, unexplored and GPS deficient environments. The proposed set up uses miniature camera and laser making it light in weight allowing more payload space for additional sensors for other applications. The system is also lower in cost when compared with commercially available sensors to just perform a take or landing.

6.2 Future Work

The initial future work would be to migrate the entire system on board the UAVs for autonomous control and navigation to perform VTOL and low altitude manoeuvring.

The next future work would be to modify the stereo rig system to include a magnetic reference north projecting a non red colour laser spot along the red circular pattern that is aligned for geographic north to start the estimation of the yaw angle. The progressive steps of yaw angle estimation will be deduced from the change in yaw angle with reference to the previous estimated yaw

angle from the captured image.

The next future work will be to modify the solution to take into consideration to eliminate the assumption to maintain identity rotation for the stereo rig consisting the laser and camera. The same needs to consider to include conditions non planar ground planes.

Appendix A

Spherical Camera Model

The advantage of choosing a spherical camera model is that this model is compromise between a very generic model, which can be difficult to calibrate and a model that does not take into consideration the important factors such as misalignment and distortion induced by the lens.

Ying in [108] showed that it is possible to use the unit sphere for fisheye camera. The modelling is possible if the calibration error is consistent with the desired application. On this proposal, Mei in [59] presents a calibration method based on the unit sphere which was extended on the work of Barreto et al. in [8], thus we make use of the same to explain the generalised spherical model for understanding.

The spherical camera uses a sphere in place of an imaging plane. The radius of the sphere is the 'focal length' of the camera. The output image is a mapping equivalent to latitude (columns) and longitude (rows). Thus for the reader it has been explained below:

A world 3D point in the mirror frame are projected onto the unit sphere is given by the equation.

$$X_{Fm} \rightarrow X_{sFm} = \frac{X}{X} = (x_s, y_s, z_s) \tag{A.1}$$

the points are then changed to a new reference frame centred in $C_p = (0, 0, \xi)$,

$$X_{sFm} \rightarrow X_{sFp} = (x_s, y_s, z_s + \xi) \tag{A.2}$$

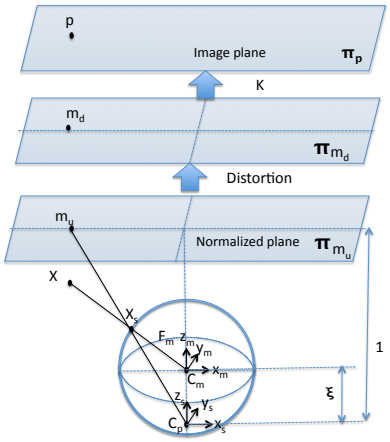

Figure A.1: The spherical projection model

they are then projected onto the normalised image plane,

$$m_u = (\tfrac{x_s}{z_s+\xi}, \tfrac{y_s}{z_s+\xi}, 1) = \hbar(X_s) \tag{A.3}$$

we then add radial and tangential distortion,

$$m_d = m_u + D(m_u, V) \tag{A.4}$$

the final projection involves a generalised camera projection matrix K (with γ the generalized focal length, $(u_0; v_0)$ the principal point, s the skew and r the aspect ratio)

$$p = Km = \begin{bmatrix} \gamma & \gamma s & u_0 \\ 0 & \gamma & v_0 \\ 0 & 0 & 1 \end{bmatrix} m = km \tag{A.5}$$

$\hbar$ lifts the point from plane π_{m_u} to the sphere :

$$\hbar^{-1}(m_u) = \begin{bmatrix} \frac{\xi+\sqrt{1+(1-\xi^2)(x^2+y^2)}}{x^2+y^2+1} x \\ \frac{\xi+\sqrt{1+(1-\xi^2)(x^2+y^2)}}{x^2+y^2+1} y \\ \frac{\xi+\sqrt{1+(1-\xi^2)(x^2+y^2)}}{x^2+y^2+1} - \xi \end{bmatrix} \tag{A.6}$$

	ξ	γ
Parabola	1	-2p*f*
Hyperbola	$\frac{df}{\sqrt{d^2+4p^2}}$	$\frac{-2pf}{\sqrt{d^2+4p^2}}$
Ellipse	$\frac{df}{\sqrt{d^2+4p^2}}$	$\frac{2pf}{\sqrt{d^2+4p^2}}$
Planar	0	-f
Perspective	0	f
d: distance between focal points 4p: latus rectum		

Table A.1: Unified model parameters.

The same steps have been represented in the figure A.1. The relationship between the (ξ, γ) and the mirror values have been detailed in Table A.

Readers are suggested to read the following references for detailed understanding, the paper by Barreto et al. in [8] and Geyer et al. in [37]

[8]: Joao P. Barreto and Helder Araujo. Issues on the geometry of central catadioptric image formation. *In Conference on Computer Vision and Pattern Recognition-CVPR 2001*, volume 2, pages 422-427, 2001.

[37]: C. Geyer and K. Daniilidis. A unifying theory for central panoramic systems and practical impli- cations.*In European Conference on Computer Vision -ECCV*, pages 445-461, 2000.

Appendix B

Papers

Papers published during PhD

[IROS2011]
Ashutosh NATRAJ, Cédric DEMONCEAUX, Pascal VASSEUR, Peter STURM, "Vision based attitude and altitude estimation for UAVs in dark environments".*IEEE/RSJ International Conference on Intelligent Robots and Systems (IROS)*, p.4006-4011, San Francisco, USA, 2011.

[ICUAS2012]
Ashutosh NATRAJ, Sang LY, Damien EYNARD, Cédric DEMONCEAUX, Pascal VASSEUR, "Omnidirectional vision for UAV: applications to attitude, motion and altitude estimation for day and night conditions",*International Conference on Unmanned Aircraft Systems (ICUAS 2012)*, Philadelphia, PA, USA, June 2012.

[IROS2012]
Ashutosh NATRAJ, Peter STURM, Cédric DEMONCEAUX, Pascal VASSEUR, "A Geometrical Approach For Vision Based Attitude And Altitude Estimation For UAVs In Dark Environments" ,*IEEE/RSJ International Conference on Intelligent Robots and Systems (IROS 2012)*, Vilamoura, Algarve, Portugal, October 2012.

[JINT2012]
Ashutosh NATRAJ, Sang LY, Damien EYNARD, Cédric DEMONCEAUX, Pascal VASSEUR, "Omnidirectional vision for UAV: applications to attitude,

motion and altitude estimation for day and night conditions", *International Journal of Intelligent and Robotic systems(JINT 2012)*, pp 1-15, Springer Netherlands, 2012.

Bibliography

[1] Pieter Abbeel, Adam Coates, Morgan Quigley, and Andrew Y. Ng. An application of reinforcement learning to aerobatic helicopter flight. In *In Advances in Neural Information Processing Systems 19*, page 2007. MIT Press, 2007.

[2] S. Ahrens, D. Levine, G. Andrews, and J.P. How. Vision-based guidance and control of a hovering vehicle in unknown, gps-denied environments. In *Robotics and Automation, 2009. ICRA '09. IEEE International Conference on*, pages 2643 –2648, may 2009.

[3] E. Altug, James P. Ostrowski, and Camillo J. Taylor. Control of a quadrotor helicopter using dual camera visual feedback. *International Journal of Robotics Research*, pages 329 –341, 2005.

[4] Omead Amidi, Takeo Kanade, and Keisuke Fujita. A visual odometer for autonomous helicopter flight. *Robotics and Autonomous Systems for Intelligent Autonomous Systems (IAS-5)*, 28(23):185 – 193, 1998.

[5] Adrien Angeli, David Filliat, Stéphane Doncieux, and Jean-Arcady Meyer. 2d simultaneous localization and mapping for micro aerial vehicles. In *EMAV 2006 European Micro Aerial Vehicles Conference*, 2006.

[6] Jorge Artieda, Jose Sebastian, Pascual Campoy, Juan Correa, Ivan Mondragan, Carol Martinez, and Miguel Olivares. Visual 3-d slam from uavs. *Journal of Intelligent Robotic Systems*, 55:299–321, 2009. 10.1007/s10846-008-9304-8.

[7] T. Bailey and H. Durrant-Whyte. Simultaneous localization and mapping (slam): part ii. *Robotics Automation Magazine, IEEE*, 13(3):108 –117, sept. 2006.

[8] J.P. Barreto and H. Araujo. Issues on the geometry of central catadioptric image formation. In *Computer Vision and Pattern Recognition, 2001. CVPR 2001. Proceedings of the 2001 IEEE Computer Society Conference on*, volume 2, pages II–422 – II–427 vol.2, 2001.

[9] J. Batlle, E. Mouaddib, and J. Salvi. Recent progress in coded structured light as a technique to solve the correspondence problem: a survey, July 1998.

[10] J.-C. Bazin, Inso Kweon, C. Demonceaux, and P. Vasseur. Uav attitude estimation by combining horizon-based and homography-based approaches for catadioptric image. In *6th IFAC/EURON Intelligent Autonomous Vehicles 2007 (IAV 07)*, may 2007.

[11] J.-C. Bazin, Inso Kweon, C. Demonceaux, and P. Vasseur. Uav attitude estimation by vanishing points in catadioptric images. In *Robotics and Automation, 2008. ICRA 2008. IEEE International Conference on*, pages 2743 –2749, may 2008.

[12] D. Bergmann. New approach for automatic surface reconstruction with coded light. In *Proceedings of Remote Sensing and Reconstruction for Three-Dimensional Objects and Scenes*, volume 2572, page 2–9, 1995.

[13] M. Blosch, S. Weiss, D. Scaramuzza, and R. Siegwart. Vision based mav navigation in unknown and unstructured environments. In *Robotics and Automation (ICRA), 2010 IEEE International Conference on*, pages 21 –28, may 2010.

[14] K. L. Boyer and A. C. Kak. Color-encoded structured light for rapid active ranging. *Pattern Analysis and Machine Intelligence, IEEE Transactions on*, PAMI-9(1):14 –28, jan. 1987.

[15] F. Caballero, L. Merino, J. Ferruz, and A. Ollero. Vision-based odometry and slam for medium and high altitude flying uavs. In Kimon P. Valavanis, Paul Oh, and Les A. Piegl, editors, *Unmanned Aircraft Systems*, pages 137–161. Springer Netherlands, 2009. 10.1007/978-1-4020-9137-7.

[16] D. Cabecinhas, R. Naldi, L. Marconi, C. Silvestre, and R. Cunha. Robust take-off and landing for a quadrotor vehicle. In *Robotics and Automation (ICRA), 2010 IEEE International Conference on*, pages 1630 –1635, may 2010.

[17] D. Cabecinhas, R. Naldi, L. Marconi, C. Silvestre, and R. Cunha. Robust take-off and landing for a quadrotor vehicle. In *Robotics and Automation (ICRA), 2010 IEEE International Conference on*, pages 1630 –1635, may 2010.

[18] S. Calinon. Robot programming by demonstration: A probabilistic approach. 2009.

[19] Pascual Campoy, Juan F. Correa, Ivan Mondragón, Carol Martínez, Miguel Olivares, Luis Mejías, and Jorge Artieda. Computer vision onboard uavs for civilian tasks. *J. Intell. Robotics Syst.*, 54(1-3):105–135, March 2009.

[20] Brian Carrihill and Robert Hummel. Experiments with the intensity ratio depth sensor. *Computer Vision, Graphics, and Image Processing*, 32(3):337 – 358, 1985.

[21] D. Caspi, N. Kiryati, and J. Shamir. Range imaging with adaptive color structured light. *Pattern Analysis and Machine Intelligence, IEEE Transactions on*, 20(5):470 –480, may 1998.

[22] G. Chazan and N. Kiryati. Pyramidal intensity-ratio depth sensor, technical report 121. *Center for Communication and Information Technologies, Department of Electrical Engineering, Technion*, Oct. 1995.

[23] Chu-Song Chen, Yi-Ping Hung, Chiann-Chu Chiang, and Ja-Ling Wu. Range data acquisition using color structured lighting and stereo vision. *Image Vision Comput.*, pages 445–456, 1997.

[24] T.D. Cornall, G.K. Egan, and A. Price. Aircraft attitude estimation from horizon video. *Electronics Letters*, 42(13):744 – 745, june 2006.

[25] Hongxia Cui, Zongjian Lin, and Jinsong Zhang. Research on low altitude image acquisition system. In *CCTA'07*.

[26] A.J. Davison. Real-time simultaneous localisation and mapping with a single camera. In *Computer Vision, 2003. Proceedings. Ninth IEEE International Conference on*, pages 1403 –1410 vol.2, oct. 2003.

[27] C. Demonceaux, P. Vasseur, and C. Pegard. Robust attitude estimation with catadioptric vision. In *Intelligent Robots and Systems, 2006 IEEE/RSJ International Conference on*, pages 3448 –3453, oct. 2006.

[28] C. Demonceaux, P. Vasseur, and C. Regard. Omnidirectional vision on uav for attitude computation. In *Robotics and Automation, 2006. ICRA 2006. Proceedings 2006 IEEE International Conference on*, pages 2842 –2847, may 2006.

[29] M.W.M.G. Dissanayake, P. Newman, S. Clark, H.F. Durrant-Whyte, and M. Csorba. A solution to the simultaneous localization and map building (slam) problem. *Robotics and Automation, IEEE Transactions on*, 17(3):229 –241, jun 2001.

[30] N.G. Durdle, J. Thayyoor, and V.J. Raso. An improved structured light technique for surface reconstruction of the human trunk. In *Electrical and Computer Engineering, 1998. IEEE Canadian Conference on*, volume 2, pages 874 –877 vol.2, may 1998.

[31] H. Durrant-Whyte and T. Bailey. Simultaneous localization and mapping: part i. *Robotics Automation Magazine, IEEE*, 13(2):99 –110, june 2006.

[32] Damien Dusha, Wageeh Boles, and Rodney Walker. Attitude estimation for a fixed-wing aircraft using horizon detection and optical flow. In *Proceedings of the 9th Biennial Conference of the Australian Pattern Recognition Society on Digital Image Computing Techniques and Applications*, DICTA '07, pages 485–492, Washington, DC, USA, 2007. IEEE Computer Society.

[33] S.M. Ettinger, M.C. Nechyba, P.G. Ifju, and M. Waszak. Vision-guided flight stability and control for micro air vehicles. In *Intelligent Robots and Systems, 2002. IEEE/RSJ International Conference on*, volume 3, pages 2134 – 2140 vol.3, 2002.

[34] D. Eynard, P. Vasseur, C. Demonceaux, and V. Freandmont. Uav altitude estimation by mixed stereoscopic vision. In *Intelligent Robots and Systems (IROS), 2010 IEEE/RSJ International Conference on*, pages 646 –651, oct. 2010.

[35] Andrew Fitzgibbon and Robert B. Fisher. A buyer's guide to conic fitting. In *In British Machine Vision Conference*, pages 513–522, 1995.

[36] Z. J. Geng. Rainbow 3-dimensional camera: New concept of high-speed 3-dimensional vision systems. In *Optical Engineering Journal*, volume 35, pages 376 –383, Feb. 1996.

[37] Christopher Geyer and Kostas Daniilidis. A unifying theory for central panoramic systems and practical implications. In *In ECCV 2000, European Conference on Computer Vision*, pages 445–461, 2000.

[38] Paul M. Griffin, Lakshmi S. Narasimhan, and Soung R. Yee. Generation of uniquely encoded light patterns for range data acquisition. *Pattern Recognition*, 25(6):609 – 616, 1992.

[39] S. Grzonka, G. Grisetti, and W. Burgard. Towards a navigation system for autonomous indoor flying. In *Robotics and Automation, 2009. ICRA '09. IEEE International Conference on*, pages 2878 –2883, may 2009.

[40] S. Grzonka, G. Grisetti, and W. Burgard. Towards a navigation system for autonomous indoor flying. In *Robotics and Automation, 2009. ICRA '09. IEEE International Conference on*, pages 2878 –2883, may 2009.

[41] Jens Gühring. Dense 3-d surface acquisition by structured light using off-the-shelf components. In *Proc. Videometrics and Optical Methods for 3D Shape Measurement*, pages 220–231, 2001.

[42] O. Hall-Holt and S. Rusinkiewicz. Stripe boundary codes for real-time structured-light range scanning of moving objects. In *Computer Vision, 2001. ICCV 2001. Proceedings. Eighth IEEE International Conference on*, volume 2, pages 359 –366 vol.2, 2001.

[43] J. Hill and W. Park. Real time control of a robot with a mobile camera. In *Proceedings of the 9th International Symposium on Industrial Robots*, pages 233–246, 1979.

[44] E. Horn and N. Kiryati. Toward optimal structured light patterns. In *3-D Digital Imaging and Modeling, 1997. Proceedings., International Conference on Recent Advances in*, pages 28 –35, may 1997.

[45] J.P. How, B. Bethke, A. Frank, D. Dale, and J. Vian. Real-time indoor autonomous vehicle test environment. *Control Systems, IEEE*, 28(2):51 –64, april 2008.

[46] H. Hugli and G. Maitre. Generation and use of color pseudo random sequences for coding structured light in active ranging. In *Proceedings of Industrial Inspection*, volume 1010, pages 75 – 82, 1989.

[47] DC Douglas Hung. 3d scene modelling by sinusoid encoded illumination. *Image and Vision Computing*, 11(5):251 – 256, 1993.

[48] S. Hutchinson, G.D. Hager, and P.I. Corke. A tutorial on visual servo control. *Robotics and Automation, IEEE Transactions on*, 12(5):651 –670, oct 1996.

[49] Karl Iagnemma and Martin Buehler. Editorial for journal of field robotics,Äîspecial issue on the darpa grand challenge. *Journal of Field Robotics*, 23(9):655–656, sep 2006.

[50] S. Inokuchi, K. Sato, and F. Matsuda. Range imaging system for 3d object recognition. In *In Proceedings of the International Conference on Pattern Recognition*, pages 806–808, 1984.

[51] Minoru Ito and Akira Ishii. A three-level checkerboard pattern (tcp) projection method for curved surface measurement. *Pattern Recognition*, 28(1):27 – 40, 1995.

[52] S. Kiyasu, H. Hoshino, K. Yano, and S. Fujimura. Measurement of the 3-d shape of specular polyhedrons using an m-array coded light source. *Instrumentation and Measurement, IEEE Transactions on*, 44(3):775 – 778, jun 1995.

[53] M. Kontitsis, K.P. Valavanis, and N. Tsourveloudis. A uav vision system for airborne surveillance. In *Robotics and Automation, 2004. Proceedings. ICRA '04. 2004 IEEE International Conference on*, volume 1, pages 77 – 83 Vol.1, april-1 may 2004.

[54] J.J. Le Moigne and A.M. Waxman. Structured light patterns for robot mobility. *Robotics and Automation, IEEE Journal of*, 4(5):541 –548, oct 1988.

[55] Yu-chi Liu and Qiong-hai Dai. A survey of computer vision applied in aerial robotic vehicles. In *Optics Photonics and Energy Engineering (OPEE), 2010 International Conference on*, volume 1, pages 277 –280, may 2010.

[56] Mark Maimone, Yang Cheng, and Larry Matthies. Two years of visual odometry on the mars exploration rovers. *Journal of Field Robotics, Special Issue on Space Robotics*, 24:2007, 2007.

[57] J. Markoff. Google cars drive themselves, in traffic. *New York Times*, oct 2010.

[58] M. Maruyama and S. Abe. Range sensing by projecting multiple slits with random cuts. *Pattern Analysis and Machine Intelligence, IEEE Transactions on*, 15(6):647 –651, jun 1993.

[59] C. Mei and P. Rives. Single view point omnidirectional camera calibration from planar grids. In *IEEE International Conference on Robotics and Automation*, April 2007.

[60] Christopher Mei, Selim Benhimane, Ezio Malis, and Patrick Rives. Constrained multiple planar template tracking for central catadioptric cameras. In *IN BRITISH MACHINE VISION CONFERENCE*, pages 4–7, September 2006.

[61] L. Merino, F. Caballero, P. Forssen, J. Wiklund, J. Ferruz, J.R. Martihez-de Dios, A. Moe, K. Nordberg, and A. Ollero. Single and multi-uav relative position estimation based on natural landmarks. In KimonP. Valavanis, editor, *Advances in Unmanned Aerial Vehicles*, volume 33 of *Intelligent Systems, Control and Automation: Science and Engineering*, pages 267–307. Springer Netherlands, 2007.

[62] Luis Merino, Fernando Caballero, J.R. Martinez-de Dios, Joaquin Ferruz, and Anibal Ollero. A cooperative perception system for multiple uavs: Application to automatic detection of forest fires. *Journal of Field Robotics*, 23(3-4):165–184, 2006.

[63] Torsten Merz, Simone Duranti, and Gianpaolo Conte. Autonomous landing of an unmanned helicopter based on vision and inertial sensing. In *ISER'04*, pages 343–352, 2004.

[64] Torsten Merz, Simone Duranti, and Gianpaolo Conte. Autonomous landing of an unmanned helicopter based on vision and inertial sensing. In Marcelo Ang and Oussama Khatib, editors, *Experimental Robotics IX*, volume 21 of *Springer Tracts in Advanced Robotics*, pages 343–352. Springer Berlin / Heidelberg, 2006.

[65] Najib Metni and Tarek Hamel. A uav for bridge inspection: Visual servoing control law with orientation limits. *Automation in Construction*, 17(1):3 – 10, 2007.

[66] I.F. Mondragon, P. Campoy, C. Martinez, and M.A. Olivares-Mendez. 3d pose estimation based on planar object tracking for uavs control. In *Robotics and Automation (ICRA), 2010 IEEE International Conference on*, pages 35 –41, may 2010.

[67] T. Monks and J. Carter. Improved stripe matching for colour encoded structured light. In Dmitry Chetverikov and Walter Kropatsch, editors, *Computer Analysis of Images and Patterns*, volume 719 of *Lecture Notes in Computer Science*, pages 476–485. Springer Berlin / Heidelberg, 1993. 10.1007/3-540-57233-3.

[68] R.A. Morano, C. Ozturk, R. Conn, S. Dubin, S. Zietz, and J. Nissano. Structured light using pseudorandom codes. *Pattern Analysis and Machine Intelligence, IEEE Transactions on*, 20(3):322 –327, mar 1998.

[69] H. Morita, K. Yajima, and S. Sakata. Reconstruction of surfaces of 3-d objects by m-array pattern projection method. In *Computer Vision., Second International Conference on*, pages 468 –473, dec 1988.

[70] Jeffrey S. Myers and Richard L. Miller. Optical airborne remote sensing. In Richard L. Miller, Carlos E. Del Castillo, Brent A. Mckee,

and Freek D. Meer, editors, *Remote Sensing of Coastal Aquatic Environments*, volume 7 of *Remote Sensing and Digital Image Processing*, pages 51–67. Springer Netherlands, 2005. 10.1007/978-1-4020-3100-7.

[71] Ashutosh Natraj, Cedric Demonceaux, Pascal Vasseur, and Peter Sturm. Vision based attitude and altitude estimation for uavs in dark environments. In *Intelligent Robots and Systems (IROS), 2011 IEEE/RSJ International Conference on*, pages 4006 –4011, sept. 2011.

[72] Ashutosh Natraj, DieuSang Ly, Damien Eynard, Cedric Demonceaux, and Pascal Vasseur. Omnidirectional vision for uav: applications to attitude, motion and altitude estimation for day and night conditions. In *International Conference on Unmanned Aircraft Systems (ICUAS 2012)*, June 2012.

[73] Ashutosh Natraj, DieuSang Ly, Damien Eynard, Cedric Demonceaux, and Pascal Vasseur. Omnidirectional vision for uav: Applications to attitude, motion and altitude estimation for day and night conditions. *Journal of Intelligent Robotic Systems*, pages 1–15, 2012.

[74] Ashutosh Natraj, Peter Sturm, Cedric Demonceaux, and Pascal Vasseur. A geometrical approach for vision based attitude and altitude estimation for uavs in dark environments. In *Intelligent Robots and Systems (IROS), 2012 IEEE/RSJ International Conference on*, Oct. 2012.

[75] Abdelkrim Nemra and Nabil Aouf. Robust airborne 3d visual simultaneous localization and mapping with observability and consistency analysis. *Journal of Intelligent Robotic Systems*, 55:345–376, 2009. 10.1007/s10846-008-9306-6.

[76] D. Nister, O. Naroditsky, and J. Bergen. Visual odometry. In *Computer Vision and Pattern Recognition, 2004. CVPR 2004. Proceedings of the 2004 IEEE Computer Society Conference on*, volume 1, pages I–652 – I–659 Vol.1, june-2 july 2004.

[77] National Commission on Oil Spill-USA. Deep water: The gulf oil disaster and the future of the offshore drilling. *A report on the BP deepwater horizon oil spill and offshore drilling*, Nov 2011.

[78] G. F. Page. Multiple view geometry in computer vision, by richard hartley and andrew zisserman, cup, cambridge, uk, 2003, vi 560 pp., isbn 0-521-54051-8. *Robotica*, 23(02):271–271, 2005.

[79] J. Pages, J. Salvi, and J. Forest. A new optimised de bruijn coding strategy for structured light patterns. In *Pattern Recognition, 2004. ICPR 2004. Proceedings of the 17th International Conference on*, volume 4, pages 284 – 287 Vol.4, aug. 2004.

[80] Martin Peternell. Rational families of conics and quadrics. In *The Mathematics of Surfaces VIII*, page pages, 1998.

[81] E.M. Petriu, T. Bieseman, N. Trif, W.S. McMath, and S.K. Yeung. Visual object recognition using pseudo-random grid encoding. In *Intelligent Robots and Systems, 1992., Proceedings of the 1992 lEEE/RSJ International Conference on*, volume 3, pages 1617 –1624, jul 1992.

[82] J.L Posdamer and M.D Altschuler. Surface measurement by space-encoded projected beam systems. *Computer Graphics and Image Processing*, 18(1):1 – 17, 1982.

[83] A. Puri, K.P. Valavanis, and M. Kontitsis. Statistical profile generation for traffic monitoring using real-time uav based video data. In *Control Automation, 2007. MED '07. Mediterranean Conference on*, pages 1 –6, june 2007.

[84] K Ro, J S Oh, and L Dong. Lessons learned: Application of small uav for urban highway traffic monitoring. In *45th AIAA Aerospace Sciences Meeting and Exhibit*, volume 1, may 2007.

[85] C. Rocchini, P. Cignoni, C. Montani, P. Pingi, and R. Scopigno. A low cost 3d scanner based on structured light. *Computer Graphics Forum*, 20(3):299–308, 2001.

[86] P. Rudol, M. Wzorek, and P. Doherty. Vision-based pose estimation for autonomous indoor navigation of micro-scale unmanned aircraft

systems. In *Robotics and Automation (ICRA), 2010 IEEE International Conference on*, pages 1913 –1920, may 2010.

[87] T. Samad, J.S. Bay, and D. Godbole. Network-centric systems for military operations in urban terrain: The role of uavs. *Proceedings of the IEEE*, 95(1):92 –107, jan. 2007.

[88] G. Sansoni, S. Lazzari, S. Peli, and F. Docchio. 3d imager for dimensional gauging of industrial workpieces: state of the art of the development of a robust and versatile system. In *3-D Digital Imaging and Modeling, 1997. Proceedings., International Conference on Recent Advances in*, pages 19 –26, may 1997.

[89] S. Saripalli, J.F. Montgomery, and G.S. Sukhatme. Visually guided landing of an unmanned aerial vehicle. *Robotics and Automation, IEEE Transactions on*, 19(3):371 – 380, june 2003.

[90] S. Saripalli and G.S. Sukhatme. Landing a helicopter on a moving target. In *Robotics and Automation, 2007 IEEE International Conference on*, pages 2030 –2035, april 2007.

[91] K. Sato. Range imaging based on moving pattern light and spatio-temporal matched filter. In *Image Processing, 1996. Proceedings., International Conference on*, volume 1, pages 33 –36 vol.1, sep 1996.

[92] Tatsuo Sato. Multispectral pattern projection range finder. In Joseph H. Nurre and Brian D. Corner, editors, *Three-Dimensional Image Capture and Applications*, volume 3640 of *SPIE Proceedings*, pages 28–37. SPIE, 1999.

[93] Ashutosh Saxena, J Driemeyer, and Andrew Y. Ng. Robotic grasping of novel objects using vision. *International Journal of Robotics Research (IJRR)*, 27 no. 2:157–173, feb 2008.

[94] D. Scaramuzza and F. Fraundorfer. Visual odometry [tutorial]. *Robotics Automation Magazine, IEEE*, 18(4):80 –92, dec. 2011.

[95] D. Skocaj and A. Leonardis. Range image acquisition of objects with non-uniform albedo using structured light range sensor. In *Pattern*

Recognition, 2000. Proceedings. 15th International Conference on, volume 1, pages 778 –781 vol.1, 2000.

[96] Andrey Soloviev and Donald Venable. Integration of gps and vision measurements for navigation in gps challenged environments. In *Position Location and Navigation Symposium (PLANS), 2010 IEEE/ION*, pages 826 –833, may 2010.

[97] H.J.W. Spoelder, F.M. Vos, E.M. Petrin, and F.C.A. Groen. Some aspects of pseudo random binary array-based surface characterization. *Instrumentation and Measurement, IEEE Transactions on*, 49(6):1331 –1336, dec 2000.

[98] J. Tajima and M. Iwakawa. 3-d data acquisition by rainbow range finder. In *Pattern Recognition, 1990. Proceedings., 10th International Conference on*, volume i, pages 309 –313 vol.1, jun 1990.

[99] S. Todorovic, M.C. Nechyba, and P.G. Ifju. Sky/ground modeling for autonomous mav flight. In *Robotics and Automation, 2003. Proceedings. ICRA '03. IEEE International Conference on*, volume 1, pages 1422 – 1427 vol.1, sept. 2003.

[100] Glenn P Tournier. Six degrees of freedom estimation using monocular vision and moir patterns. In *PhD thesis, Massachusetts Institute of Technology Press*, June 2006.

[101] M. Trobina. Error model of a coded-light range sensor. Technical Report 164, Communication Technology Lab, Image Science Group, ETH, September 1995.

[102] R.J. Valkenburg and A.M. McIvor. Accurate 3d measurement using a structured light system. *Image and Vision Computing*, 16:99–110, 1996.

[103] P. Vuylsteke and A. Oosterlinck. Range image acquisition with a single binary-encoded light pattern. *Pattern Analysis and Machine Intelligence, IEEE Transactions on*, 12(2):148 –164, feb 1990.

[104] C. De. Wagter and J. Mulder. Towards vision-based uav situation awareness. In *AIAA Guidance, Navigation, and Control Conference and Exhibit*, August 2005.

[105] M. Walter, F. Hover, and J. Leonard. Slam for ship hull inspection using exactly sparse extended information filters. In *Robotics and Automation, 2008. ICRA 2008. IEEE International Conference on*, pages 1463 –1470, may 2008.

[106] G. Wiora. High resolution measurement of phase-shift amplitude and numeric object phase calculation. In *Proceedings of Vision Geometry IX*, volume 4117, page 289–299, October 2000.

[107] Clarence Wust and David W. Capson. Surface profile measurement using color fringe projection. *Machine Vision and Applications*, 4:193–203, 1991. 10.1007/BF01230201.

[108] Xianghua Ying and Zhanyi Hu. Can we consider central catadioptric cameras and fisheye cameras within a unified imaging model. In Tomas Pajdla and Jir Matas, editors, *Computer Vision - ECCV 2004*, volume 3021 of *Lecture Notes in Computer Science*, pages 442–455. Springer Berlin / Heidelberg, 2004. 10.1007/978-3-540-24670-1-34.

[109] Chengxin Yu, Li Zhao, Na Xu, and Shaolin Li. Study of computer vision and robot control technology in as/rs. In *Automation and Logistics, 2007 IEEE International Conference on*, pages 876 –879, aug. 2007.

[110] Li Zhang, Brian Curless, and Steven M. Seitz. Rapid shape acquisition using color structured light and multi-pass dynamic programming. In *The 1st IEEE International Symposium on 3D Data Processing, Visualization, and Transmission*, pages 24–36, June 2002.

[111] Zhengyou Zhang. Flexible camera calibration by viewing a plane from unknown orientations. In *Computer Vision, 1999. The Proceedings of the Seventh IEEE International Conference on*, volume 1, pages 666 –673 vol.1, September 1999.